

EGG-TMI-6580  
September 1984  
(Draft)

TMI PARTICLE CHARACTERIZATION DETERMINED  
FROM FILTER EXAMINATIONS--DRAFT

PATENT CLEARED

Charles S. Olsen  
Richard E. Mason  
Timothy E. Doyle  
Richard R. Hobbins

<del>TU</del> SEP 14 1993
<del>Stella Steele 5-13-99</del>
sheryl Silberman 5-24-00

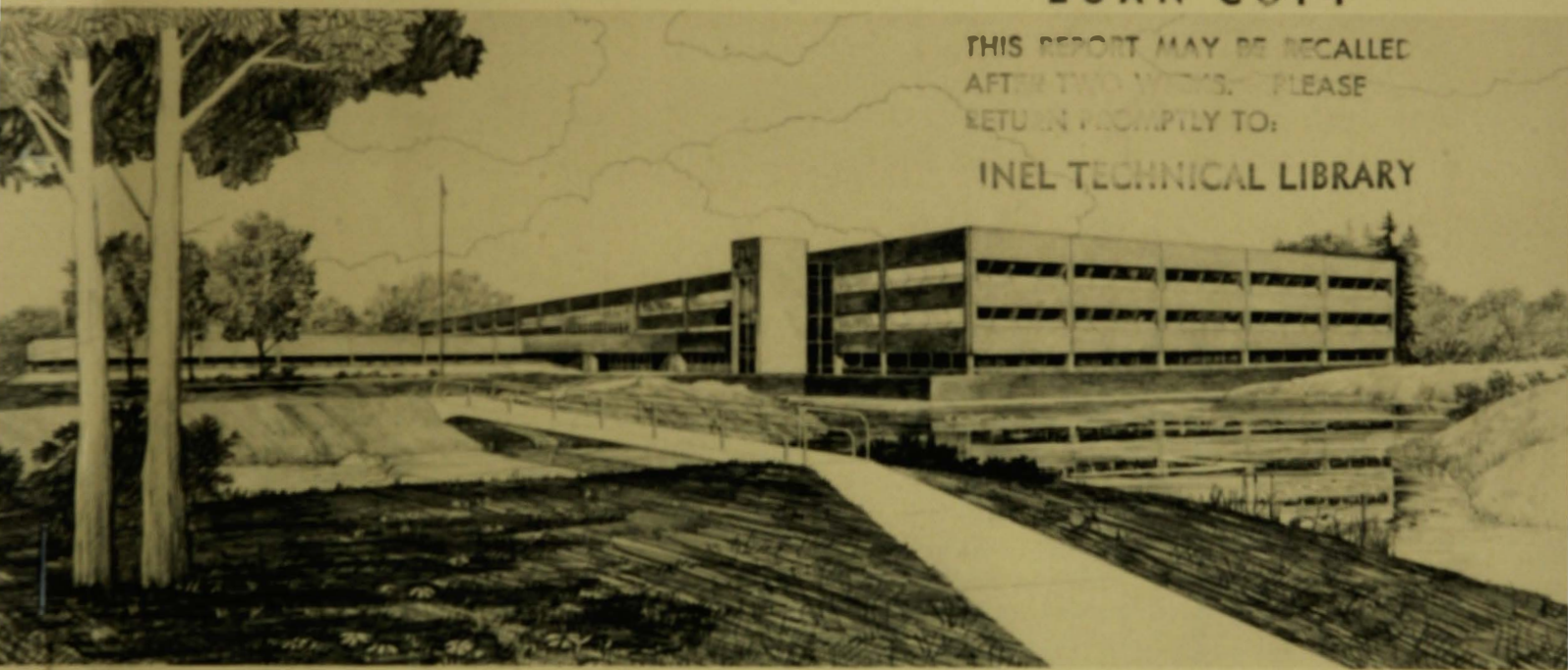
**Idaho National Engineering Laboratory**  
Operated by the U.S. Department of Energy

**Informal Report**

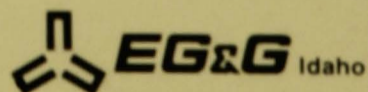
**LOAN COPY**

THIS REPORT MAY BE RECALLED  
AFTER TWO YEARS. PLEASE  
RETURN PROMPTLY TO:

**INEL TECHNICAL LIBRARY**



Prepared for the  
**U.S. DEPARTMENT OF ENERGY**  
Under DOE Contract No. DE-AC07-76ID01570



## DISCLAIMER

This book was prepared as an account of work sponsored by an agency of the United States Government. Neither the United States Government nor any agency thereof, nor any of their employees, makes any warranty, express or implied, or assumes any legal liability or responsibility for the accuracy, completeness, or usefulness of any information, apparatus, product or process disclosed, or represents that its use would not infringe privately owned rights. References herein to any specific commercial product, process, or service by trade name, trademark, manufacturer, or otherwise, does not necessarily constitute or imply its endorsement, recommendation, or favoring by the United States Government or any agency thereof. The views and opinions of authors expressed herein do not necessarily state or reflect those of the United States Government or any agency thereof.

EGG-TMI-6580  
September 1984  
(Draft)

**TMI PARTICLE CHARACTERIZATION DETERMINED FROM FILTER EXAMINATIONS--DRAFT**

Charles S. Olsen  
Richard E. Mason  
Timothy E. Doyle  
Richard R. Hobbins

Published September 1984

EG&G Idaho, Inc.  
Idaho Falls, Idaho 83415

Prepared for the  
U.S. Department of Energy  
Idaho Operations Office  
Under DOE Contract No. DE-AC07-76ID01570

## ABSTRACT

Filters from the purification/makeup system of the Three Mile Island Unit 2 Reactor were examined after the March 28, 1979, accident to determine the character of the debris transported to the filters. The physical condition of the filters was recorded, and material from the filters was examined. The elemental and radionuclide chemistry of the debris is discussed with regard to particle size distribution and fission product release from the core and transport in the primary system. Data on material characterization should be useful in reconstructing the TMI-2 accident events, in determining the propensity of different materials to form fine particles and scatter through the system, and in providing debris chemistry and radionuclide content.

## ACKNOWLEDGMENTS

We thank the personnel at Argonne National Laboratory-East, Los Alamos National Laboratory, Exxon Nuclear Idaho Company, and the EG&G Idaho Hot Cells, Physics, and Fuel Behavior branches who have worked with, examined, or analyzed the data present in this report. We especially thank the principal investigators: C. V. McIsaac and R. L. Nitschke, both of EG&G Idaho; N. D. Stalnaker, Los Alamos National Laboratory, and R. V. Strain, Argonne National Laboratory.

CONTENTS

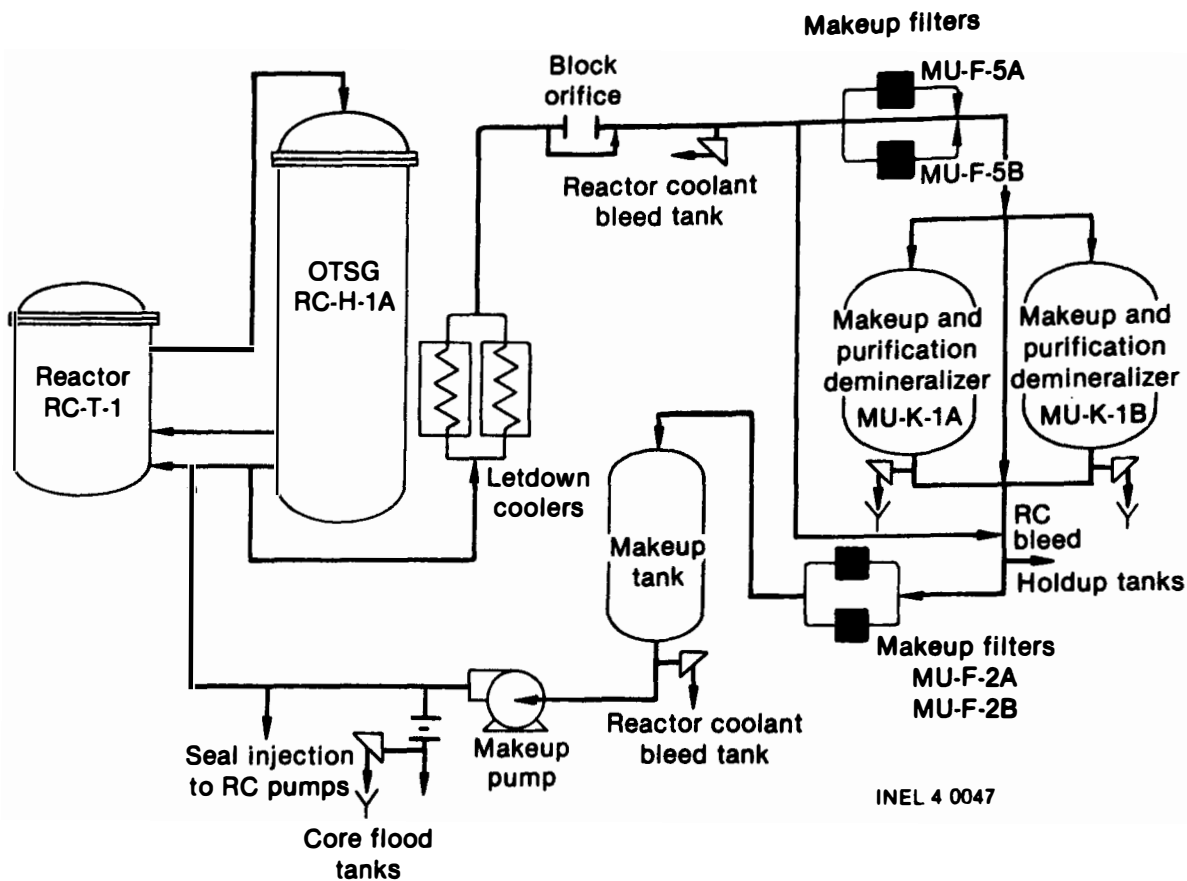
ABSTRACT .....	ii
ACKNOWLEDGMENTS .....	iii
INTRODUCTION .....	1
HISTORY OF FILTER OPERATION .....	7
Reactor Coolant Makeup and Purification System Accident Operations .....	7
FILTER CONDITION .....	9
RADIONUCLIDE DISTRIBUTION .....	15
MATERIAL CHARACTERIZATION .....	21
SUMMARY .....	36
REFERENCES .....	37
APPENDIX A--FINAL REPORT BY ARGONNE NATIONAL LABORATORY .....	A-1
APPENDIX B--FINAL REPORT BY LOS ALAMOS NATIONAL LABORATORY .....	B-1

## INTRODUCTION

The accident at Three Mile Island Unit 2 (TMI-2) on March 28, 1979, provides a opportunity to investigate severe accident damage and advance the knowledge of light water reactor safety. Recognizing this opportunity, four organizations--General Public Utilities, Electric Power Research Institute, Nuclear Regulatory Commission, and Department of Energy--called the GEND group, are conducting a variety of data acquisition and reactor recovery tasks. One task is an examination of the purification/makeup filters and vacuum cartridge filters from the TMI-2 reactor. The examinations were conducted as a joint venture among INEL, Los Alamos National Laboratory, and Argonne National Laboratory-East. The Department of Energy funded examinations at INEL and LANL. The Nuclear Regulatory Commission funded the examinations at Argonne-East. The final report by Argonne National Laboratory is presented in Appendix A, and the final report by Los Alamos National Laboratory is presented in Appendix B.

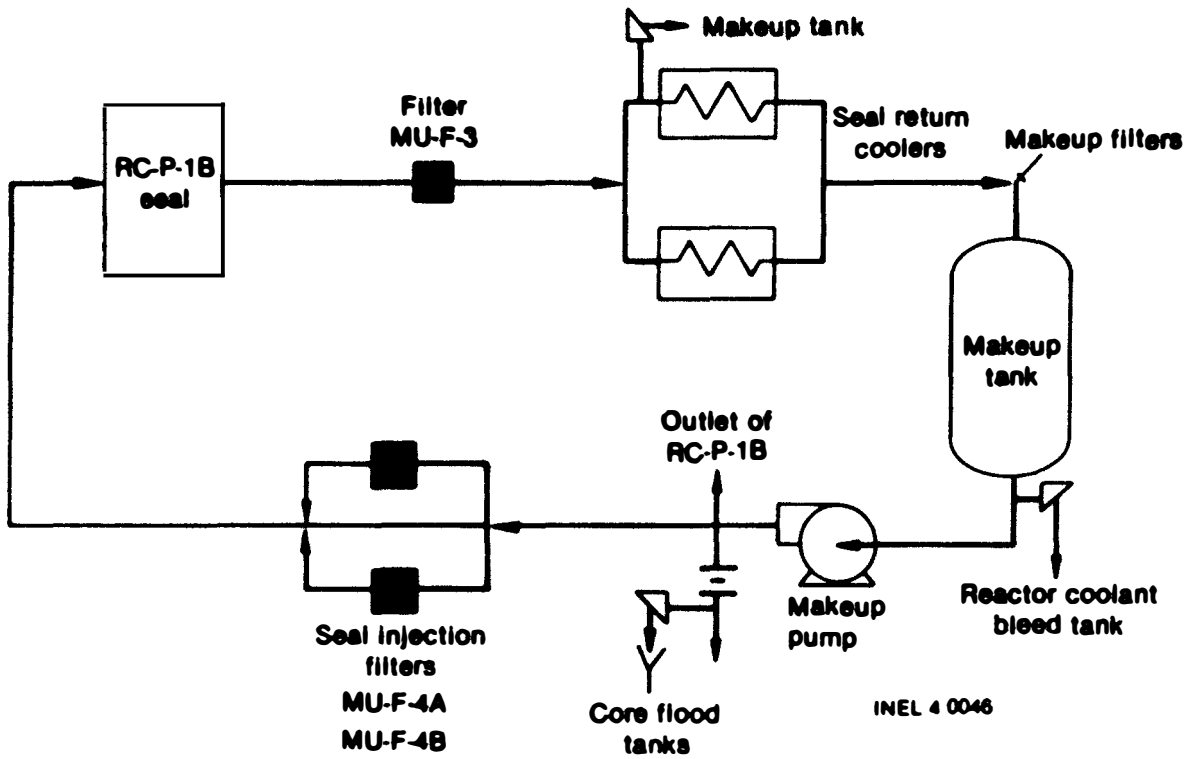
The reason for examining filters was to provide information on light water reactor behavior under severe accident conditions. Specifically, the goal of the filter examination is to assist in the reconstruction of the TMI-2 accident events by indicating which core components are prone to form fine particles that redistribute through the primary coolant system of a light water reactor during a severe accident and providing data on debris chemistry and radionuclide concentrations. To accomplish this goal, the chemical composition of the bulk material and individual particles was measured along with the particle shape and size distributions.

Three long (0.6-m-long) and two short (0.3-m-long) filters from the purification/makeup system were selected for examination (Figure 1 shows schematics for the primary coolant and pump seal coolant systems). The long filters (MUF-5B, -2A, and -2B) were located upstream of the makeup tank. The short filters (MUF-4A and -4B) preceded the injection to the primary pump seal. Each filter had a cylindrical perforated stainless steel backing covered by pleated paper. The pleated paper on the large filters was composed of a minimum of four layers of paper. The outer paper layer consisted of a treated composite of cellulose and glass fiber cardboard type paper. The smaller filters were composed of a perforated stainless steel backing covered



(a) Primary coolant system

Figure 1. Schematic of the purification/makeup filter system in the TMI-2 reactor.



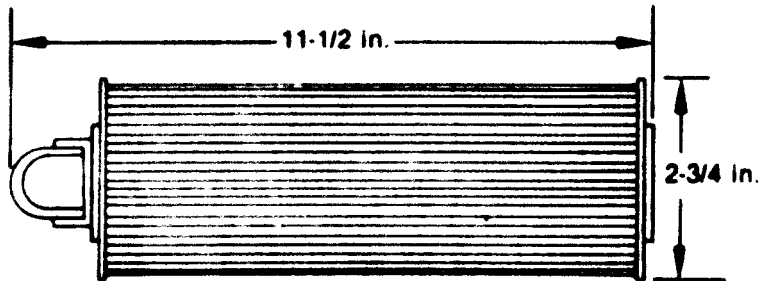
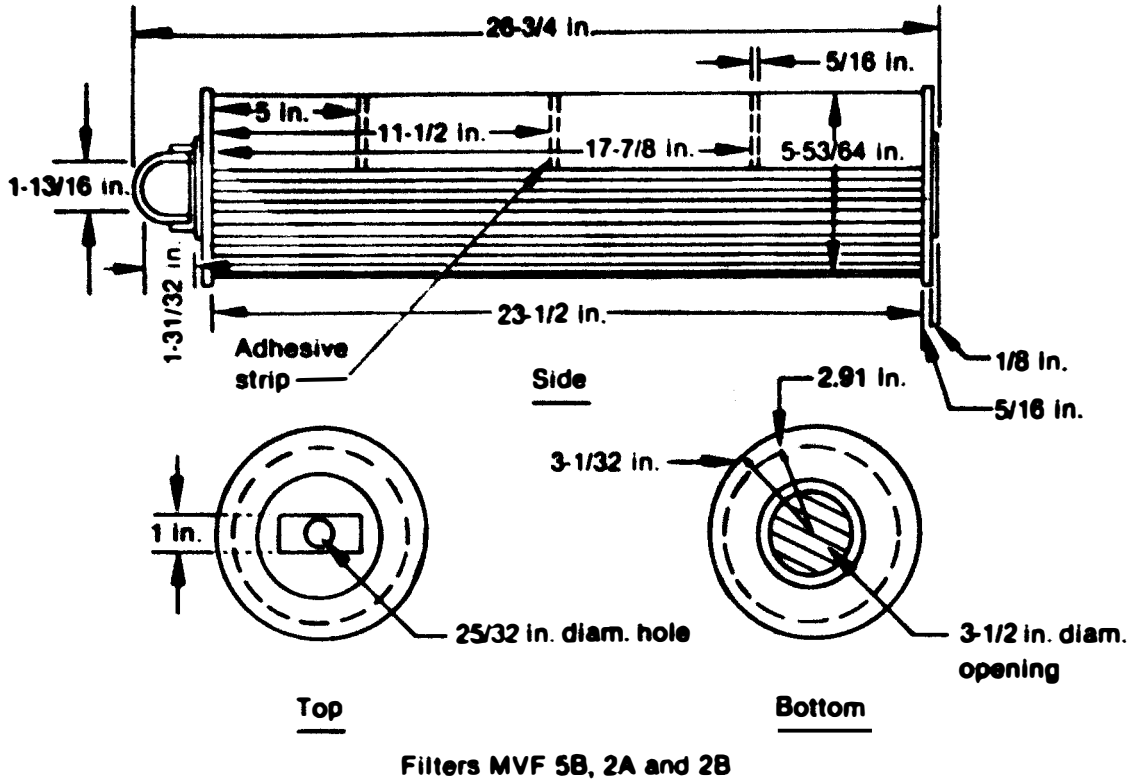
(b) Pump seal coolant system  
Figure 1. (continued)

with only one layer of treated cellulose cardboard paper. The coolant flows into the cylindrical paper filter from outside and then out the perforated stainless steel cylinder. The filters are illustrated in Figure 2.

In addition to the purification/makeup system filters, eight vacuum cartridge filters were used to vacuum loose debris out of the filter housings after the system filters were removed. These cartridge filters also were examined. The vacuum filters were enclosed in metal canisters and sealed on both ends by spring closed caps, as illustrated in Figure 3.

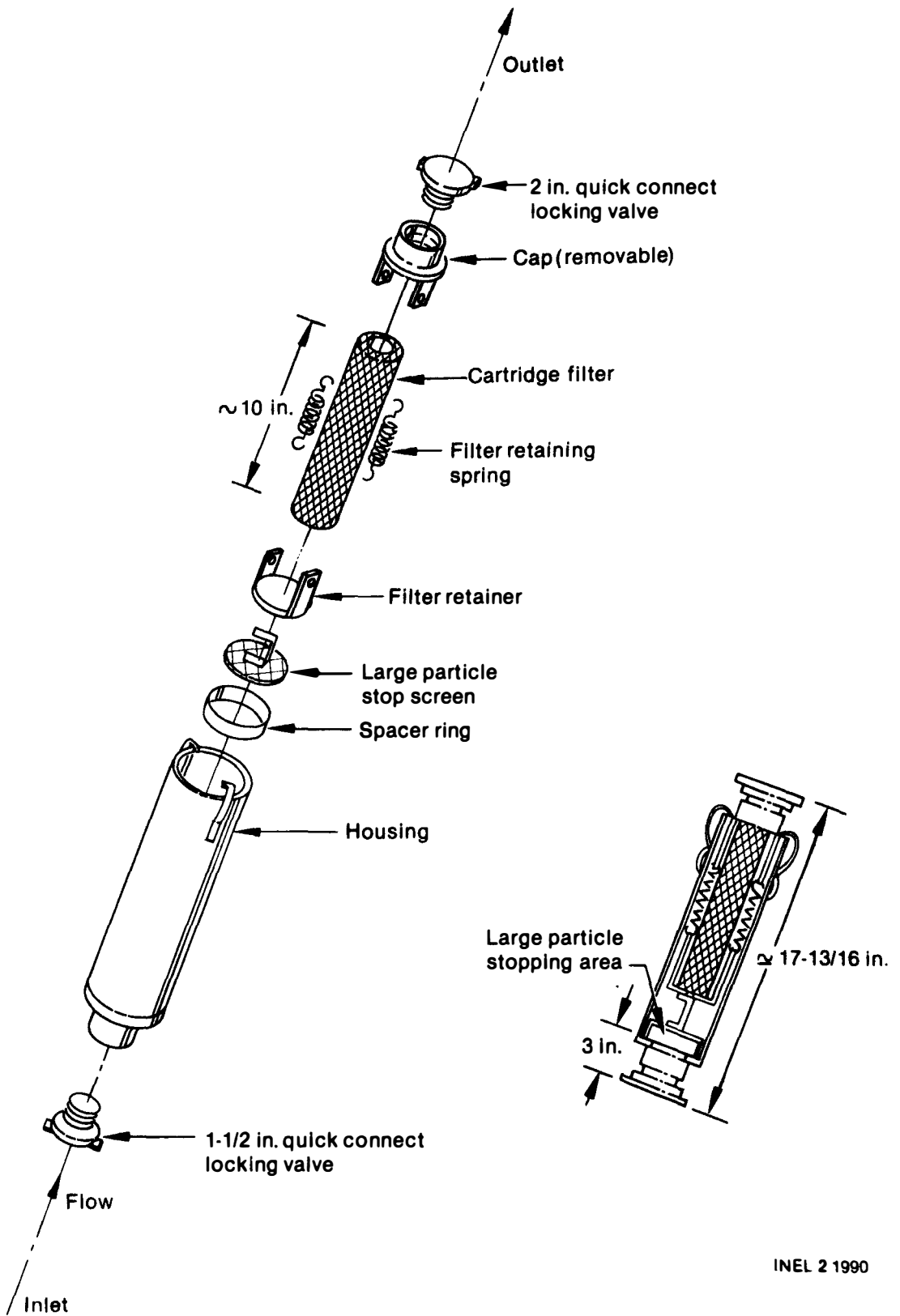
The accident history is discussed in terms of the events that affected the filters, followed by a discussion of the condition of the filters and the distribution of radionuclides in the filter debris. Material behavior, as derived from particle size measurements, chemical analyses, and scanning electron microscopy measurements are also presented.

TMI-2 Purification Filters



INEL 2 1989

Figure 2. Schematic of the TMI-2 purification/makeup filters.



INEL 2 1990

Figure 3. Schematic of the TMI-2 vacuum filter.

## HISTORY OF FILTER OPERATION

### Reactor Coolant Makeup and Purification System Accident Operations

The makeup and purification system filters and demineralizes a portion of the reactor coolant on a continuous basis during reactor operation. A portion of the reactor coolant flow (letdown) is drawn from the reactor coolant line at the suction side of RC-P-1A. The letdown water flows through the letdown cooler where its temperature is reduced from 555 to 120°F and then through the block orifice where the pressure is reduced from 2155 to 100 psig. The water then flows through makeup and purification demineralizer filters (MUF-5A or MUF-5B), to the demineralizers (MUK-1A or MUK-1B) and the makeup filters (MUF-2A or MUF-2B). Fresh makeup water is added to the system between the demineralizers and the makeup filters. The letdown flow at the outlet of the makeup filters is joined with flow from the reactor coolant pump seal return. Both of these flows go to the makeup tank (MUT-1). From the makeup tank the makeup flow passes through the makeup pumps (MUP-1A, B, C) and the seal injection filters (MUF-4A or MUF-4B). A portion of the makeup is then discharged to the reactor coolant pump seals and the remainder is returned to the reactor coolant system.

The system is designed to operate at flows between 40 and 110 gpm. At the time of the accident, the system was operating at 40 gpm with one set of filters/demineralizers on-line. There is no record of which set of filters/demineralizers were on-line at the time of the accident but past accident examinations indicate that the 'A train' was probably in operation. After the accident, letdown flows fluctuated for a brief period but finally stabilized at about 70 gpm. By 1630 hours on March 28, 1979 letdown flows began to fluctuate from lows of 40 gpm to highs of 159 gpm until letdown flow was lost at 2234, apparently as a result of letdown cooler plugging. By 0631 hours on March 29, 1979 a letdown flow of 25 gpm had been established with all system filters and the demineralizers bypassed. The exact time of component bypassing is unknown and the demineralizers were not totally isolated until the effluent stop/check valves were closed on March 30, 1979. GPU Nuclear estimated 46,000 gallons

of water was processed through the makeup system during the 16.5 hours it was in operation after reactor shutdown. During this period, sometime after 1630 hours in March 28, 1979 water was diverted to the reactor coolant bleed tanks caused by overpressurization in the makeup tanks. When letdown flow was reestablished at 0631 hours on March 29, 1979 letdown was being discharged to the reactor coolant bleed tanks and then batch fed to the makeup tank.

## FILTER CONDITION

Three large and two short purification filters, and eight vacuum cartridge filters were shipped in their original steel canisters from TMI-2 to INEL in April 1982. The physical condition of filters MUF-5B, -2A, -2B, -4A, and -4B when they were removed from their containment bags is shown in Figures 4 through 8, respectively. Little filter paper or debris remained on the steel frames of the three large filters (Figures 4, 5, and 6). However, Filter MUF-4A (Figure 7) was received with almost all the filter paper and debris still on the frames of metal filters. The filter paper was friable and debris and paper fell off as the filter was handled. Also, the top half of the metal filter frame had collapsed, (Figure 7). Because there was no indication that the filter had been crushed during shipping, a pressure differential during use at TMI probably caused the filter to collapse from flow blockage after the filter had been loaded with debris. Nearly all filter paper and debris was scraped from the filter and weighed 82.7 g. Short purification Filter MUF-4B also was received intact. However, it was not loaded with the dark debris found on all the other filters but the filter paper was swollen (Figure 8).

The total weight of the debris (filter paper and material collected by the filter) from each filter is given in Table 1. Some debris could have been lost after removing the filters from the plant. The filters, although deteriorated, still retained their debris in containment bags.

Although the high coolant temperatures, coupled with the pressure drops across the filters, may have contributed to the filter deterioration, the beta/gamma field from the entrapped particles is probably the major contributor to the filter degradation as evidenced from the intactness of the pump seal filters 4A and 4B and from the smaller particle content on these filters.

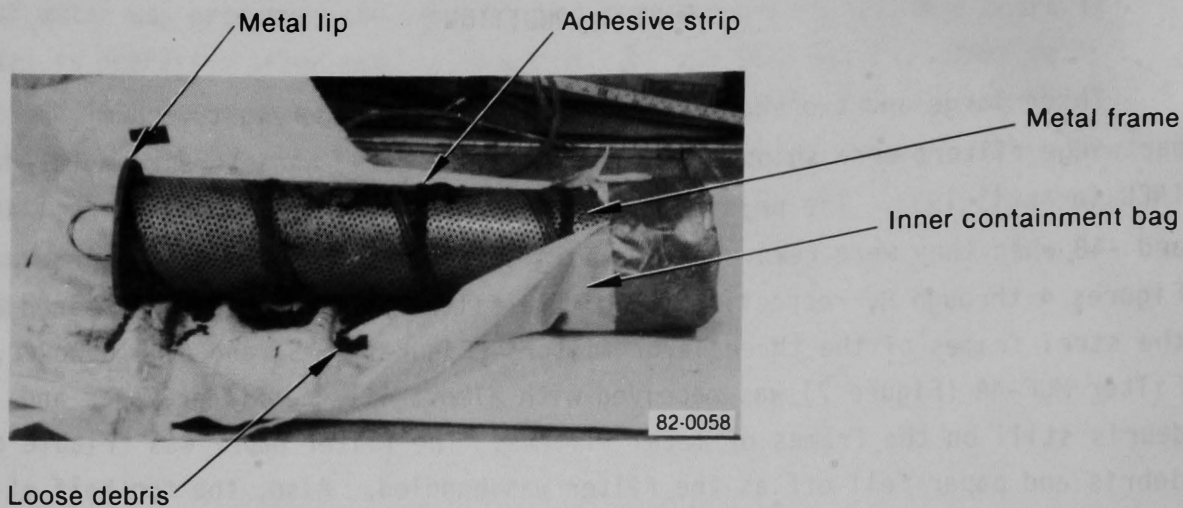


Figure 4. Purification/makeup Filter MUF-5B.

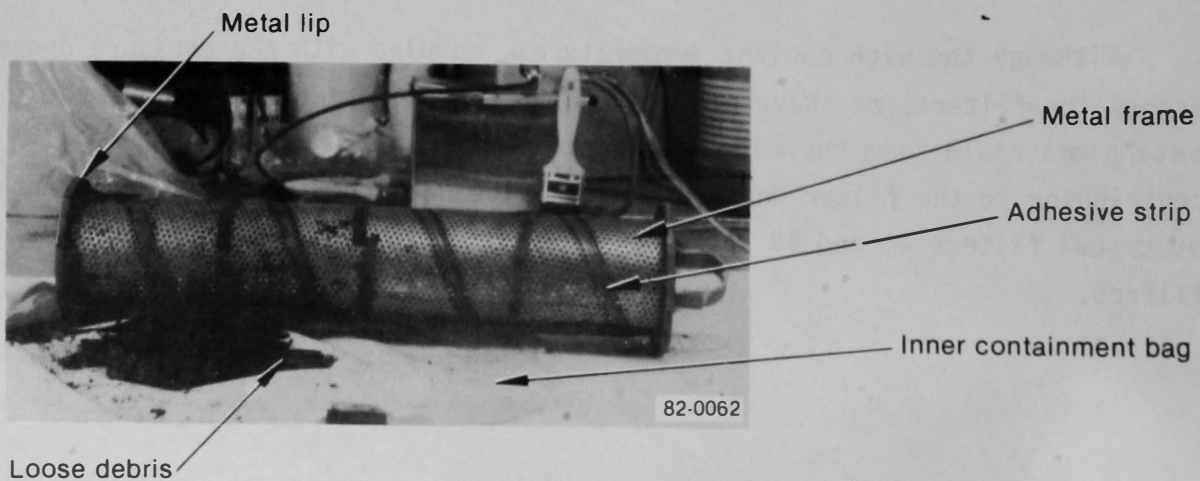


Figure 5. Purification/makeup Filter MUF-2A.

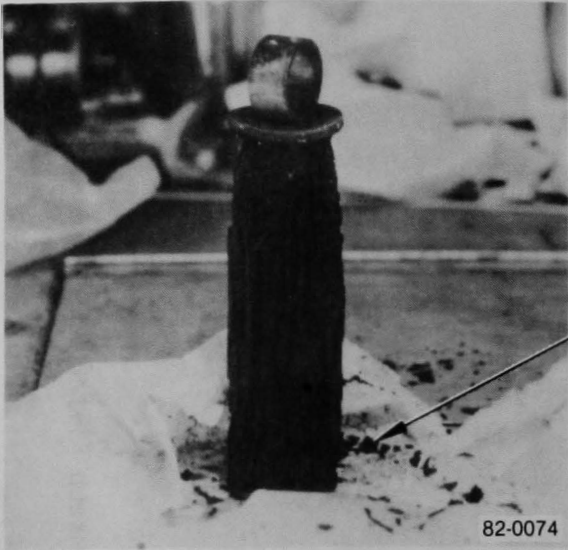


Section of filter paper and debris



Figure 6. Purification/makeup Filter MUF-2B.

0°



Loose debris

82-0074

90°

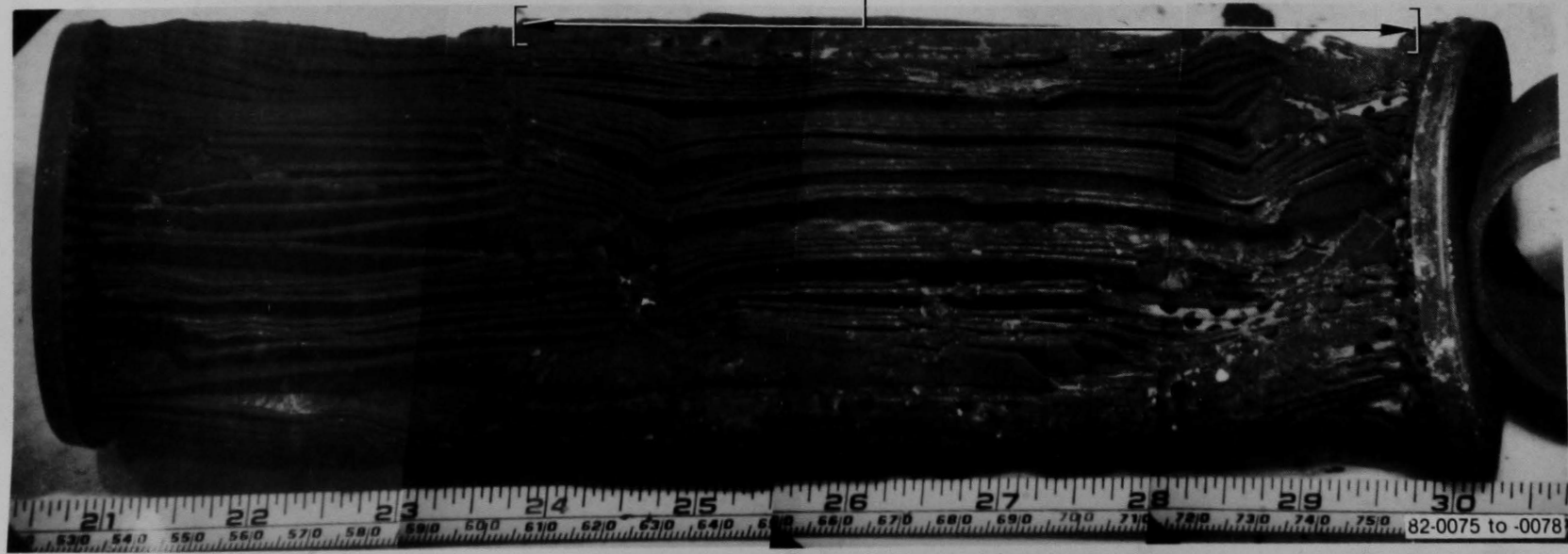


Collapsed region

82-0073

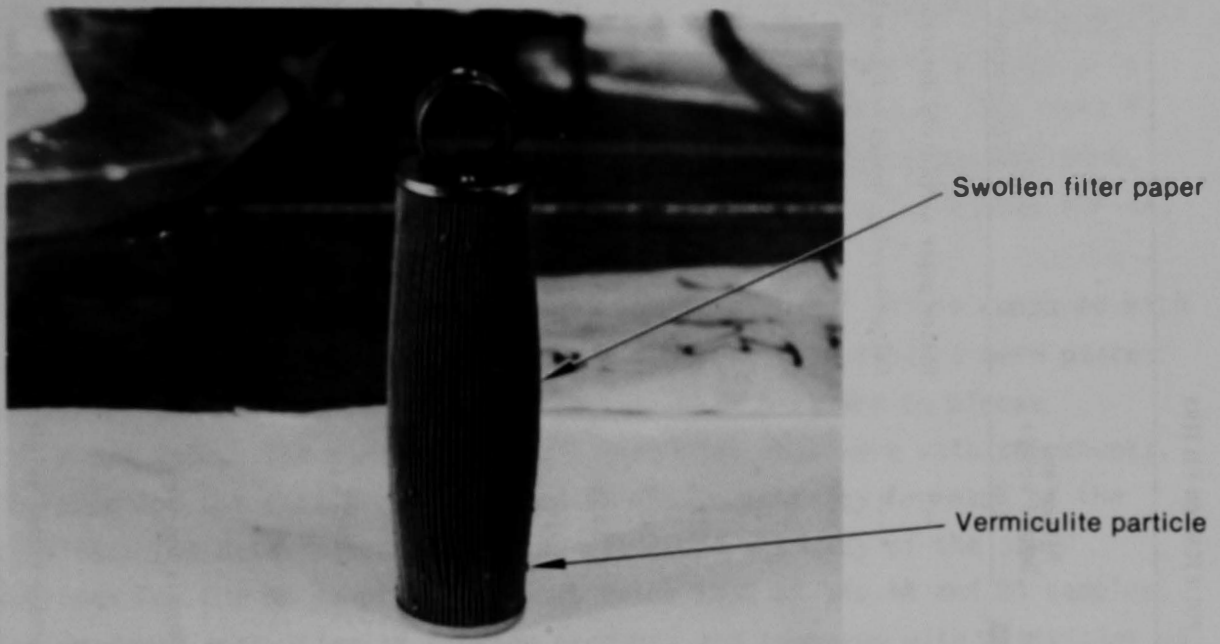
Collapsed region

12



0°

Figure 7. Purification/makeup Filter MUF-4A.



82-0072

Figure 8. Purification/makeup Filter MUF-4B.

TABLE 1. NET WEIGHT OF DEBRIS COLLECTED FROM TMI-2 PURIFICATION FILTERS

Filter	Debris Weight <sup>a</sup> (g)	Estimated Content		Filter and Debris Weight (g)	Description
		Uranium <sup>b</sup> Weight (g)	Storage Drum Identification		
MUF-5B	203.9	10.2	--c	--d	Filter paper completely deteriorated
MUF-4A	82.7	4.1	03	--d	Filter heavily loaded and intact
MUF-4B	--d	0	03	--d	Filter very lightly loaded and intact
MUF-2A	405.7	20.3	--c	--d	Filter paper completely deteriorated
MUF-2B	206.2	10.3	--c	--d	Filter paper completely deteriorated
VAC-MUF-2A-1	340 <sup>e</sup>	17.0	09	577.6	Heavily loaded
VAC-MUF-2A-2	~6 <sup>e</sup>	0.3	09	245.7	Lightly loaded
VAC-MUF-2A-3	~90 <sup>e</sup>	4.5	03	330.5	Moderately loaded
VAC-MUF-2B	~0	0	RCBTA	236	Very lightly loaded--side had a few dark spots
VAC-MUF-4A	~80 <sup>e</sup>	~4.0	04	327	Moderately loaded
VAC-MUF-4B	~0	0	04	242	Moderately loaded--one side was loaded with dark debris
VAC-MUF-5B	~0	0	04	269	Very lightly loaded
VAC-MUF-5A	~0	0	14	242.5	Very lightly loaded--one side was colored light gray with debris and a few large particles were on the surface

a. Damp weights.

b. Estimate based on the assumption that 5% of the debris was UO<sub>2</sub>.

c. Metal filter frames were discarded as hot waste.

d. Not applicable.

e. Estimation based on the assumption that the cartridge filter weighted 240 g.

## RADIONUCLIOE DISTRIBUTION

Filters MUF-5B, MUF-4A, and -4B, and MUF-2A and -2B were examined to determine the concentrations of radioactive isotopes on the filters. A gross gamma scan of Filter MUF-4A and -4B (Figure 9) shows that radioactive debris were located preferentially at one end. Figure 10 shows a spectral gamma scan of the filter at about midheight that indicates that the primary species were Cs, Sb, Ru, Ce/Pr, Ag, Mn, and Co. Filter MUF-4B contained Cs and Co, as indicated by the gamma spectrum shown in Figure 11. The gross gamma scan of Filter MUF-4B is compared with the MUF-4A scan in Figure 9. Because Filter 4B was not opened to the makeup tank during the accident, the gamma field of Filter MUF-4B is much lower than that of Filter MUF-4A.

The results of gamma spectroscopy from Filter MUF-5B are compared with the other filters in Table 2. The chunks reported in Table 2 were pieces of the filter that varied in size from  $\sim 1/16$  inch square to pieces  $1/4 \times 3/4$  inch. The fines were small particles that were with the chunks. In Table 2b, the data are normalized to the Cs activity for each of the samples. The data indicate that the ratios of activity of the other nuclides for the 5B samples are about twice that of the 4A and 2A samples. The measured activities of fission products are compared with activities in the fuel calculated for the TMI-2 power history using the ORIGEN2 code<sup>1</sup> (see Table 3). The measured and calculated  $^{144}\text{Ce}$  activities are in good agreement, which indicates that  $^{144}\text{Ce}$  has stayed with the fuel and is a good indicator for the presence of  $\text{UO}_2$ . The measured activity of the Cs isotopes is about eight times that expected from the calculated inventory in the fuel, and the ratio is about 9 for  $^{90}\text{Sr}$ , 20 to 70 for  $^{125}\text{Sb}$ , 60 for  $^{129}\text{I}$ , and 2 for  $^{106}\text{Ru}$ . The presence of those fission products in the debris, in amounts greatly exceeding the inventory in the fuel, strongly suggests that those isotopes were released from the fuel during the high-temperature portion of the accident and transported along with nonfuel components. Cesium, iodine, and strontium generally tend to form compounds that are soluble in water such as halides and hydroxides. The presence of these fission products in the filter debris after washing with primary coolant suggests that they have chemically combined with the debris.

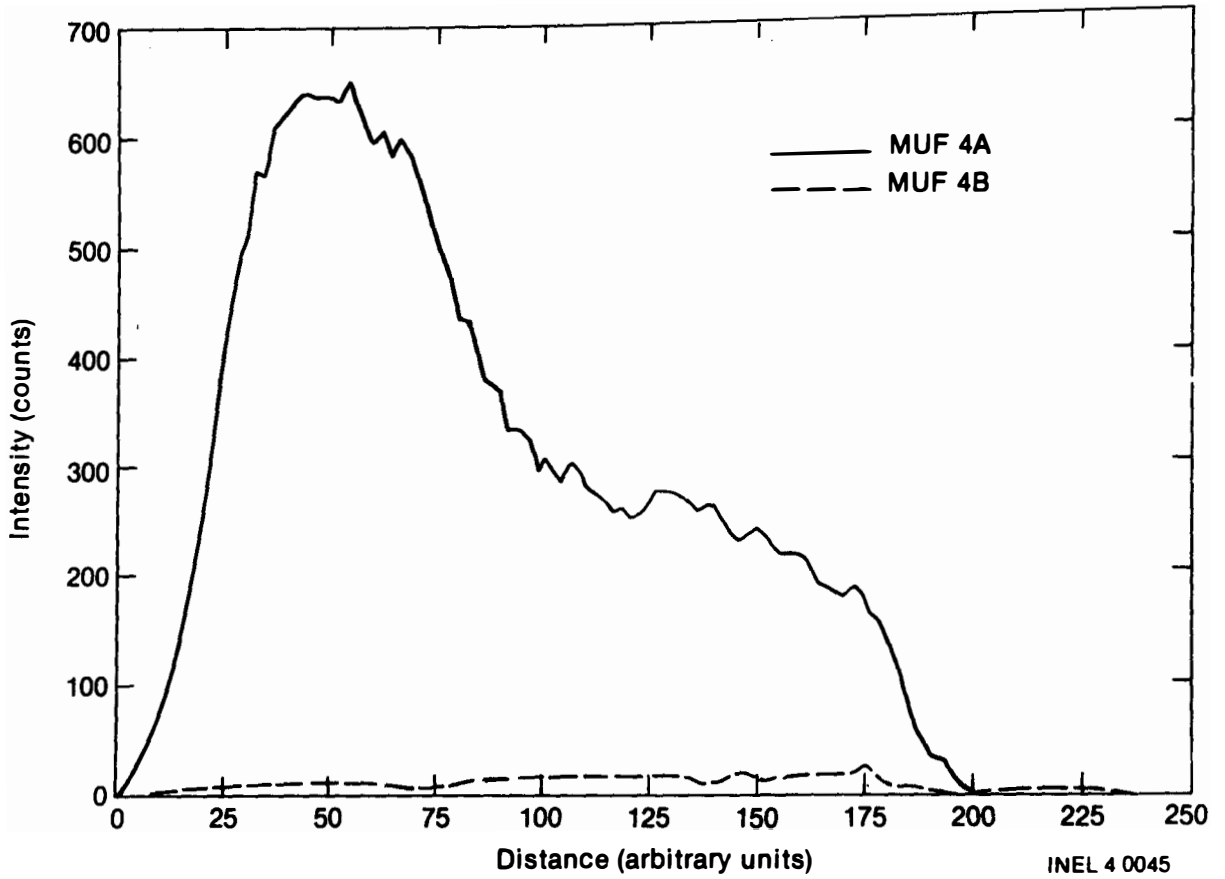


Figure 9. Gross gamma radiation profiles of TMI-2 filters MUF-4F and -4B.

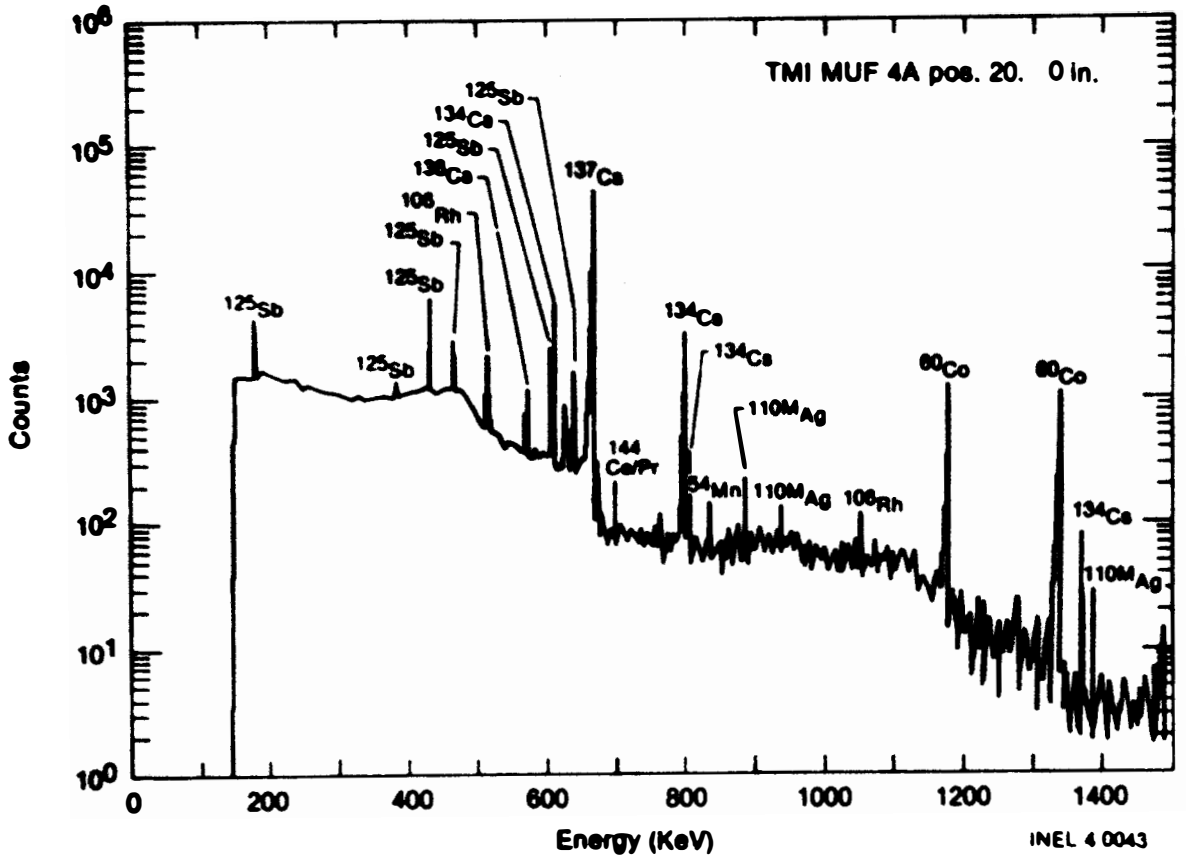


Figure 10. Gamma spectrum of Filter MUF-4A.

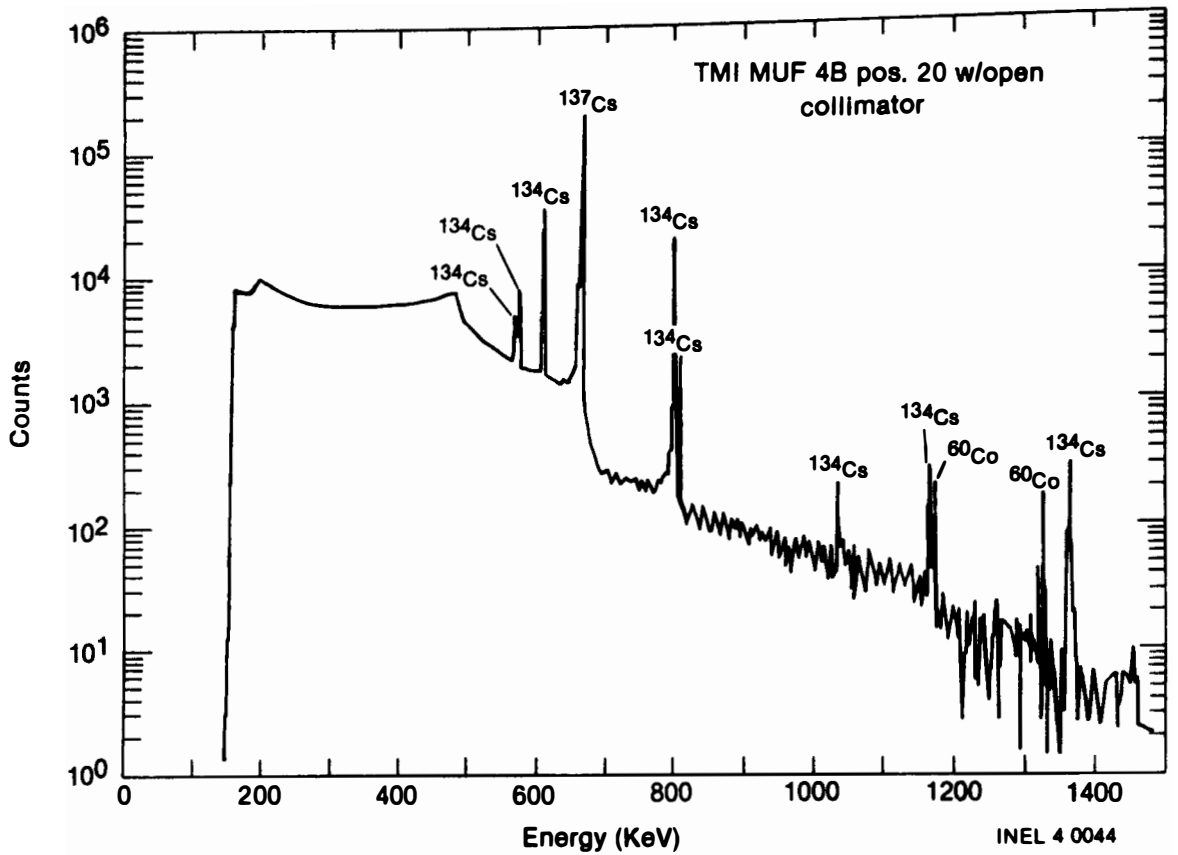


Figure 11. Gamma spectrum of Filter MUF-4B.

TABLE 2. RADIOISOTOPES FROM FILTER MUF-5B

(a) Content ( $\mu\text{Ci/gm}$ )						
	<u>MUF-2A Chunks</u>	<u>MUF-2A Fines</u>	<u>MUF-5B Chunks</u>	<u>MUF-5B Fines</u>	<u>MUF-4A Chunks</u>	<u>MUF-4A Fines</u>
Cs-137	31561.50	28025.66	16708.67	26286.27	6331.09	22090.83
Sb-125	8037.43	4327.94	8457.66	13646.03	1267.15	3967.44
Cs-134	2278.07	2046.85	1164.31	1856.87	453.38	1585.26
Ce-144	1983.96	1081.99	2449.60	4632.50	451.06	1696.6
Ru-106	2032.09	1132.18	2071.57	4177.95	432.46	1645.24
Co-60	748.66	429.45	1179.44	2427.47	199.95	719.79
Ag-110	48.13	27.89	65.52	87.04	16.28	51.41
Mn-54	25.13	15.62	36.34	61.90	8.14	31.71

(b) Isotopic Curie Ratio (based on Cs-137)						
	<u>MUF-2A Chunks</u>	<u>MUF-2A Fines</u>	<u>MUF-5B Chunks</u>	<u>MUF-5B Fines</u>	<u>MUF-4A Chunks</u>	<u>MUF-4A Fines</u>
Cs-137	1.00	1.00	1.00	1.00	1.00	1.00
Sb-125	0.25	0.15	0.51	0.52	0.20	0.18
Cs-134	0.07	0.07	0.07	0.07	0.07	0.07
Ce-144	0.06	0.04	0.15	0.18	0.07	0.08
Ru-106	0.06	0.04	0.12	0.16	0.07	0.07
Co-60	0.02	0.02	0.07	0.09	0.03	0.03
Ag-110	0.00	0.00	0.00	0.00	0.00	0.00
Mn-54	0.00	0.00	0.00	0.00	0.00	0.00

TABLE 3. FISSION PRODUCT ANALYSIS

<u>Nuclide</u>	<u>Filter</u>	<u>Activity<sup>a</sup></u>	<u>Calculated Activity<sup>c</sup></u>	<u>Ration of Measured to Calculated Activities</u>
<sup>144</sup> Ce	MUF-5B	18,400 (μCi/gU)	24,360 (μCi/gU)	0.76
<sup>137</sup> Cs	MUF-5B	76,200 (μCi/gU)	9,740 (μCi/gU)	7.8
<sup>134</sup> Cs	MUF-5B	8,300 (μCi/gU)	840 (μCi/gU)	8.8
<sup>125</sup> Sb	MUF-5B	53,000 (μCi/gU)	760 (μCi/gU)	70
<sup>106</sup> Ru	MUF-5B	12,400 (μCi/gU)	6,040 (μCi/gU)	2.1
<sup>90</sup> Sr	MUF-5B	80,000 <sup>b</sup> (μCi/gU)	8,500 (μCi/gU)	9.4
<sup>129</sup> I	MUF-2A	1,180 (ppm)	16 (ppm)	73.8
<sup>129</sup> I	MUF-2B	1,000 (ppm)	16 (ppm)	62.5

a. The activity for the first five nuclides was measured January 6, 1982, and the sample weight was 0.0239 g. The uranium concentration was assumed to be 5% of the total weight.

b. The activity was measured February 2, 1982. The uranium concentration was assumed to be 5% of the total weight.

c. The calculated activity values are based on ORIGEN2 code calculations.

## MATERIAL CHARACTERIZATION

Photomicrographs of cross sections of the filter show some stratification of the materials (Figure 12). Reflective material of large particle sizes is located on the outer layers of the filters. Smaller particles are located below this layer of larger particles. The volume fraction of metallic (reflective) materials is estimated at 10%.

Results of emission spectroscopy used to determine the elemental content of the debris from Filter MUF-5B are shown in Table 4. The amount of uranium contained in the debris varies between 5 and 7% by weight. Based on this content, an amount of uranium between 70 and 100 g was received with the purification and vacuum filters. The remaining residue consists of control materials, Ag (12%), Cd (11%), and In (5%); fuel rod cladding materials, Zr (5 to 25%), and Sn (2 to 3%), and stainless steel and Inconel, Fe (6%), Ni (5%), Cr (1%), Mo (0.8%), and Si (0.3%). Also, large amounts of carbon (18%) probably from the filter paper and possibly the demineralizer resin beads, were measured in two of the four samples analyzed by emission spectroscopy.

Particle size analysis was performed on samples from filters MUF-5B, MUF-2A, and MUF-2B using metallographically mounted filter sections. Particle sizing was performed with a Zeiss IM-35 metallograph coupled to a Hamamatsu image analyzer (Appendix B). The average particle sizes for all samples ranged between 1 and 2  $\mu\text{m}$ . However, some particles were observed to be as large as 50  $\mu\text{m}$ . Another measurement indicated particles on filters MUF-5B and -2B ranged from submicron size to 50  $\mu\text{m}$ . A histogram of particle sizes on Filter MUF-5B is shown in Figure 13, and cumulative distributions of particle sizes from filters MUF-5B and 2A are shown in Figure 14. The apparent mean particle diameter is 6  $\mu\text{m}$ . The particle size measurements indicate that the majority (80%) of the particles deposited on the filters were less than 10  $\mu\text{m}$  with a mean size of about 2 to 6  $\mu\text{m}$ .

Coolant containing the reactor debris had to travel through the steam generator, the letdown coolers, and the block orifice before it reached the



Figure 12. Metallographic mount of the MUF-5B grab sample.

TABLE 4. EMISSION SPECTROSCOPIC ANALYSIS OF THE MUF-5B FILTER DEBRIS

Element	Elemental Composition of Debris (wt%)			
	B&W <sup>a</sup>	ENICO		
		Sample 0104 <sup>a</sup>	Sample 0105 <sup>a</sup>	Sample 0111 <sup>b</sup>
C	--c	17.5	18	--c
Ag	6 to 12	11.1	13	12.2
Al	0.6	0.55	0.43	~0.5
B	2	0.62	0.64	~0.1
Ca	0.2	--	--	--
Cd	11	11.4	11.2	--
Co	0.08	--	--	--
Cr	0.4	1.0	0.8	2.1
Cu	0.5	0.22	0.23	~0.5
Fe	7	5.7	5.2	3.9
Gd	<0.1	--	--	--
In	--	5.7	5.5	4.5
K	--	--	--	~4.5
Mg	<0.05	0.02	0.02	~0.01
Mn	0.1	0.10	0.10	~0.06
Mo	0.8	0.82	0.86	~0.08
Na	0.06	--	--	--
Nb	--	0.05	0.03	--
Ni	6	4.9	4.5	~0.9
Pb	<0.03	--	--	--
Si	1.8	<0.3	<0.3	~0.16
Sn	3	2.3	2.2	--
Ti	0.1	0.07	0.07	--
U	6	~5	~5	7.27
V	<0.05	--	--	--
Zn	<0.2	--	--	--
Zr	>25	5.4	5.7	12.6
Total	77.27	72.75	73.78	47.78

a. Homogenized sample that fell from the filter during a 1981 filter removal attempt.

b. Specimen taken from the MUF-5B filter. This specimen was homogenized in a plastic jar with Al<sub>2</sub>O<sub>3</sub> milling pellets.

c. Not measured.

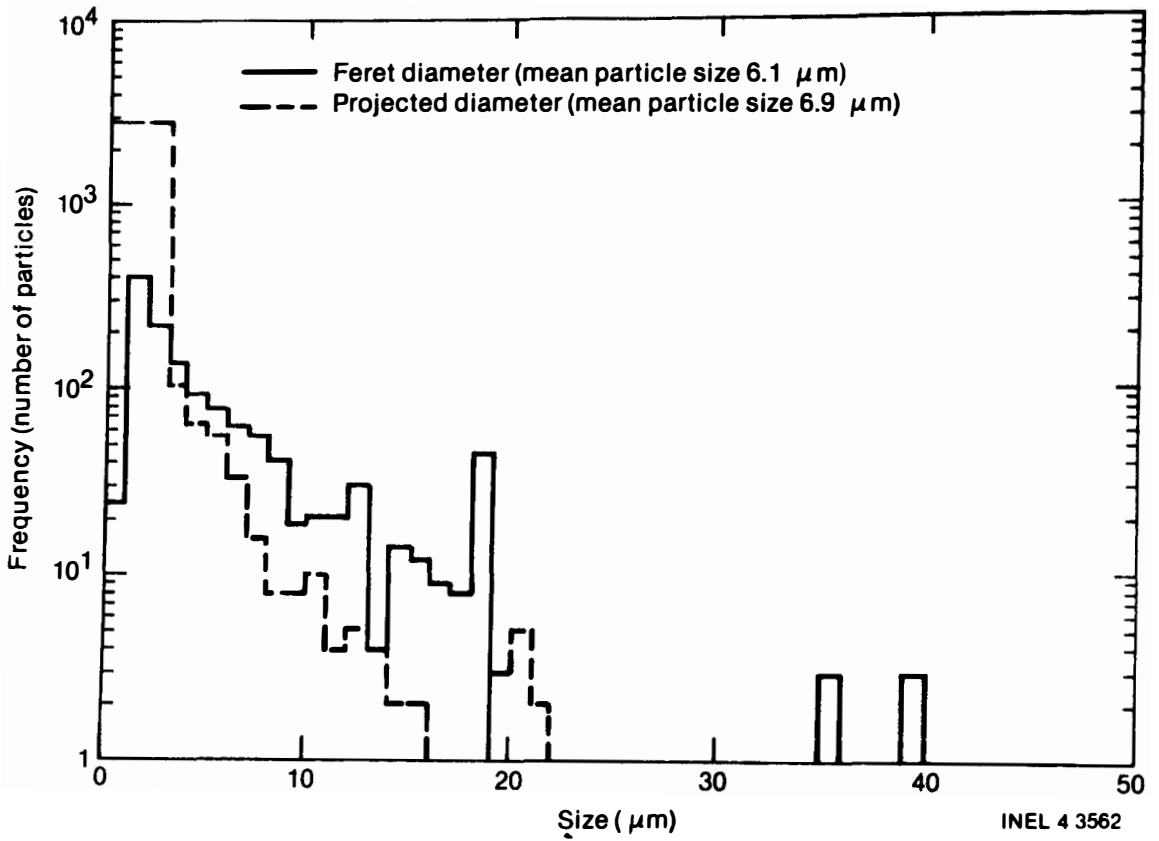


Figure 13. Size distribution of particles from Filter MUF-5B.

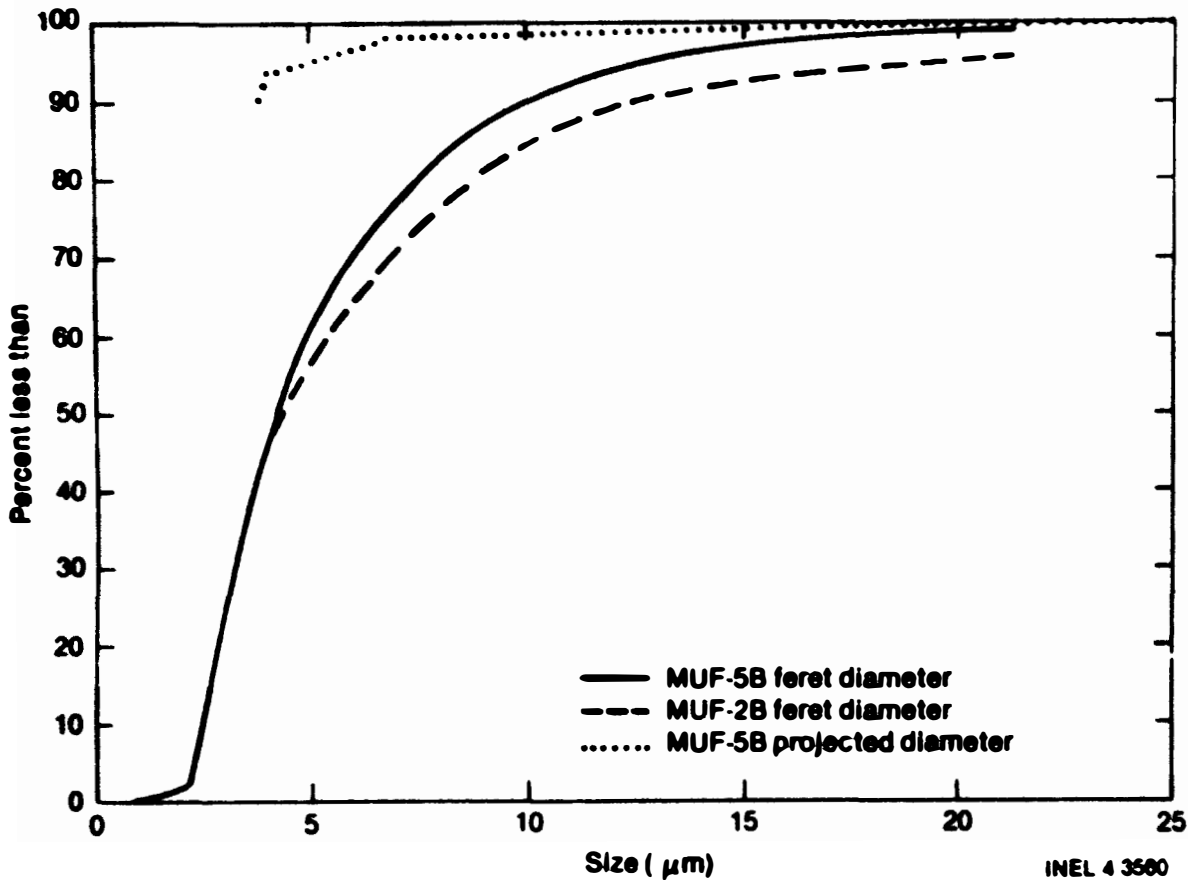


Figure 14. Cumulative particle size distribution from filters MUF-5B and -2A.

filters. These structural components may have limited the maximum particle size that would reach the filters and may also have provided surfaces for deposition of small particles.

The sphericity of particles from the MUF-58 debris was determined from SEM photomicrographs. Sphericity is the ratio of the projected diameter to the diameter<sup>a</sup> of a circle that just circumscribes the particle, and the overall sphericity of the particles is a gross indicator of the particle shape. A particle sphericity histogram of the debris examined on the SEM is illustrated in Figure 15. The mean sphericity of the particles was about 0.61, indicating quite irregular particles.

Examinations of 47 particles in one sample and 28 particles in another sample show that occasionally the debris particles may contain essentially one metallic element, such as zirconium or uranium, but generally the particles have complex compositions containing a number of elements from the fuel, cladding, stainless steel, Inconel, and control materials (Table 5). Expected elemental ratios for the core components are compared with the ratios derived from the elemental measurements in Table 6. Based on the measured Ni/Fe and Mo/Fe ratios, it would appear that the debris likely contain material from both stainless steel and Inconel components, although a somewhat higher Cr/Fe ratio would be expected (from the Inconel source) than was measured. The very high Mo/Fe and the high Cu/Fe ratios are not understood, but suggest some partitioning of the Mo and Cu from their respective alloys.

More than 70% of the particles containing Cd had essentially no Ag or In in them, but instead had steel, Inconel, and/or zirconium components. Cadmium and indium did not occur together in any zircaloy analyzed. Cadmium probably vaporized to a greater extent than did the silver or indium, because of its higher vapor pressure. Vaporization of cadmium from failed control rods has been observed experimentally at ORNL<sup>2</sup> in simulated core-melt tests using light water reactor (LWR) type fuel and control rods. The ORNL tests indicate that cadmium volatilized,

---

a. The projected particle diameter is the diameter of a circle whose area is equal to the area defined by the profile of the particle.

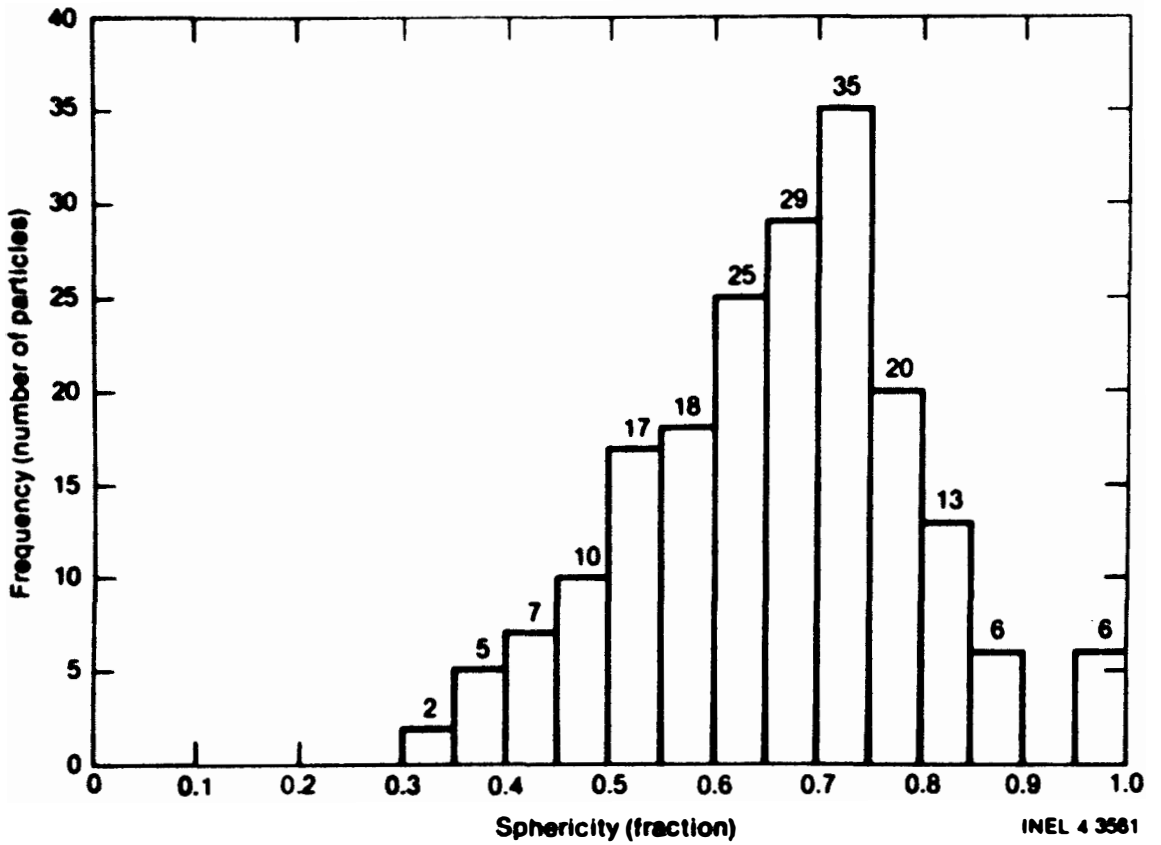


Figure 15. Sphericity distribution of particles from Filter MUF-5B.

TABLE 5. SEM/EDS RESULTS OF PARTICLES REMOVED FROM FILTER MUF-5B

Particle Elemental Composition	Frequency (Number of Particles)	Total Particles Examined (%)
Zirconium	2	7
Uranium <sup>a</sup>	4	14
Zirconium--uranium <sup>b</sup>	2	7
Zirconium--uranium--stainless steel/Inconel	2	7
Zirconium--control materials--stainless steel/ Inconel	1	4
Zirconium--uranium and/or control materials-- stainless steel/Inconel <sup>c</sup>	12	43
Control material <sup>d</sup>	2	7
Aluminum	3	11

a. Particle X-ray spectra generally included small zirconium peaks.

b. Particle X-ray spectra generally contained small peaks from elements associated with stainless steel or Inconel (chromium, iron and nickel).

c. Uranium L-series X-ray peaks were not observed. However, the counting statistics were not sufficient to rule out uranium.

d. X-ray peaks are too broad to be the result of X-ray activation of one element. These particles probably contain Cd, In, and Ag elements from control rods.

TABLE 6. STRUCTURAL MATERIAL MASS RATIOS<sup>a</sup>

<u>Material</u>	<u>Ni/Fe</u>	<u>Cr/Fe</u>	<u>Cu/Fe</u>	<u>Mo/Fe</u>	<u>Si/Fe</u>	<u>Al/Fe</u>	<u>Fe/Total Weight</u>
Stainless steel	0.14	0.27	0	0	0	0	0.65 to 0.76
Inconel	2.84	1.03	0.01	0.19	0.01	0.03	0.19
Bulk filter debris	0.8	0.2	0.06	0.1	0.1	0.09	0.06
LANL microanalysis	1.7	0.2	--	2.7	1.1	0.08	--

a. Based upon iron and compared with similar ratios of TMI-2 filter debris.

left the control rods, and formed CdO when oxygen was available. In the absence of oxygen, vaporized cadmium formed small spherical particles which agglomerated, the agglomerates being <8.6  $\mu\text{m}$  in diameter. The spherical particles and agglomerate structures in the ORNL tests were very similar in morphology to those found in the TMI filter debris.

Energy dispersive X-ray analysis of different particles on Filter MUF-5B confirm the above findings. Round particles such as that located on a long fiber (presumed to be fiberglass because of geometry and silicon content) in Figure 16 were generally found to contain control materials (Ag, In, and Cd). Particles containing zirconium were angular and of varying sizes from 1 to 10  $\mu\text{m}$ . The particles high in stainless steel components (Fe, Cr, and Ni) were small (1 to 5  $\mu\text{m}$ ) angular particles. The angular shape of the nickel, iron, and zirconium bearing particles indicate that these materials did not achieve melting temperatures, whereas the spherical control materials indicate that these materials did melt.

Examination of Filter MUF-2A indicated that the size and shapes of the particles were similar to those seen in the sample from Filter MUF-5B. Two uranium dioxide particles from this filter, identified from elemental chemistry and polyhedral shape, are shown in Figure 17. A rectangular particle below the  $\text{UO}_2$  particles was high in uranium, but also appeared to contain zirconium. This particle may have resulted from the reaction of fuel and cladding. High-magnification photographs of fuel grains (Figure 18) show that small particles (0.1 to 0.5  $\mu\text{m}$ ) have been deposited on the fuel particles. Elements appearing in the X-ray spectra of the fuel particles may result from the deposition of these particles.

Micro-Raman analysis was performed on a sample from Filter MUF-5B with the use of the molecular optical laser examiner microprobe (MOLE). Because the sample stage is a conventional light microscope, no special preparation was needed to examine the particles beyond mounting the sample on a glass slide. The Raman spectra of the particles reveal differences in the crystalline structure of the samples that may provide information about processes that occurred in the TMI-2 core.

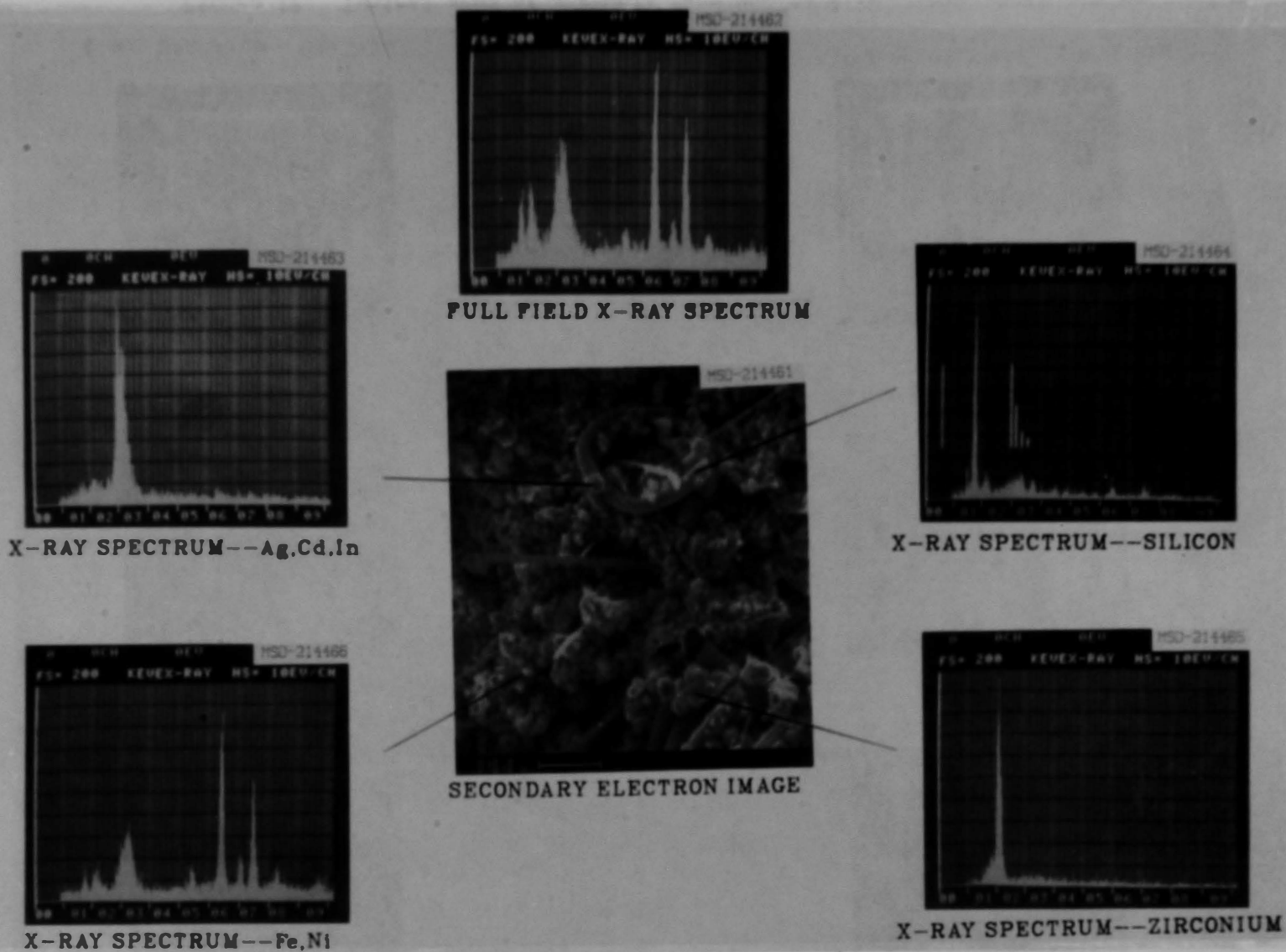


Figure 16. Typical area of a sample from MUF-5B filter with X-ray spectra of some of the particles.

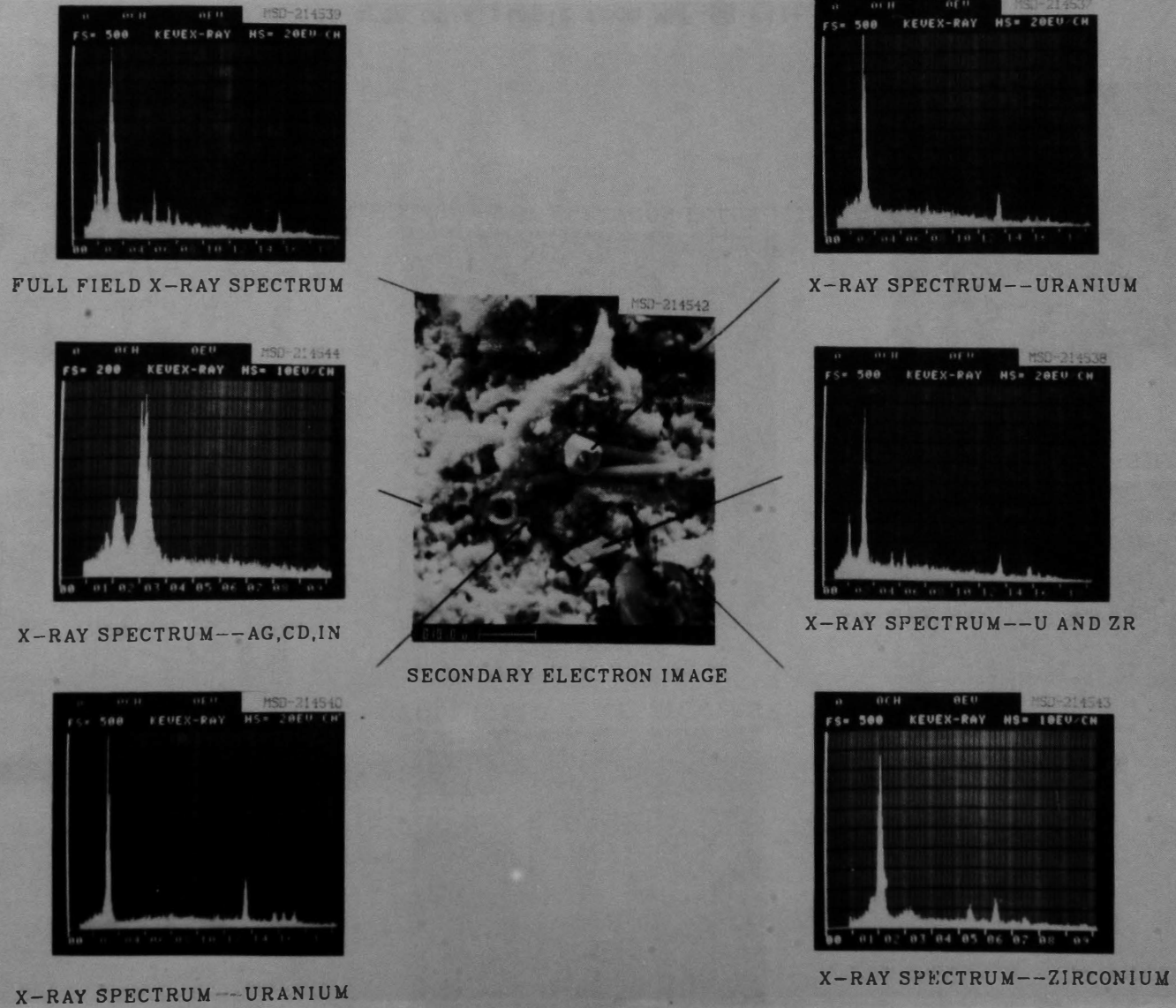


Figure 17. Typical area of a sample from MUF-2A filter with X-ray spectra of some of the particles.

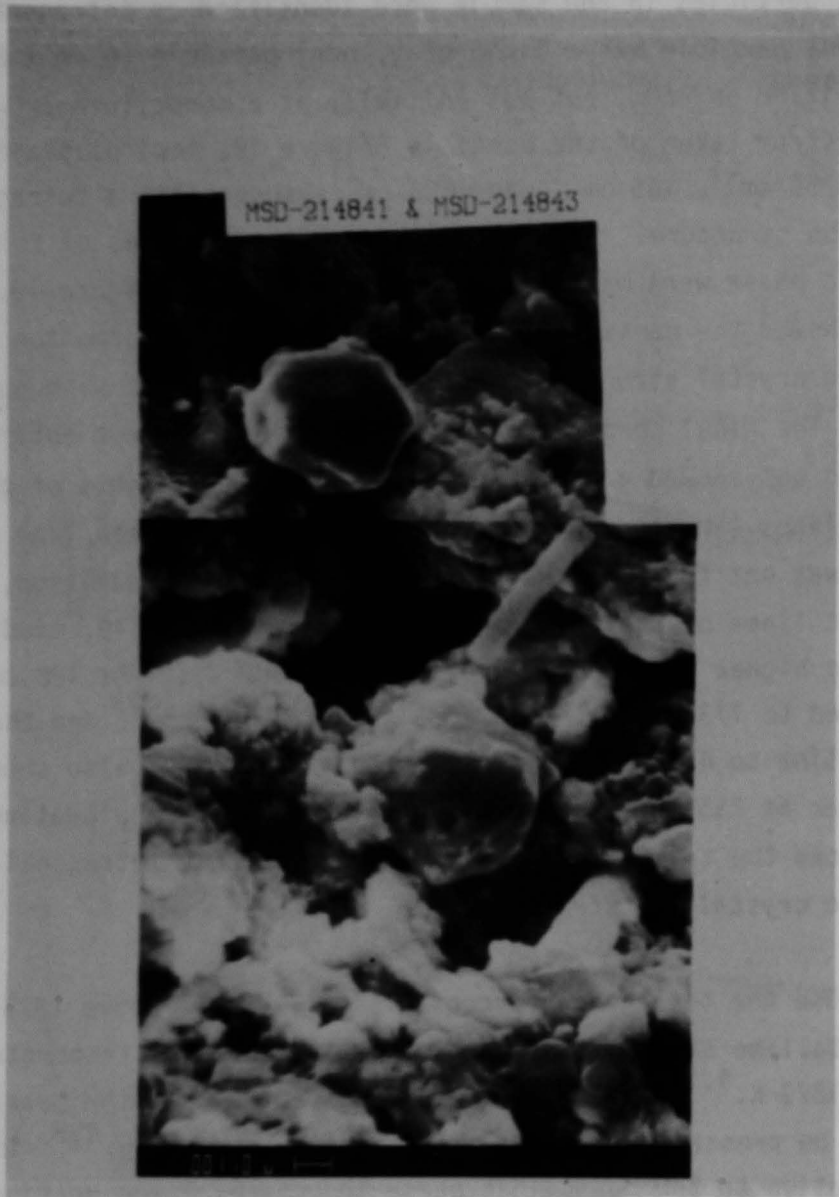


Figure 18. Secondary electron image showing two fuel particles in a piece of the MUF-2A filter.

Four particles in the sample were identified as tetragonal zirconium oxide. One particle was a light gray, oval particle (6  $\mu\text{m}$  x 8  $\mu\text{m}$ ) and was identified as  $\text{ZrO}_2$ , but not initially as a monoclinic  $\text{ZrO}_2$ . The first spectrum taken of the particle (Figure 19, top) displayed weak, broad lines at 256  $\text{cm}^{-1}$ , 465  $\text{cm}^{-1}$ , and 628  $\text{cm}^{-1}$ , suggesting a tetragonal crystalline structure. The 180  $\text{cm}^{-1}$  and 192  $\text{cm}^{-1}$  lines of the monoclinic phase were missing. Subsequent spectra (Figure 19, middle and bottom) showed the particle undergoing a phase transformation to the monoclinic crystal structure that became more dominant with successive spectra. The final spectrum (Figure 19, bottom) was not entirely monoclinic but showed a disparity in the relative heights of the 337 476  $\text{cm}^{-1}$  lines (shifted to 332 and 471  $\text{cm}^{-1}$ ), and a weak line at 216  $\text{cm}^{-1}$  was not found in the standard spectrum. In addition, the major monoclinic lines of the intermediate spectrum (Figure 19, middle) were shifted to higher frequencies (lower wave numbers). The 180  $\text{cm}^{-1}$  line was shifted to 173  $\text{cm}^{-1}$ , the 192  $\text{cm}^{-1}$  line to 186  $\text{cm}^{-1}$ , and the 476  $\text{cm}^{-1}$  line to 465  $\text{cm}^{-1}$ . The intermediate spectrum also showed a strong peak at 255  $\text{cm}^{-1}$ , not a monoclinic line. Sample heating from the laser caused the transformation from the metastable tetragonal to monoclinic crystalline structures.

Because the tetragonal zirconia is only stable above 1373 to 1473 K, this crystalline structure suggests that the cladding temperature may have exceeded 1373 K.<sup>4,5</sup> It is not normally expected that the tetragonal phase can be preserved at low temperatures by quenching.<sup>4,5</sup> The transformation to the monoclinic phase induced by laser heating cannot be resolved with present information. Impurities could also stabilize the high-temperature phase at room temperature, but in this case subsequent heating with the laser would not be expected to induce the transformation to the monoclinic phase.

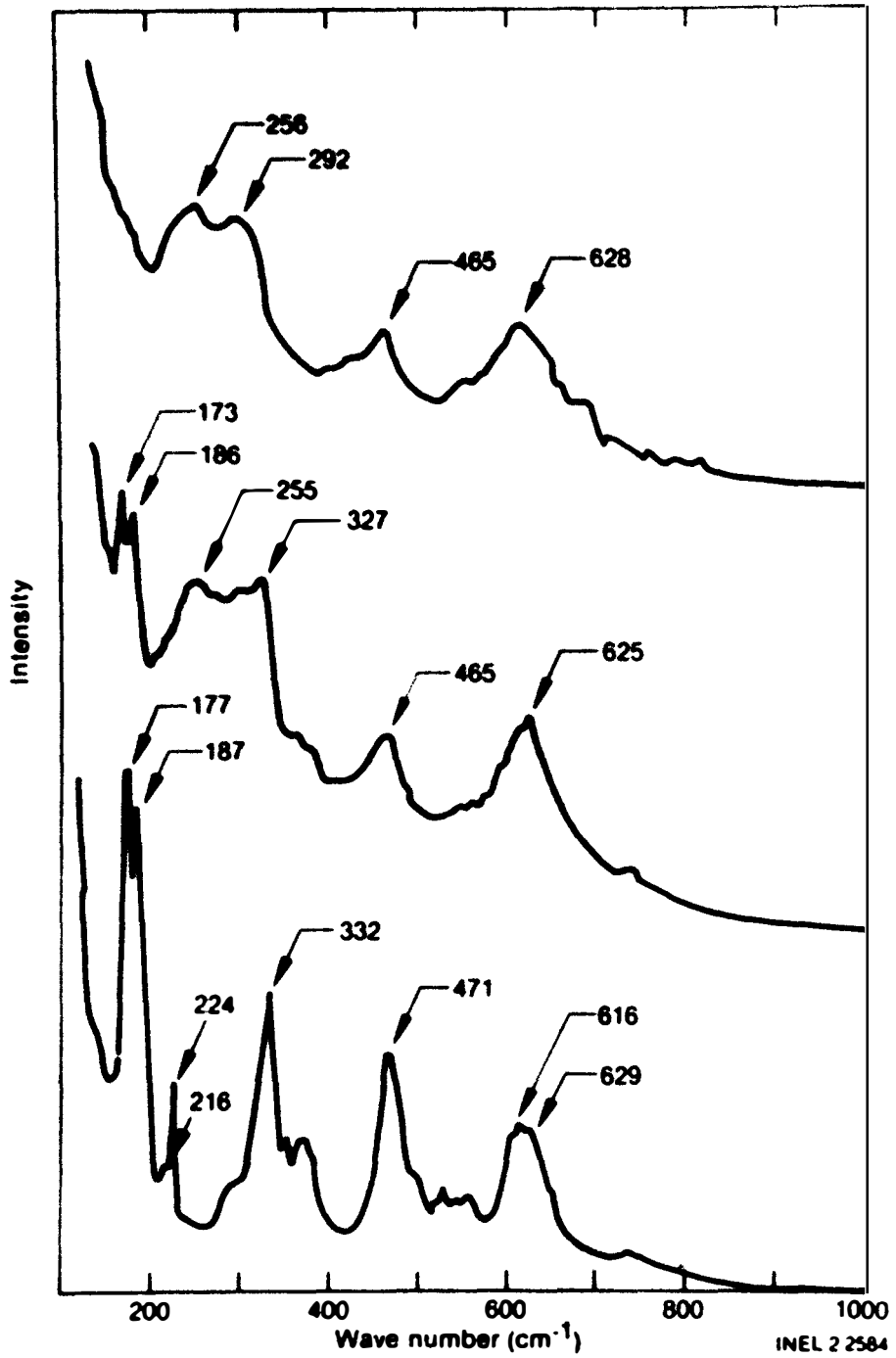


Figure 19. Raman spectra of  $ZrO_2$  particle.

## SUMMARY

Materials from all of the core components were deposited in the purification/makeup filters at TMI including the stainless steel control rod, Inconel spacer grids, silver, indium cadmium control material, and the zircaloy cladding and  $UO_2$  fuel.

The amounts of cesium and iodine present in the filter debris greatly exceeded the amount expected from the fuel and indicate that these materials were transported differently than the fuel. Vapor transport or a mechanism in which vapors are deposited on aerosols of other core components is possible. The cesium and iodine are apparently deposited in insoluble forms on or within particles in the debris.

Antimony and ruthenium fission products were also found in the debris in greater proportions than can be accounted for from the fuel.

The spherical shape of the Ag, In, and Cd bearing particles indicates that these control materials were molten during the TMI-2 accident. The angular shapes of the Fe, Ni, Zr, and U bearing particles indicate that these elements are probably in largely oxide forms that did not melt during the accident.

## REFERENCES

1. R. E. Mason et al., Interim Report on the TMI-2 Purification Filter Examination, EGG-TMI-6181.
2. R. E. Adams and M. L. Tobias, "Aerosol Release and Transport Program-Quarterly Progress Report for October-December 1981," NUREG/CR-2299, Vol. 4, ORNL/TM-8307, May 1982.
3. A. Feinberg and C. H. Perry, "Structural Disorder and Phase Transitions in  $ZrO_2$ - $Y_2O_3$  System," Journal of the Physics and Chemistry of Solids, **42**, 1981, pp. 513-518.
4. R. C. Garvie, "The Occurrence of Metastable Tetragonal Zirconia as a Crystallite Size Effect," The Journal of Physical Chemistry, **69**, 4, 1965, pp. 1238-1243.
5. R. C. Garvie, "Stabilization of the Tetragonal Structure in Zirconia Microcrystals," The Journal of Physical Chemistry, **82**, 2, 1978, pp. 218-224.

REFERENCES

1. W. L. Ridd, J. Am. Chem. Soc., 61, 1111 (1939)

2. W. L. Ridd, J. Am. Chem. Soc., 61, 1111 (1939)

3. W. L. Ridd, J. Am. Chem. Soc., 61, 1111 (1939)

4. W. L. Ridd, J. Am. Chem. Soc., 61, 1111 (1939)

5. W. L. Ridd, J. Am. Chem. Soc., 61, 1111 (1939)

APPENDIX A  
FINAL REPORT BY ARGONNE NATIONAL LABORATORY

THE NATIONAL ARCHIVES  
COLLECTION OF THE NATIONAL ARCHIVES

**RESULTS FROM THE EXAMINATION OF TMI-2 FILTER SAMPLES AT ANL-8**

by

**R. V. Strain**

**Materials Science and Technology Division  
ARGONNE NATIONAL LABORATORY  
9700 South Cass Avenue  
Argonne, Illinois 60439**

**October 1983**

## RESULTS FROM THE EXAMINATION OF TMI-2 FILTER SAMPLES AT ANL-E

### 1. Introduction

Five samples of material from TMI-2 makeup/letdown filters were received at the Alpha-Gamma Hot-Cell Facility (AGHCF) at ANL-E for examination. Material from three of these five samples was examined to characterize the debris from filters MUF-5B, MUF-2A and MUF-4A. Greatest emphasis was placed on the examination of material from the MUF-4A filter as material from this filter was not being examined elsewhere. Material from filter MUF-4B was not examined, and no examinations were performed on a second sample of material from filter MUF-5B, which had been homogenized by ball milling. The purpose of the examinations was to characterize the debris from the filters by size, shape, and chemical composition. The examinations or analyses that were performed on samples of material from each filter are listed in Table I. The results of each of the examinations or analyses listed in Table I are described and a short discussion of those results is provided in this report.

### 2. Visual Examination

Visual examination of debris samples from filters MUF-5B and MUF-2A in the hot-cell showed them to consist of irregular rectangular pieces of fibrous material and fine particles. The pieces of fibrous material were thin slabs that varied in size from  $\sim 1/16$  in. square to pieces  $1/4 \times 3/4$  in. Visual examination of a small piece of the fibrous material in a glovebox indicated that it was composed of layers of fine particles on an underlay of the fibrous filter material. The filter material itself appeared to be composed of fiberglass that was formed into a mat. The MUF-4A filter material was examined visually and determined to consist of irregular, rectangular pieces of  $\sim 1/16$  in. thickness of and fine particles. The MUF-4A filter material was

much less fibrous than the material from the other filters and broke up quite easily when handled. This filter material appeared to be composed only of paper.

### 3. Gamma Spectroscopy

Two different types of samples were counted for radioactivity to determine the types of radionuclides present and their relative activity. Small pieces of the filter (chunks) as well as random samples of the fine particles (fines) from each of the three filters (MUF-5B, MUF-2A, and MUF-4A) were counted to see if the radionuclides were segregated on the filter material. The gamma activities for the samples as of April 1, 1983 are given in Table II. These data indicate that the Cs activity was higher for the debris from the MUF-2A filter than for debris in the other two filters. Normalization of the data for each of these samples (see Table III) to the activity of  $^{137}\text{Cs}$  indicates that the activity ratios of the rest of the radionuclides in the 2A chunks and both 4A samples are similar. The activity ratios of the other radionuclides in the 5B samples are about twice those of the 4A and 2A chunks, while the ratios for the 2A fines are significantly less. These variations in gamma activity may be indicative of variations in quantities of debris trapped by the 2A and 5B filters. Another possibility is that the variations are a result of the difficulty of obtaining truly representative samples of the material. It is likely that the variation in activity of the two types of samples (chunks and fines) from the 2A filter is a result of the types of sampling techniques employed.

### 4. Optical Microscopy

At least two samples of debris from each of the three filters examined were prepared for optical microscopy by placing small pieces in epoxy resin and polishing them according to standard procedures. Low-magnification photos

indicate that the debris had collected on the filters in layers. The small size of the samples made it difficult to determine whether the debris was trapped as several layers within the filter or whether the multiple layers resulted from inclusion of several folds of the filter in the sample. Typical areas of the filters at a magnification of 250X are shown in Figs. 1, 2, and 3. From photos it is apparent that the quantity of reflective material varies significantly within each of the mounted samples. Stereology measurements show that 10% of the MUF-5B sample volume is occupied by highly reflective material that is concentrated in bright-phase areas such as in the center of the upper left photograph in Fig. 1. Examination of optical photographs of the MUF-4A filter revealed that less than 1% of the area of this sample is represented by the highly reflective material as shown in the left photograph in Fig. 3. The highly reflective (bright) material in these optical micrographs is thought to be metallic since the oxides of uranium, iron, and Zircaloy are not this highly reflective. The large (10-50- $\mu\text{m}$ -long) particles appear to have collected on the outermost layer of the filters, particularly the MUF-5B filter. The smaller (1 to 5  $\mu\text{m}$ ) particles are found in layers below the large particles in the two fiberglass filters, MUF-2A and MUF-5B. The quantity of highly reflective material trapped by the paper filter MUF-4A was comparatively small and large particles were insufficient in number to form layers. The filter material itself and many of the ceramic particles do not appear as prominent features in the optical micrographs of these samples. Apparently the filter material, particularly the glass fibers, and zirconium oxide particles are transparent or translucent and have optical properties similar to the epoxy resin that was used as the mounting medium.

## 5. SEM Examinations

SEM examinations were performed on two types of samples — small pieces of the filter material that were mounted directly on sample stubs and polished samples that were examined by optical microscopy.

### 5.1 MUF-5B

Small samples of material from the MUF-5B filter were mounted directly on a sample stub for SEM examination. A typical area near the edge of a piece of filter material is shown in Fig. 4. The large (sometimes angular) pieces of material and the strands shown in the secondary electron (SE) image are believed to be the filter itself. Energy dispersive X-ray analysis\* showed that the large, medium-gray pieces of material produce no characteristic X-ray spectrum. They are assumed to be materials of low atomic number and are probably the cellulose in the filter itself. X-ray spectra of various particles in the secondary electron image are also shown in Fig. 4. Materials easily identified in the full field spectrum are listed in Table IV. The primary constituent or constituents of several particles are identified by the captions under the X-ray spectra in Fig. 4. The broad peak at ~3 keV is composed of Ag, Cd, In, and possibly U. Uranium can be identified by its  $L_{\alpha}$  peak at 13.6 keV with use of a 30 V accelerating voltage. However, the uranium  $L_{\alpha}$  peak was not found in a spectrum of this field of view, and therefore, none of these particles contain significant amounts of uranium. The close proximity of the X-ray peaks for Ag, Cd, and In makes identification of the individual elements imprecise. The presence of certain elements in the particles in this field of view indicates that these elements also were present in the reactor core as the control materials (Ag,

\*Only elements with atomic no. 11 (sodium) and above can be identified using energy dispersive X-ray analysis.

Cd, In), and in components such as the control rod cladding (stainless steel), the fuel rod cladding (Zr), and the Inconel straps (Cr). The clear identification of silicon in the fibers and the strong presence of silicon in the full-field spectrum of the sample confirmed that the filter was constructed of fiberglass.

Figure 5 shows another typical area of the MUF-5B sample along with the X-ray spectra of this field of view and of the individual particles. This area is adjacent to the area shown in Fig. 4, but is closer to the edge of this piece of filter. The number of particles per unit area is greater in the area shown in Fig. 5 than that in Fig. 4, but the materials found are mostly the same. Again, the materials present represent the control material (Ag, Cd, In), the fuel rod cladding (Zr), the control rod cladding (Fe, Cr, Ni), and the silicon in the glass filter fibers. The lack of a spectral peak at 13.6 keV indicates that no uranium is present in this field of view; however, uranium was found in other views of the MUF-5B sample but no photos were taken of the particles that contained uranium. The small round particles, visible in Fig. 5, were generally found to contain control materials (Ag, Cd, In). Zirconium-containing particles generally were found to be angular and of sizes varying from 1- to 10- $\mu\text{m}$  across. The particles high in stainless steel components (Fe, Cr, Ni) generally were also small (1- to 5- $\mu\text{m}$  across) angular particles. None of the large metallic particles seen through optical microscopy of the mounted samples from MUF-5B were observed during the SEM examination of this piece of filter material.

## 5.2 MUF-2A

The SEM examination of a sample of the MUF-2A filter revealed that the size and shapes of the particles (from the reactor core) were similar to those seen in the sample from MUF-5B. Energy dispersive X-ray analysis showed

that the same materials (listed in Table IV) were present except that a  $L_{\alpha}$  uranium peak was also present. A backscattered secondary electron (BSE) image was used to locate particles\* containing uranium. A typical area of the MUF-2A filter sample that contained uranium-rich particles is shown in Fig. 6. The full-field X-ray spectrum of this area indicated the presence of Si, Zr, Ag, Cd, In, Cr, Fe, Ni and U. The particles in the center of this field of view contained only uranium and appear to be grains of the  $UO_2$  fuel as the particles are of the polyhedral shape that is typical of  $UO_2$  grains. The rectangular particle below the  $UO_2$  grain was high in uranium content but also appeared to contain Zr. The presence of Zr indicates that this particle was created by a reaction between the fuel and cladding. A third uranium-rich particle that appeared to be partially covered by smaller particles was located near the center of this field of view. Figure 6 also shows the X-ray spectra of a large Zr-rich particle, a small particle of control material, and a glass fiber (Si). Additional SEM examination of this MUF-2A sample showed the commonness of particles that appear to be grains of fuel. Higher magnification (5000X) photographs of fuel grains (see Fig. 7) show that small particles (0.1 to 0.5  $\mu m$ ) have been deposited on the fuel particles. This finding suggests that other materials appearing in the X-ray spectra of the fuel particles may also exist as small depositional particles rather than as a true two-phase material. These high-magnification photographs also show surface features that apparently are gas bubbles that have formed on the grain faces as a result of the temperature excursion in TMI-2.<sup>6</sup> Transient testing of

\*The higher atomic number materials appear light in shade and the low atomic number materials dark in shade in the BSE image.

LWR fuel has shown that fission gas accumulates in bubbles on grain boundaries and that agglomeration of these bubbles is a primary mechanism of fission gas release.

A polished sample from the MUF-2A filter was given a cursory SEM examination. This examination indicated the presence of many more particles than were revealed through optical microscopy of the sample. No correlation could be made, however, between the optical image and the secondary electron (SE) image in order to find a specific particle location on the sample; therefore, a detailed examination was not performed.

### 5.3 MUF-4A

Examination of a piece of the MUF-4A filter revealed its similarity to the MUF-2A filter; however, no fibers containing silicon were present. The number of particles per unit area was lower than in either the MUF-5B or -2A filter samples. Grains of fuel were found in an abundance similar to that in the MUF-2A sample. The photographs in Figs. 8, 9, and 10 show typical grains of fuel that were found in the MUF-4A filter sample. The backscattered secondary electron (BSE) images in Figs. 8 and 9 show debris samples containing light-colored material of high atomic number that was identified as uranium. Figure 8 shows a whole  $UO_2$  grain (5 or 6  $\mu m$  across) and several smaller (0.1- to 0.5- $\mu m$ ) pieces of material with high contents of uranium. A  $UO_2$  grain with gas bubbles on its surface and a particle of high Zr content are visible in the centers and upper-right corners, respectively, of the photographs in Fig. 9. Three  $UO_2$  grains, a Zr-rich particle, and a sharply pointed Fe-rich particle are shown in Fig. 10. Figure 11 shows particles with unique shapes and high contents of Zr (a) and Fe (b). These photographs, taken at relatively high magnification, again show the presence of a large number of very small (0.1- to 0.5- $\mu m$ ) particles on the filter. It was

difficult to determine the exact composition of these small particles, but the BSE images indicate that elements of a wide range of atomic numbers are represented.

Two samples from the MUF-4A filter that were mounted and polished for examination by optical microscopy were also examined in some detail by SEM. Because there was only a small amount of material (particularly the bright phase) several specific shapes were easily identified in these samples. Three areas shown in 250X optical micrographs (Fig. 12A-C) were also examined at 250X with the SEM. Specific areas within these fields of view were then examined at higher magnifications so that the primary constituents of individual particles could be identified. The first of these areas, area A in Fig. 12, is a region in which optical microscopy allowed identification of four bright particles; however, SEM examination revealed that this area actually contains six or seven particles. Figure 13 shows SE images of area A at higher magnification (2500X). The principal constituents of these particles were determined from the X-ray spectrum of each particle. All of the particles except the bright particle near the center of the BSE image were composed mainly of Zr. The bright particle in the BSE image was mostly composed of uranium. Note that two of the Zr-rich particles and the U-rich particle were not apparent in the optical image.

Figure 14 shows the bright particle in Area B (of Fig. 12) at 2500X along with its X-ray spectrum which shows it to contain Cr, Ni, and Fe in ratios that identify this material as Inconel from the fuel bundle straps.

Figure 15 comprises high-magnification (2500X) SE, BSE, and X-ray images of area C. The X-ray images of this area show that all of the material that is present in great abundance in the core is also present in this region. The SE images reveal that although some of the Zr-rich particles

appear as bright material in the optical image, not all of the Zr-rich particles are visible in the optical image. The Fe-rich particle visible at the bottom of these photographs did not appear as a bright particle in the optical image and did not contain a significant amount of Cr. This particle appears to be composed of an iron oxide rather than stainless steel.

A second area photographed at 250X contained a large (40- $\mu\text{m}$ -long) bright particle and is shown in Fig. 16. Again, the SE image revealed many particles that were not apparent in the optical image. Higher-magnification (2500X) photographs show that the very large bright particle is stainless steel.

A third area that was examined with both optical microscopy and SEM is shown in Fig. 17, which provides optical, SE, BSE, and X-ray images (at 250X) of an extremely long (100- $\mu\text{m}$ ) stainless steel particle. Several of the bright particles in the optical image do not contain Fe, and therefore, are not stainless steel. The area near the top of the large stainless steel particle is shown at higher magnification (1000X) in Fig. 18. It was found that Zr is the primary constituent of many of the bright particles (in the optical image) in this area. The Zr-rich particle, located (in Fig. 17) just above the large stainless steel particle exhibits some polishing scratches that also indicate its metallic nature. The control material (Ag, Cd, In), the fuel cladding (Zr), the fuel (U), and the control rod cladding (SST) are all represented by particles in this area.

## 6. Discussion

Initial planning for the examination of material from these samples included examination of polished samples with an electron microprobe. The electron microprobe can more positively identify the elements Ag, Cd, In, and U by diffraction of the X-ray beam. However, the much better resolution of

the images that is produced by the SEM, as well as the qualitative separation of the elements by atomic number that is provided by the back-scattered secondary electron images, made examination with the SEM preferable to the electron microprobe. Evidence of disassociation of the components of the control material was not readily obtained from the SEM analysis; however, this deficiency was atoned for by the sharpness of imagery of comparable sample areas that was obtained with both optical microscopy and SEM.

Attempts to quantify the amount of the bright phase (metallic material) present in the polished samples were unsuccessful because of difficulties in defining a representative area. The large variation in the size of the particles also tended to make such an analysis difficult. The large particles were overdetected when the detection limit was set to include the small particles and the small particles went undetected when the large particles were properly detected. As mentioned earlier, it was very difficult to see some of the ceramic particles in the optical micrographs, so no comparison of the relative amounts of metallic and ceramic material could be made.

Examination of the optical and SEM results indicated that the particles could be grouped into three different size ranges; 0.1 to 0.5  $\mu\text{m}$ , 1 to 5  $\mu\text{m}$ , and 5 to 100  $\mu\text{m}$ . The particles that fell into largest size range were all metallic particles that appeared to be ductile shards. The similarity of shape between the large particles identified as stainless steel in the MUF-4A filter and the largest particles in the other two filters indicates that all of these large particles were stainless steel. Particles in the middle size range could be identified according to shape and reflectivity. The round metallic particles generally were the control materials Ag, Cd, and In. The rectangular metallic particles in the middle size range were generally Zr and the nonreflective particles were generally either fuel particles (U-rich

particles assumed to be  $UO_2$ ) or Zr-rich particles (assumed to be  $ZrO_2$ ). A few Fe-rich particles (assumed to be iron-oxide) also fit into this category. Although the composition of the small particles was not specifically determined, they appeared according to the BSE images, to contain the same elements as particles in the middle size range.

The energy dispersive X-ray analyses performed during this examination indicated that Zr, Ag, Cd, In, Fe, Cr, U and Ni were present as major constituents of particles trapped in the filter. Silicon was present in samples from the MUF-5B and MUF-2A filters as glass fibers from the filter itself. X-ray spectra of the individual fuel grains indicated that Ru or Rh was present in small quantities in the fuel. During examination of the small piece of the MUF-4A filter that was mounted on a sample stub, Mo was detected in a few fields of view. In each of these cases, no particle that was high in Mo content could be located, and X-ray images indicated no areas of high Mo concentration. Two Sn-rich particles were found in the polished sample (see Fig. 15). Other than the few exceptions above, the debris on the filter was found to be composed of elements that were major components of the materials present in the reactor core.

The major uncertainty in the examination was whether the examined samples were truly representative of the debris on the filters. The gamma-spectroscopy of the two samples from the MUF-2A indicates that variations in the type of sample taken may affect the results. If one assumes that the filter itself, particularly the cellulose in the filter, had been saturated with water containing dissolved cesium, then the data in Table III indicate that the sample of fines contained fewer particles than the sample of chunks. However, if one assumes that the samples of chunks are representative samples, then some additional inferences can be drawn from these data. The gamma

spectroscopy data indicate that the MUF-5B filter contained about twice as many particles as the MUF-2A and -4A filters, which is in general agreement with the results of the optical and SEM examinations. The quantity of particles per unit mass of the sample appears to be about the same for the MUF-2A and MUF-4A filters. Optical microscopy indicated that there was less material on the MUF-4A filter than on either of the other two filters. It may be that the quantity of particles by weight is similar for the 4A and 2A filters, but the particles on the 4A filter are generally smaller in size and, therefore, were not as apparent under examination by optical microscopy.

#### 7. Conclusions

An examination of materials from three filters of the makeup/letdown system of the TH1-2 reactor has shown that the debris is composed of particles of materials that were present in the core in great abundance. The materials included the fuel ( $UO_2$ ), the fuel rod cladding (Zr from the Zircaloy), the control material (Ag, Cd, In alloy), the control rod cladding (stainless steel), and fuel rod bundle straps (Inconel 715). Gamma spectroscopy has shown that fission products and activation products were present, but in relatively small quantities. The presence of Si in the fibers found in samples of the MUF-5B and -2A filters confirmed that these filters were reinforced with fiberglass. The size of the particles on the filters ranged from about 0.1 to 100  $\mu m$ . The largest particles generally appeared to be stainless steel. Some of the Zr-rich particles appeared to be in the form of  $ZrO_2$  and were difficult to see in the optical images. Many of the Zr-rich particles were bright in the optical images and appeared to be metallic in nature. Whole grains of fuel, some with gas bubbles on their faces, were

common in the samples of the MUF-2A and -4A filters. Optical microscopy indicated that there were fewer large metallic particles in the debris from the MUF-4A than in the debris from the other two filters.

8. Acknowledgments

The author would like to acknowledge the work of Chester Gebo and Joe Florek in performing the optical microscopy and the assistance of John Sanecki in the SEM examinations. The gamma spectroscopy was done by Bob Heinrich of the Chemical Technology Division.

**Table 1. Examinations or Analyses Performed on TH1-2  
Makeup/Latdown System Filter Debris at ANL-E**

<b>Filter</b>	<b>Examination description</b>
<b>MUF-5B</b>	Visual examination Gamma spectroscopy Optical microscopy of mounted samples SEM of small samples
<b>MUF-2A</b>	Visual examination Gamma spectroscopy Optical microscopy of mounted samples SEM of small samples SEM of mounted sample (limited)
<b>MUF-4A</b>	Visual examination Gamma spectroscopy Optical microscopy of mounted samples SEM of small samples SEM of mounted samples

Table II. Gamma Spectroscopy Data\* for Samples  
 from TMI-2 Makeup/Letdown System Filters  
 Activity,  $\mu\text{Ci/g}$

Sample	Wt., g	$^{137}\text{Cs}$	$^{125}\text{Sb}$	$^{134}\text{Cs}$	$^{144}\text{Ce}$	$^{106}\text{Ru}$	$^{60}\text{Co}$	$^{110}\text{Ag}$	$^{54}\text{Mn}$
MUF-2A Chunks	0.1870	5902	1503	426	371	380	140	9	4.7
MUF-2A Fines	0.1793	5025	776	367	194	203	77	5	2.8
MUF-5B Chunks	0.1984	3315	1678	231	486	411	234	13	7.2
MUF-5B Fines	0.1034	2718	1411	192	479	432	251	9	6.4
MUF-4A Chunks	0.4301	2723	545	195	194	186	86	7	3.5
MUF-4A Fines	0.1167	2578	463	185	198	192	84	6	3.7

\*Decay corrected to 4/1/83.

Table III. ~~Gamma~~ Spectroscopy Data Normalized to  $^{137}\text{Cs}$  Activity

Sample	$^{137}\text{Cs}$	$^{125}\text{Sb}$	$^{134}\text{Cs}$	$^{144}\text{Ce}$	$^{106}\text{Ru}$	$^{60}\text{Co}$	$^{110}\text{Ag}$	$^{54}\text{Mn}$
MUF-2A Chunks	1	.2547	.0722	.0629	.0644	.0237	.0015	.0008
MUF-2A Fines	1	.1544	.0730	.0386	.0404	.0153	.0010	.0006
MUF-5B Chunks	1	.5062	.0697	.1466	.1240	.0706	.0039	.0022
MUF-5B Fines	1	.5191	.0706	.1762	.1589	.0923	.0033	.0024
MUF-4A Chunks	1	.2001	.0716	.0712	.0683	.0316	.0026	.0013
MUF-4A Fines	1	.1796	.0718	.0768	.0745	.0326	.0023	.0014

Table IV. Elements Present in the Full-Field X-Ray Spectrum Shown in Figure 4

Element	Characteristic X-ray Energies, keV					
	$K_{\alpha_1}$	$K_{\alpha_2}$	$K_{\beta_1}$	$L_{\alpha_1}$	$L_{\alpha_2}$	$L_{\beta_1}$
Silicon	1.740	1.739	1.832			
Chromium	5.414	5.405	5.946			
Iron	6.403	6.390	7.057			
Nickel	7.477	7.460	8.264			
Zirconium				2.042	2.040	2.124
Silver				2.984	2.978	3.151
Cadmium				3.133	3.127	3.316
Indium				3.287	3.279	3.487
Uranium	3.171*	3.337*		13.613	13.438	

\* $M_{\alpha_1}$  and  $M_{\alpha_2}$  Lines.

**Results of X-ray Fluorescence Analysis of Debris  
from NUF-2A**

<b>Element</b>	<b>wt. %*</b>
<b>Ag</b>	<b>NA</b>
<b>Cr</b>	<b>0.3</b>
<b>Pb</b>	<b>1.1</b>
<b>Ni</b>	<b>0.9</b>
<b>Zr</b>	<b>5.5</b>
<b>Cd</b>	<b>3.5</b>
<b>In</b>	<b>4.9</b>
<b>U</b>	<b>2.8</b>

\*The relative error of the analyzed wt. % is  $\pm 10\%$ .

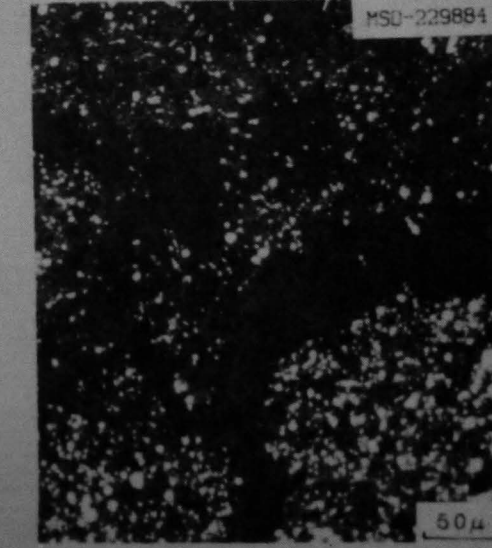
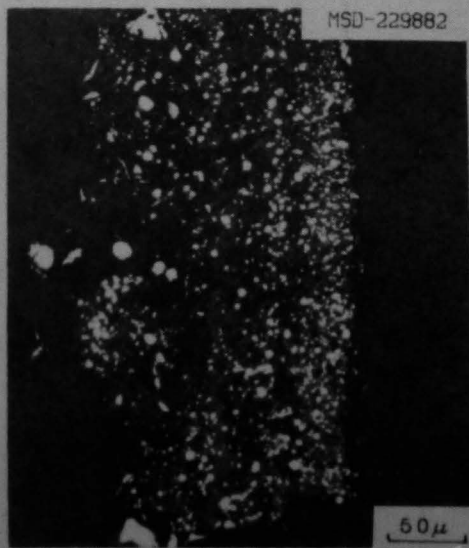
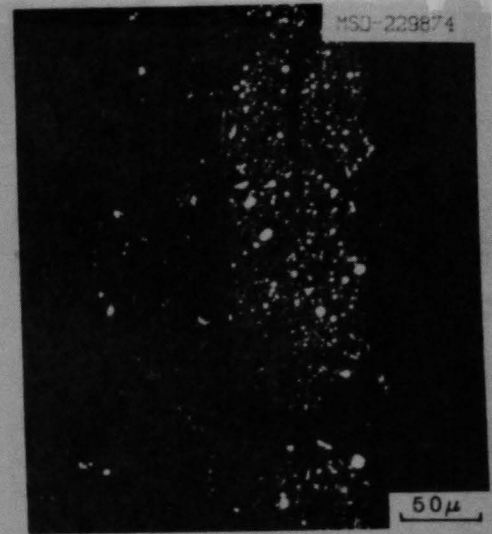


Fig. 1. Optical images of a sample of material from the MUF-5B filter that was mounted in epoxy and polished.

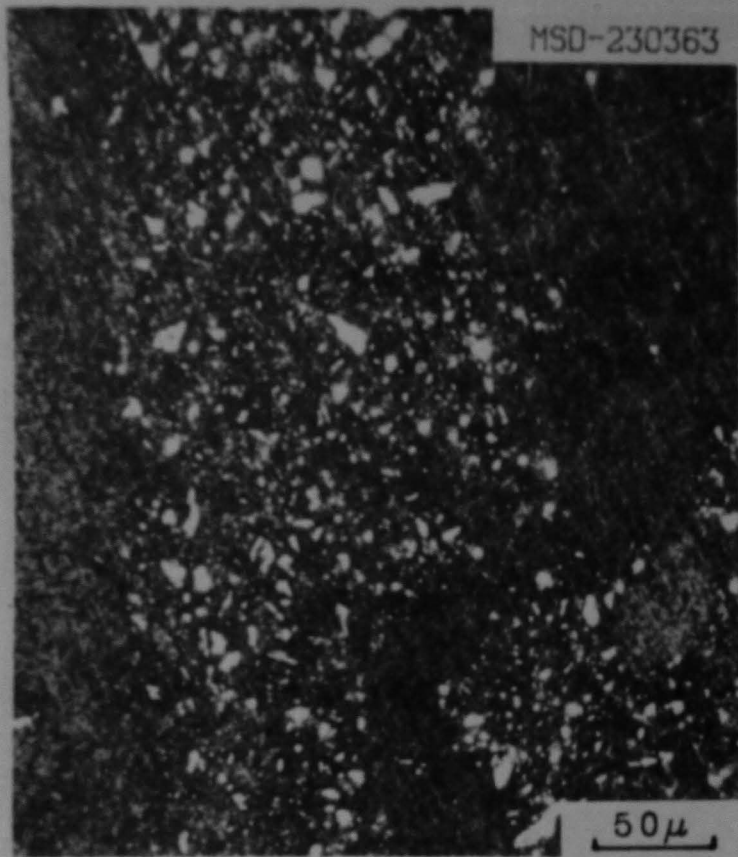


Fig. 2. Optical images of a sample of material from the MUF-2A filter that was mounted in epoxy and polished.



Fig. 3. Optical images of a sample of material from the MUF-4A filter that was mounted in epoxy and polished.

A-25

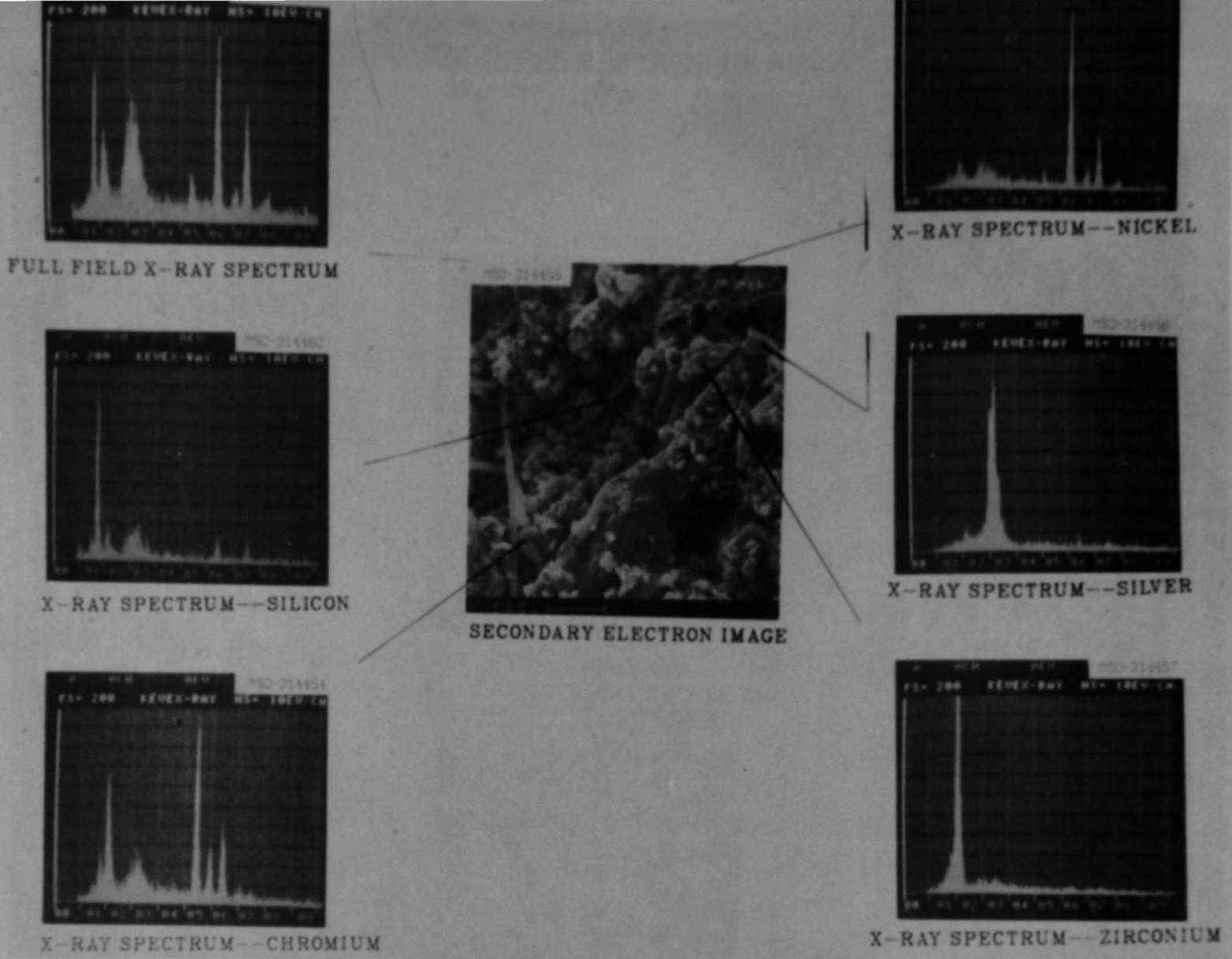


Fig. 4. Typical area of a piece of the MUF-5B filter with X-ray spectra of some of the particles.

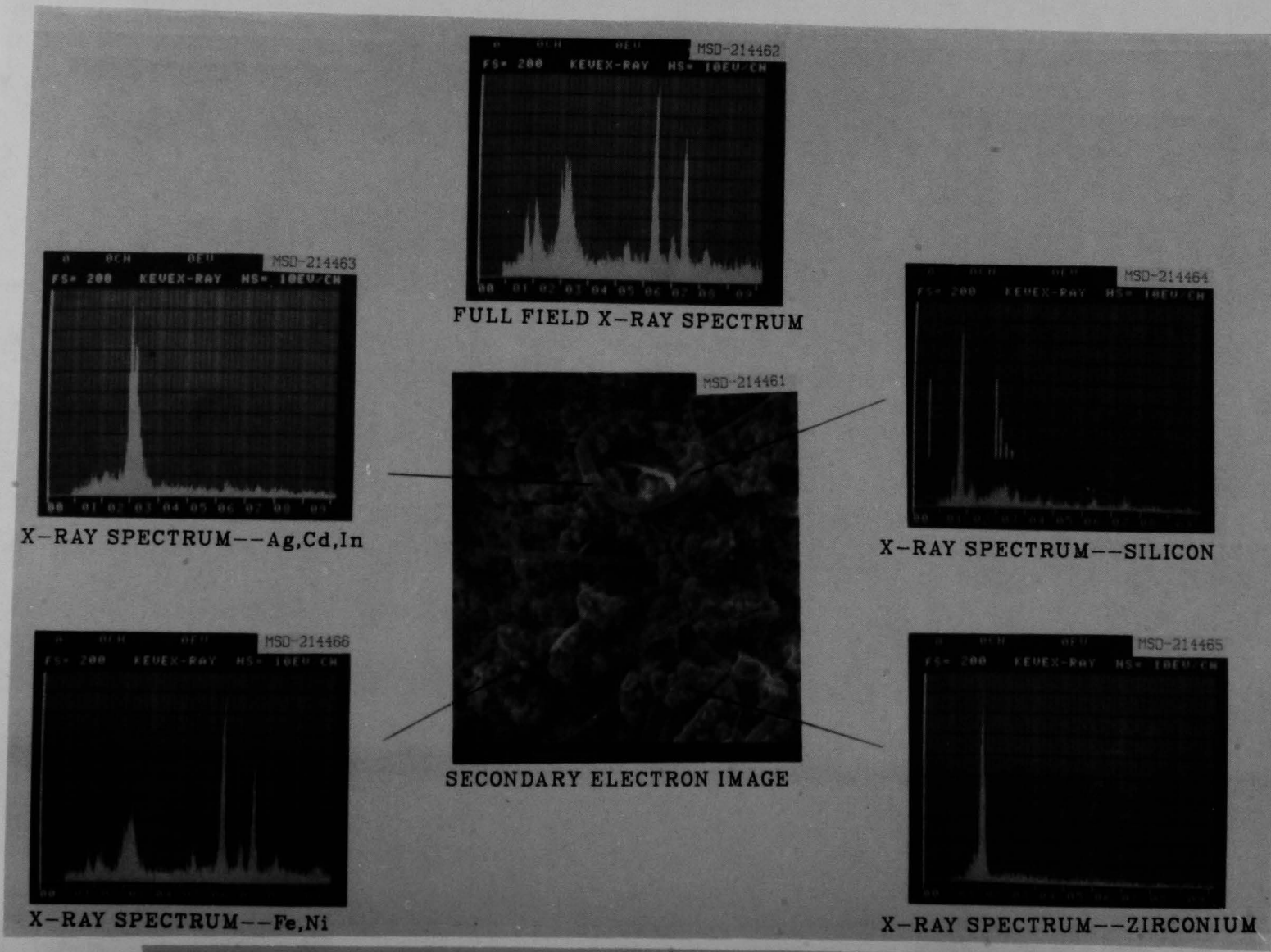


Fig. 5. A second typical area of a piece of the MUF-5B filter with X-ray spectra of some of the particles.

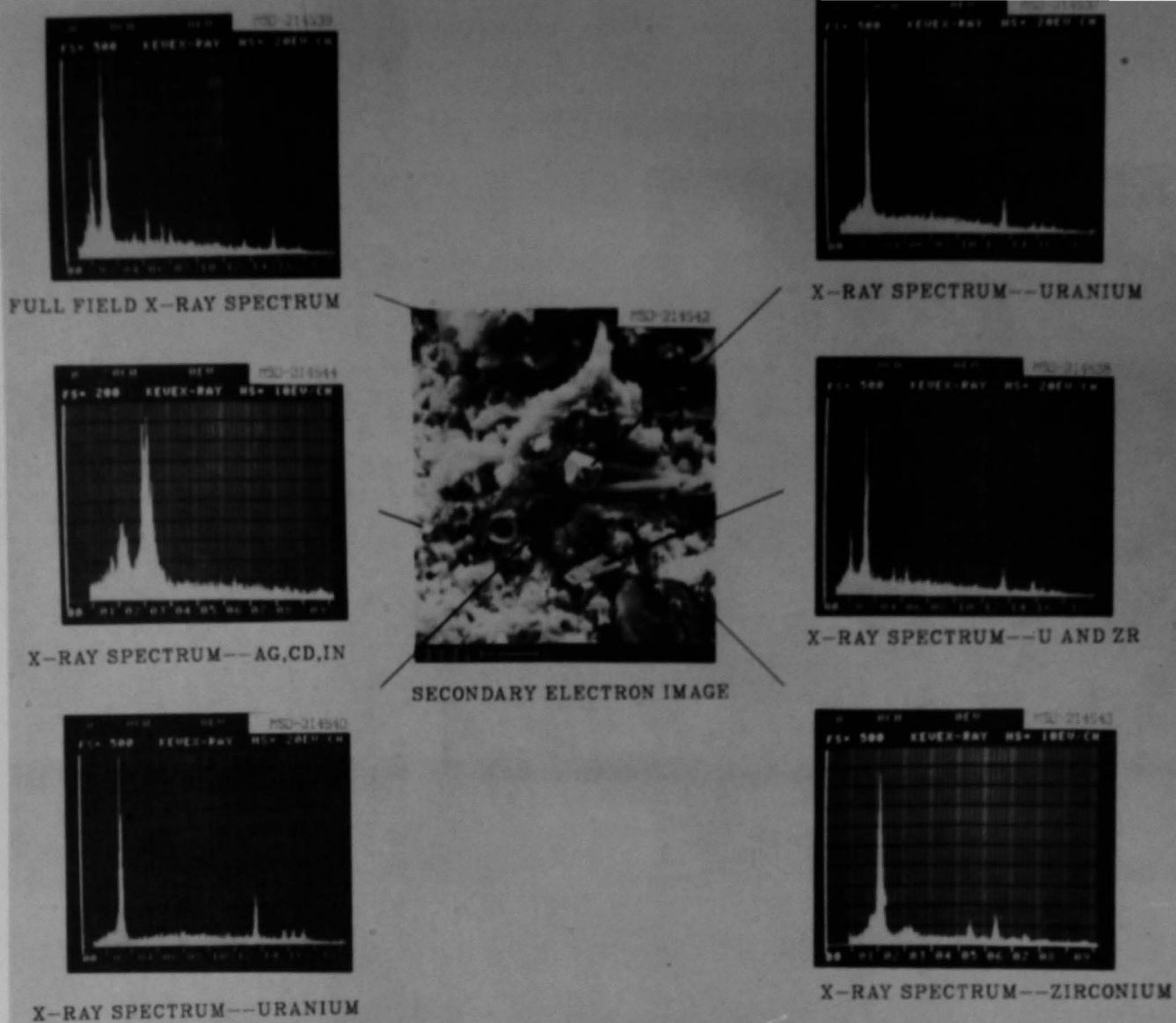


Fig. 6. Typical area of a piece of the MUF-2A filter with X-ray spectra of some of the particles.

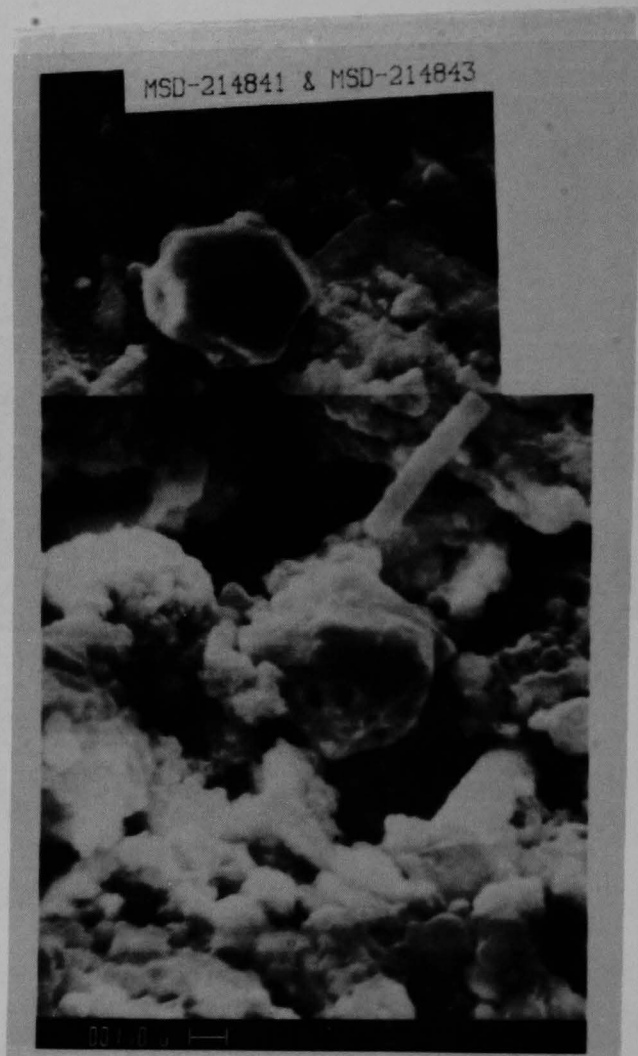
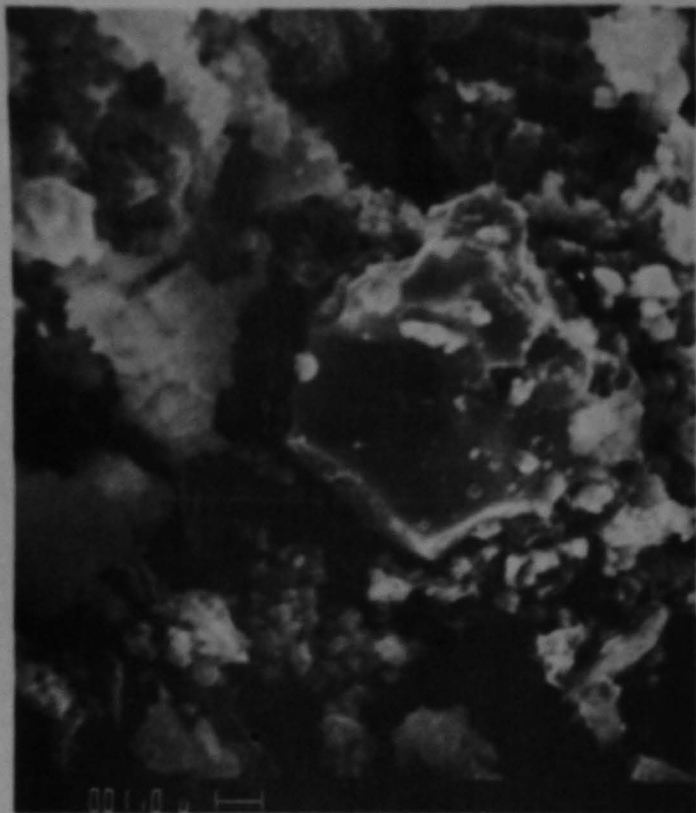


Fig. 7. Secondary electron image showing two fuel particles in a piece of the MUF-2A filter. Note the gas bubbles on the grain surfaces of the lower particle.

MSD-214872



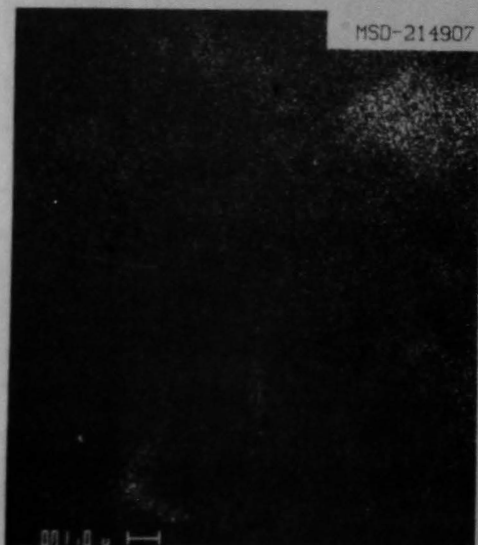
SECONDARY ELECTRON IMAGE

MSD-214874

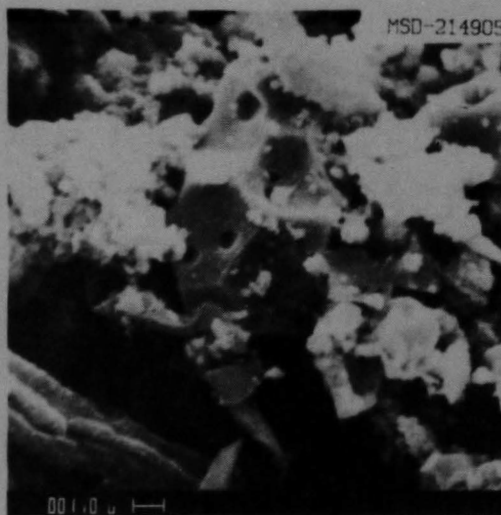


BACKSCATTERED S.E. IMAGE

Fig. 8.  $\text{UO}_2$  grain and small particles present in a piece of the MUF-4A filter.



ZIRCONIUM X-RAY IMAGE



SECONDARY ELECTRON IMAGE



BACKSCATTERED S.E. IMAGE



URANIUM X-RAY IMAGE

Fig. 9.  $\text{UO}_2$  grain with gas bubbles on its faces (center of photos) and particle with high Zr content (upper-right of photo) in a piece of the MUF-4A filter.

MSD-214891

MSD-214891



PARTICLES FUEL-ZIRCONIUM



ZIRCONIUM X-RAY IMAGE

MSD-214882

MSD-214880



IRON X-RAY IMAGE



URANIUM X-RAY IMAGE

g. 10. UO<sub>2</sub> grains, a particle high in Zr, and a pointed particle high in Fe from the MUF-4A filter.

MSD-214903



HIGH ZIRCONIUM PARTICLE

MSD-214915

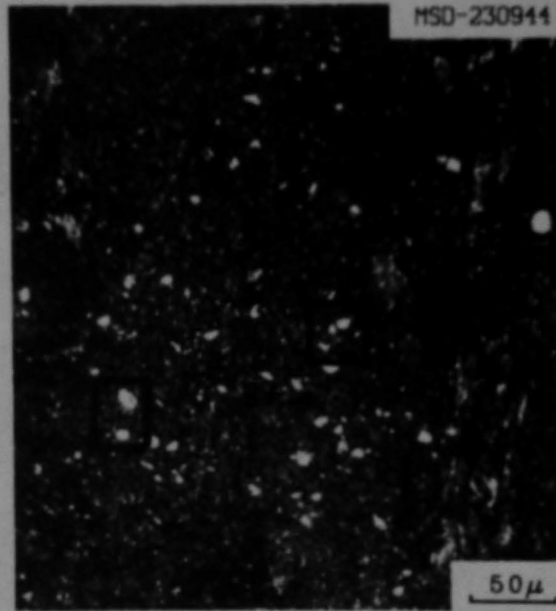


HIGH IRON ROD

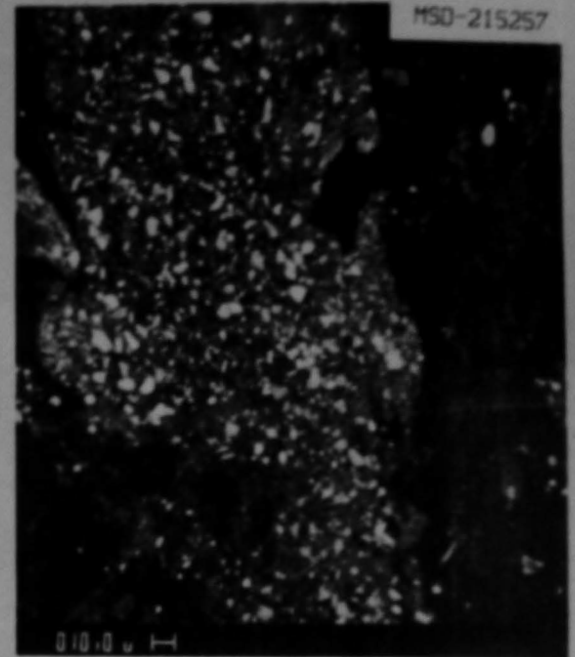
Fig. 11. Uniquely shaped Zr-rich and Fe-rich particles from the MUF-4A filter.



S.E. IMAGE



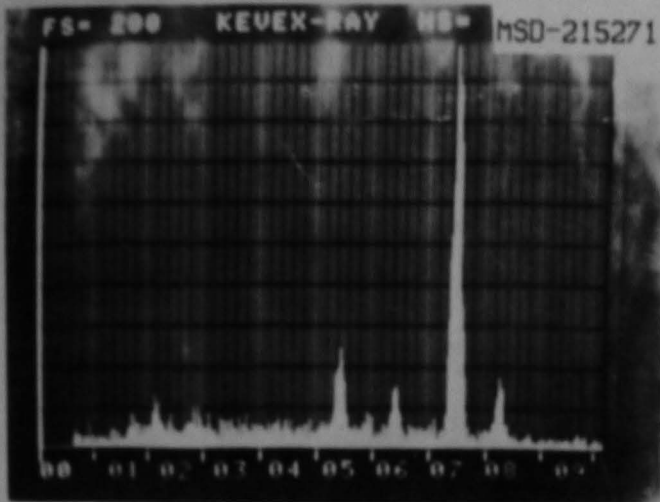
OPTICAL IMAGE



B.S.E. IMAGE

Fig. 12. Area of a polished sample from the MUF-4A filter at 250X.



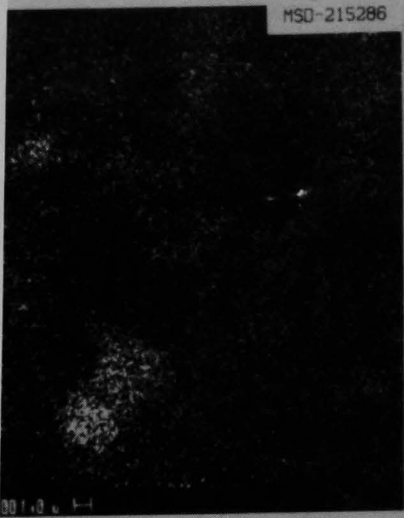


X-RAY SPECTRUM--Ni,Cr,Fe



S.E. IMAGE

Fig. 14. Inconel particle in Area B.



Sn X-RAY IMAGE



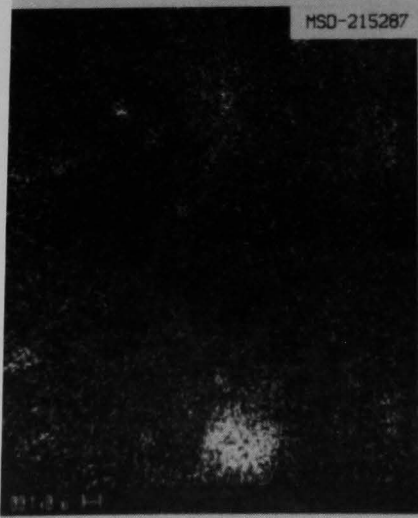
Zr X-RAY IMAGE



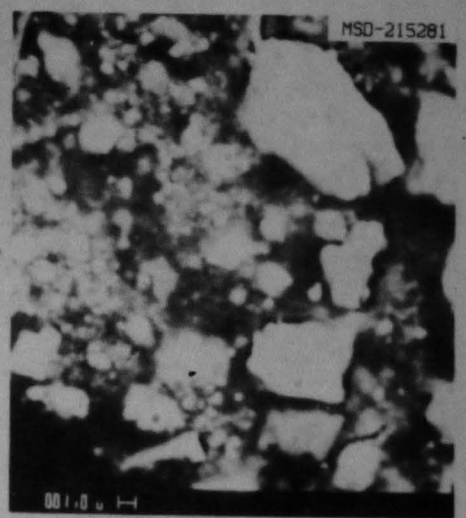
Ag X-RAY IMAGE



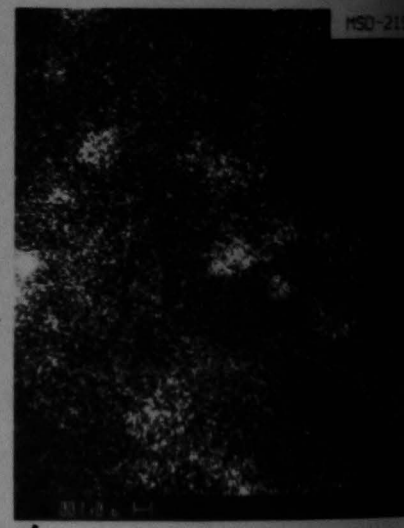
S.E. IMAGE



Fe X-RAY IMAGE



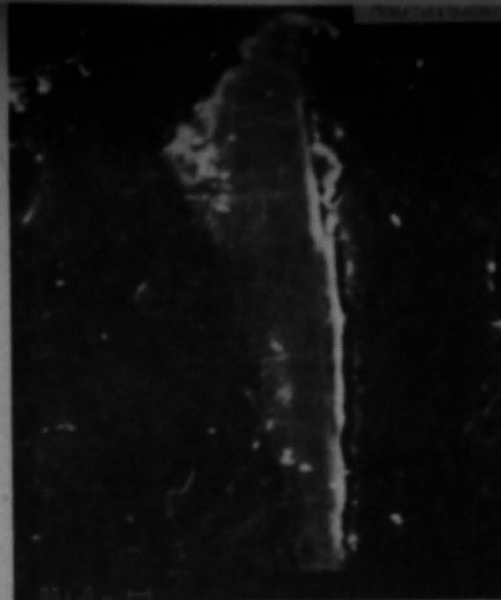
B.S.E. IMAGE



U,Cd X-RAY IMAGE



OPTICAL IMAGE



S.E. IMAGE



Cr X-RAY IMAGE



S.E. IMAGE



Zr X-RAY IMAGE



Fe X-RAY IMAGE

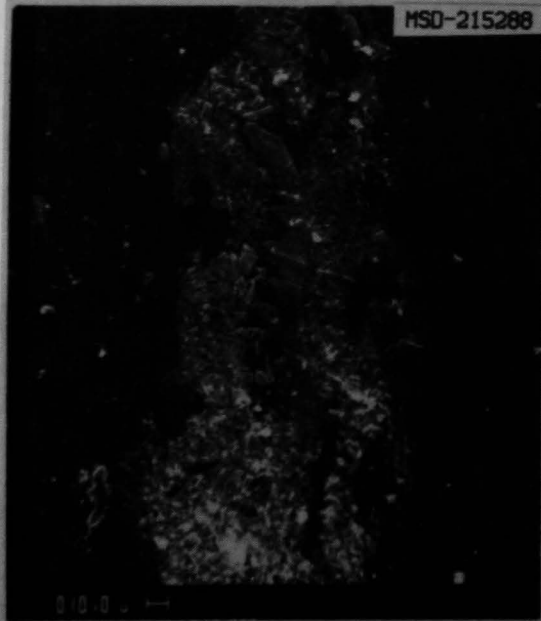
Fig. 16. Area of a polished sample from the MUF-4A filter showing a very large particle.



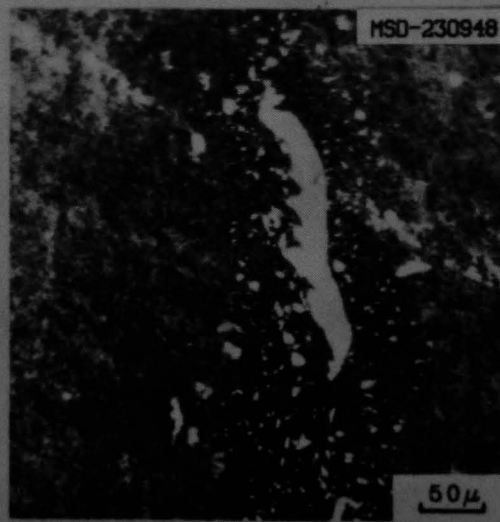
Zr X-RAY IMAGE



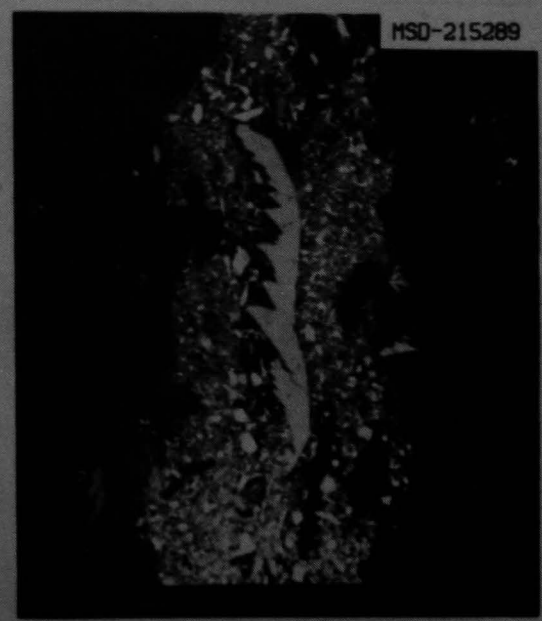
Fe X-RAY IMAGE



S.E. IMAGE

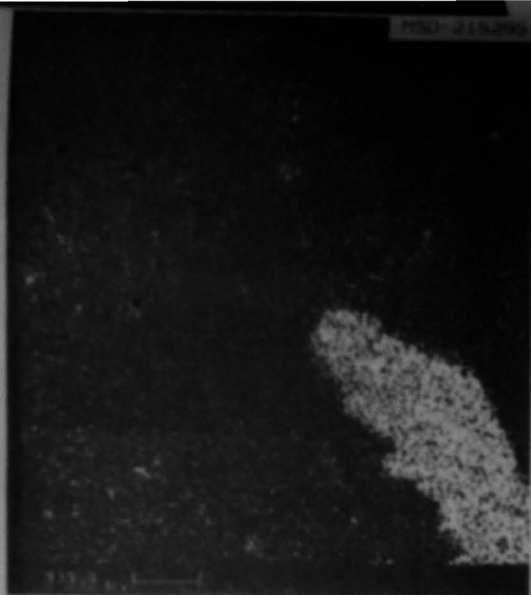


OPTICAL IMAGE

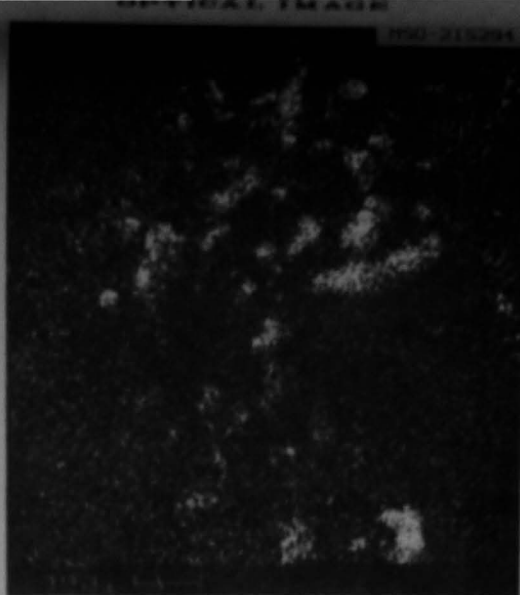


B.S.E. IMAGE

Fig. 17. A third area of the polished sample from the MUF-4A filter at 250X.



Fe X-RAY IMAGE



Zr X-RAY IMAGE



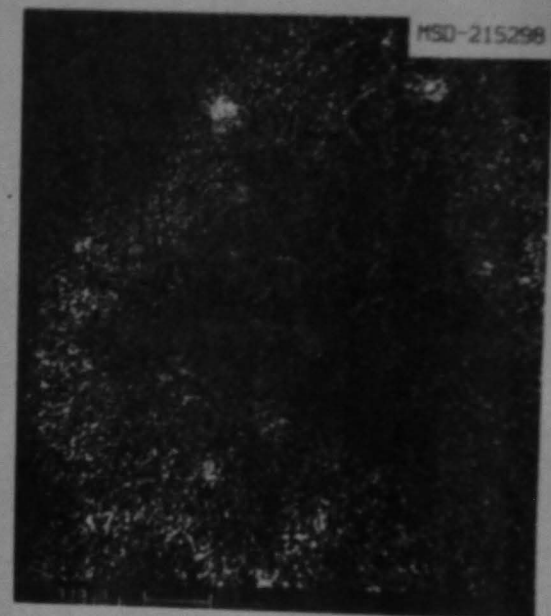
Ag X-RAY IMAGE



Cr X-RAY IMAGE



S.E. IMAGE



Cd,U X-RAY IMAGE

Fig. 18. Area near the top of the stainless steel particle shown in Fig. 17



APPENDIX B  
FINAL REPORT BY LOS ALAMOS NATIONAL LABORATORY

Author: J. J. ...  
Date: ...

Submitted to: ...

APPENDIX B

REPORT OF THE LABORATORY

TITLE FINAL REPORT ON THE ANALYSIS OF THREE MILE ISLAND CORE DEBRIS

AUTHOR(S): M. D. Stalnaker  
J. H. Cook

SUBMITTED TO EG&G, Idaho Falls, Idaho 83415

By acceptance of this article the publisher recognizes that the U.S. Government retains a nonexclusive royalty-free license to publish or reproduce the published form of this contribution or to allow others to do so for U.S. Government purposes.

The Los Alamos National Laboratory requests that the publisher identify this article as work performed under the auspices of the U.S. Department of Energy.

Los Alamos Los Alamos National Laboratory  
Los Alamos, New Mexico 87545

FINAL REPORT ON THE ANALYSIS OF  
THREE MILE ISLAND CORE DEBRIS

Analysis of MUF-2A, MUF-2B, and MUF-5B Filter Samples

by

N. D. Stalnaker, J. H. Cook, A. G. Nicol, D. S. Shaffer,  
J. D. Farr, J. N. Quintana, A. S. Murray  
O. R. Simi, D. L. Gallimore, W. B. Hutchinson, and J. M. Hansel

Los Alamos National Laboratory  
Los Alamos, New Mexico 87545

June 22, 1983

## SUMMARY

Core debris of the TMI-2 reactor, which was collected on the MUF-2A, MUF-2B and MUF-5B purification/makeup water system filters, was analyzed to determine some of its physical and chemical characteristics. This was done to assist in recovery from the accident and to provide knowledge of what events occurred during the accident and in what sequence.

The debris particle size was determined by image analysis. The mean diameter for particles  $> 0.9 \mu\text{m}$  was 1.5 to 1.9  $\mu\text{m}$ . The particles were generally either spherical or very irregular in shape.

The elements found in the samples of debris include those from all of the major core components; fuel, fuel cladding, control rod alloy, inconel and stainless steel. Many instances of separation of the elements from the parent alloy were found in the emission spectroscopy and electron microprobe analysis results. For example, the Ag, Cd and In of the control rod alloy separated to give particles with a wide variety of elemental concentrations. Also, the filter debris contained relatively high concentrations of tin which was released from the Zircaloy fuel cladding at some time in the accident.

The principal gamma emitting radionuclides in the debris were Cs-137, Cs-134, Sb-125, Ru-106/Rh-106, Ag-110m, Ce-144/Pr-144, Co-60 and Mn-54. The Cs-137 was the major gamma emitter at the time of the analysis comprising  $>49\%$  of the activity in all of the samples. The activities of Cs-137 correspond to a concentration range of 32 to 65 ppm. Cerium -144 activity was found to correlate with the uranium concentration in the debris.

Iodine -129 was determined by neutron activation analysis to have a minimum concentration of ~50 ppm in debris collected on the MUF-2A and MUF-2B filters.

Information on the sequence of events that took place in the reactor during the accident was looked for in stratification of materials in the debris collected on the filters using the electron microprobe. No evidence of stratification of materials was found. The materials were generally intimately mixed in the regions examined.

Analysis of individual debris particles by electron microprobe revealed a wide range of compositions. Several particles were found to contain U, Fe and Cr and other particles contained Zr, Cr and Fe. Some, but not a large number, of particles contained U, Fe, Cr and Zr. At present, it is not known if the formation of these materials with unusual compositions is limited to small particles. Pure uranium oxide and zirconium oxide particles were also abundant.

The uranium and plutonium isotopic analyses done by mass spectroscopy showed all three filters collected fuel of identical isotopic composition. The U-235 content was  $2.30 \pm 0.01$  weight percent of the uranium present.

The debris collected on the three separate filters was qualitatively the same in composition.

## I. INTRODUCTION

This report compiles all of the information obtained during the physical and chemical characterization of debris collected on

the TMI-2 purification/ makeup water system filters. The data reported in two previous reports to EG&G is repeated to provide a complete description in a single final report of the work done by the Los Alamos National Laboratory.

Materials from the MUF-5B, MUF-2A and MUF-2B filters were analyzed. The principal methods employed in the analysis of the debris include gamma scanning, particle sizing by image analysis, gamma ray spectroscopy, neutron activation analysis, electron microprobe analysis, mass spectroscopy, carbon analysis, and emission spectroscopy. Application of these methods and the end results are presented in this report.

## II. EXPERIMENTAL

This section describes the methods used in preparing the purification/ makeup water system filter samples for analysis by various methods. A large part of the work was done in hot cells.

The sample identification used in this report corresponds to the specimen description sent to Los Alamos National Laboratory with the samples.

### A. Loading of Samples for Gamma Scanning

Two sets of gamma scans were run on the filter debris. The first set of scans was run on the TMI-0104 sample and the second set of scans was run on seven samples of the MUF-2A, MUF-2B and MUF-5B debris.

TMI-0104 (~250 mg of homogenized debris) was received in on ~1-cm diameter by ~2-cm high plastic vial. To mount the vial for gamma scanning, the container vial was placed in a longer plastic snap-cap vial which was then placed in a stainless steel tube that was compatible with the gamma scanner mounts.

The seven samples from the MUF-2A, MUF-2B and MUF-5B filters were first placed in 15-mm o.d. x 58-mm long plastic vials with screw caps. These vials were then loaded into plastic screw cap bottles with dimensions of 32-mm o.d. x 91-mm long. The seven bottles were stacked in a ~1-m long aluminum tube which had an o.d. of 50.8 mm and i.d. of 47.6 mm. The caps of the plastic bottles were 44 mm in diameter, which limited the lateral movement of the samples within the tube to <5 mm. A brass spacer was placed on top of the seven bottles to hold them in place in the tube. Figure 1 diagrams the sample loading.

Some of the samples were too bulky for the gamma scanning containers to hold all of the material without crushing the intact pieces of filter. An estimated 10 to 20% of the MUF-2A, MUF-2B, and MUF-5B Grab samples were analyzed. The percentage of material analyzed for the other samples was estimated >80%.

#### B. Preparation of Samples for Electron Microprobe and Image Analyses

Two methods of sample preparation were used on the filter debris samples. The homogenized TMI-0104 sample was dispensed onto a metallographically mounted and polished piece of graphite. Dispersion of the powder with an insufflator was adopted after several unsuccessful attempts to disperse the material with solvents. A grab sample, visually estimated to be ~25 mg, was taken from the ~250 mg of homogenized debris and placed in a DeVilbiss-119 powder insufflator which had most of the sample reservoir filled with epoxy to reduce the volume to an appropriate size for the small sample. Graphite mounts were coated with a

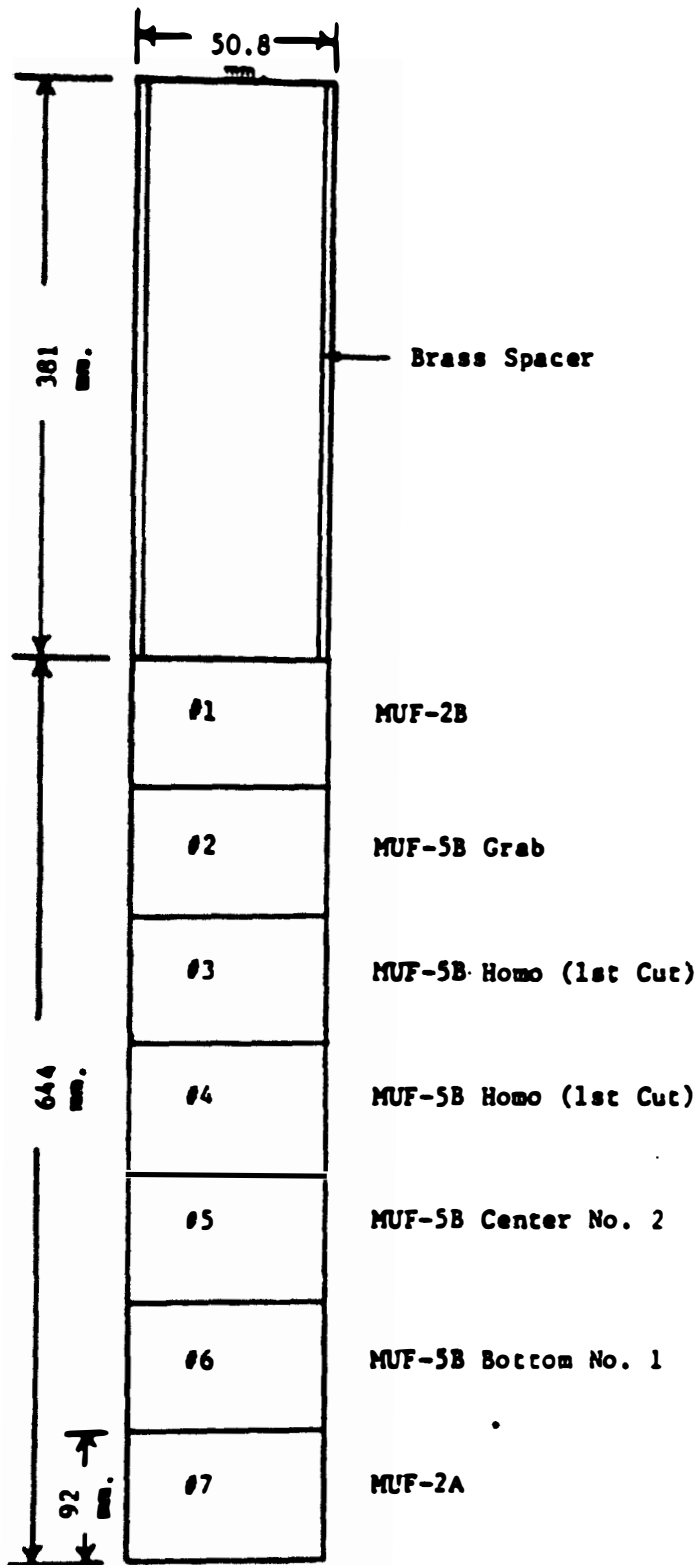


Fig. 1. Sample loading diagram for gamma scanning.

thin film of a solution of TEM replicating tape dissolved in xylene. After drying, the mounts were placed on the bottom of a 5-cm wide x 25-cm high x 30.5-cm long enclosure. All the mounts were placed near one end of the box. At the opposite end of the box, the outlet of the insufflator was placed in a small hole near the top of the box. Sample material was dispersed from the insufflator into the box. The cloud of powder settled to the bottom of the box and onto the mounts.

For the filter samples, MUF-5B Grab, MUF-5B Top No. 3, MUF-2A, and MUF-2B, the sample was examined and portions of filter that had remained intact were selected from several samples. The selected pieces were then sectioned perpendicular to the vertical line at two points with a razor blade (see Fig. 2). The sections were mounted with epoxy cement in metallographic molds in such a way as to expose the cut surfaces. The samples were vacuum potted in Epon-815 with 1 to 10 diethylenetriamine hardener and then pressurized to 2000 psi with  $N_2$ . After curing, the samples were ground with 180 to 600 mesh silicon carbide paper using kerosene as a coolant. Polishing of the ground samples was done with a 3- $\mu$ m Texmet mat using ethylene glycol coolant. The MUF-5B Homo sample powder was handled the same way as the filter pieces except for sectioning.

For electron microprobe work the samples were vacuum carbon coated to provide electrical conductivity which is necessary for electron beam stability. A metallographically mounted and polished sample is shown in Fig. 3 .



Fig. 2. MUF-2B filter sectioned for metallographic mounting.



Fig. 3. Metallographically mounted section of MUF-2B filter ready for examination.

### C. Division of Homogenized Filter Debris Samples Using a Spinning Riffler

Division of the homogenized filter debris samples into fractions that were of appropriate mass for analysis was done using a spinning riffler. A spinning riffler was chosen because it satisfied the two principal requirements for sampling powders, i.e. sample a moving stream and sample frequently for short intervals to obtain a composite sample (1).

Using the spinning riffler, the ~225 mg of sample TMI-0104 was divided into ten fractions.

The division of the 13.5 g of MUF-5B homogenized sample was done using the same spinning riffler. The sample was divided first into 10 parts (first cut); one of the 10 parts was selected at random and further subdivided into 10 parts (second cuts). The initial division proved difficult because of sample clumping and required enlargement of the sample holder tip. The exact number of revolutions during the first division were not counted. The second cut required 52 revolutions for distribution of the entire cut. A cut of the second cuts was divided to give ten third cuts. Less than 10 revolutions of the spinning riffler were required to dispense all of the material into the ten vials.

### D. Dissolution of Filter Debris Samples for Radiochemical and Mass Spectroscopy Analysis

Two dissolution procedures were used to prepare the filter debris samples for analysis. Three of the 10 sample cuts of sample TMI-0104 were dissolved in concentrated HCl using the

sealed-tube dissolution method described in Ref. 2. After dissolution, examination of the sealed tubes showed only pieces of filter paper and crystals of silver chloride. After transfer of each solution to 100-mL volumetric flasks some very small black particles could be seen. These may be carbon contamination from the dissolution procedure. The amount of black material in each flask was estimated to be less than a tenth of a milligram.

One sample from each of the MUF-2A, MUF-2B, and MUF-5B Homo filters was dissolved in ~10 hours in a mixture of dilute  $\text{HNO}_3$  and  $\text{HCl}$  at temperatures between  $65^\circ\text{C}$  and  $95^\circ\text{C}$ . As the solution evaporated more acid was added. A couple of drops of concentrated  $\text{HF}$  was added to the samples initially. The solutions were filtered through  $0.45\text{-}\mu\text{m}$  Millipore filters. The filter and collected material was fused with  $\text{K}_2\text{S}_2\text{O}_7$  and the salt cake, was dissolved in dilute  $\text{HNO}_3$ , and was transferred to the flask holding the acid solution from the initial step.

#### E. Preparation of Samples for I-129 Analysis by Neutron Activation

To determine I-129 content by neutron activation analysis, samples of filter and debris from MUF-2A and MUF-2B were weighed and placed in a ~4-mm i.d. by 150-mm long quartz tubes which were sealed at one end. A plug of quartz wool was placed in the tube ~2 cm away from the sample at the sealed end of the tube. The end of the tube containing sample was heated for ~1 hr at temperatures estimated to be  $\sim 750^\circ\text{C}$ . The walls of the tubes were then heated with a driven Bunsen burner for a few minutes. The quartz wool now presumed to contain I from the samples, was removed from the tubes, sealed in clean quartz tubes of ~4-mm i.d. by 100-mm

long, and activated for 7 hr at a neutron flux of  $\sim 1.6 \times 10^{13}$  n/cm<sup>2</sup>/sec. Approximately 24 hr later the samples were counted with an appropriate standard using high-resolution gamma ray spectrometer system.

### III. RESULTS AND DISCUSSION

This section provides the results of all analyses, and discusses some of the observation.

#### A. Gamma Scanning

All of sample TMI-0104 was gamma scanned except for a small grab sample. The scan was done to determine if any gross inhomogeneities existed in the distribution of gamma emitting isotopes. A diametral and an axial gross gamma scan were taken using a 1.27 mm primary collimator with a 7.62 mm secondary collimator taking 0.051-mm steps.\* The results of the scans are shown in Figs. 4 and 5. No gross inhomogeneities are evident in the sample.

An axial multielement gamma scan of the sample was taken using a 1.27 mm primary collimator with a 7.62 mm secondary collimator taking 1.27 mm steps at 2 hours per increment. This scan provided the distributions of the gamma-emitting isotopes Cs-137, Co-60, Sb-125 and Cs-134. No unusual distribution of these isotopes were found.

---

\*The gamma scanning system is described in Ref. 3.

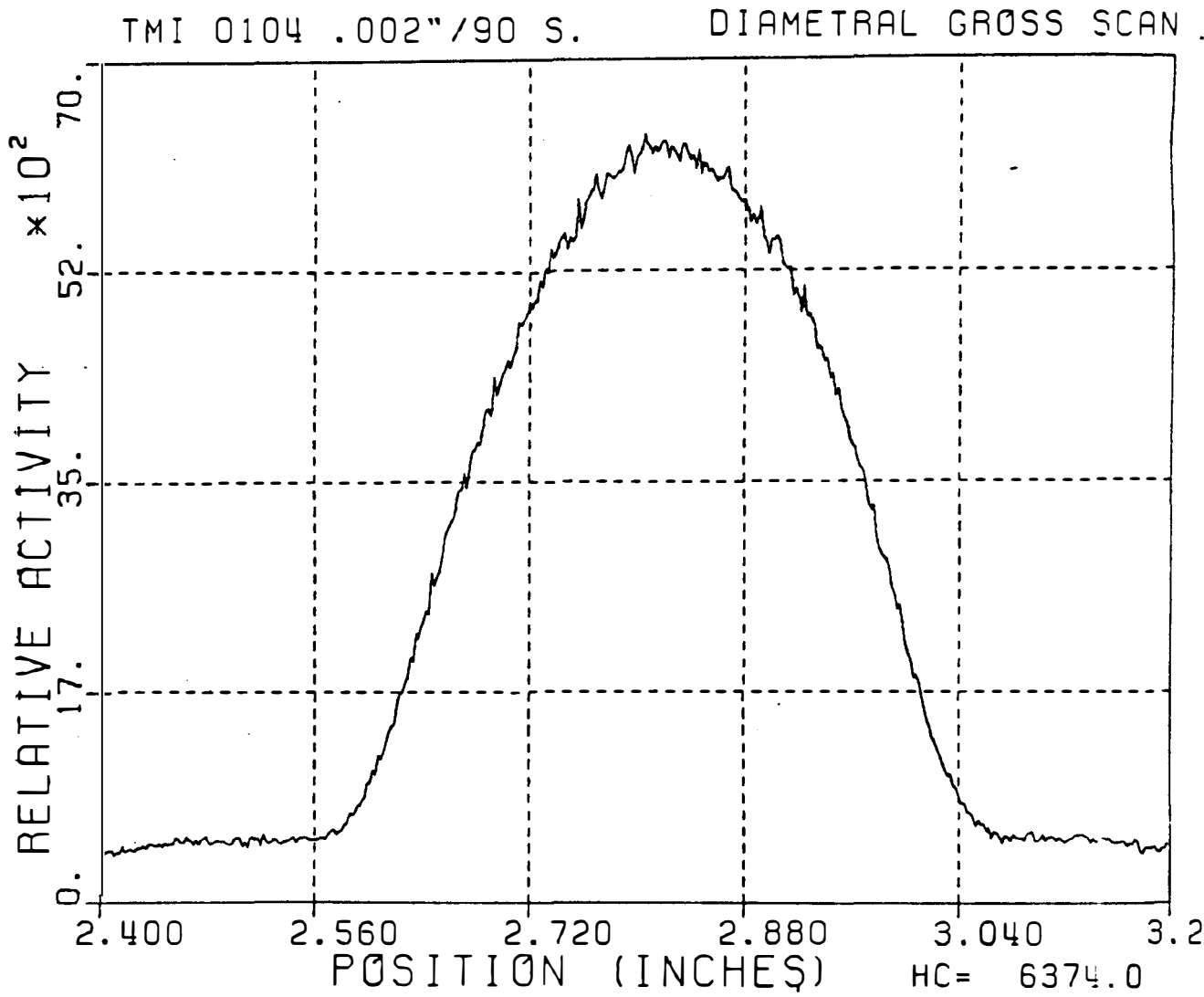


Fig. 4. Diametral gross gamma scan of sample TMI-0104.

TMI 0104 .002"/30 S.

AXIAL GROSS GAMMA SCAN

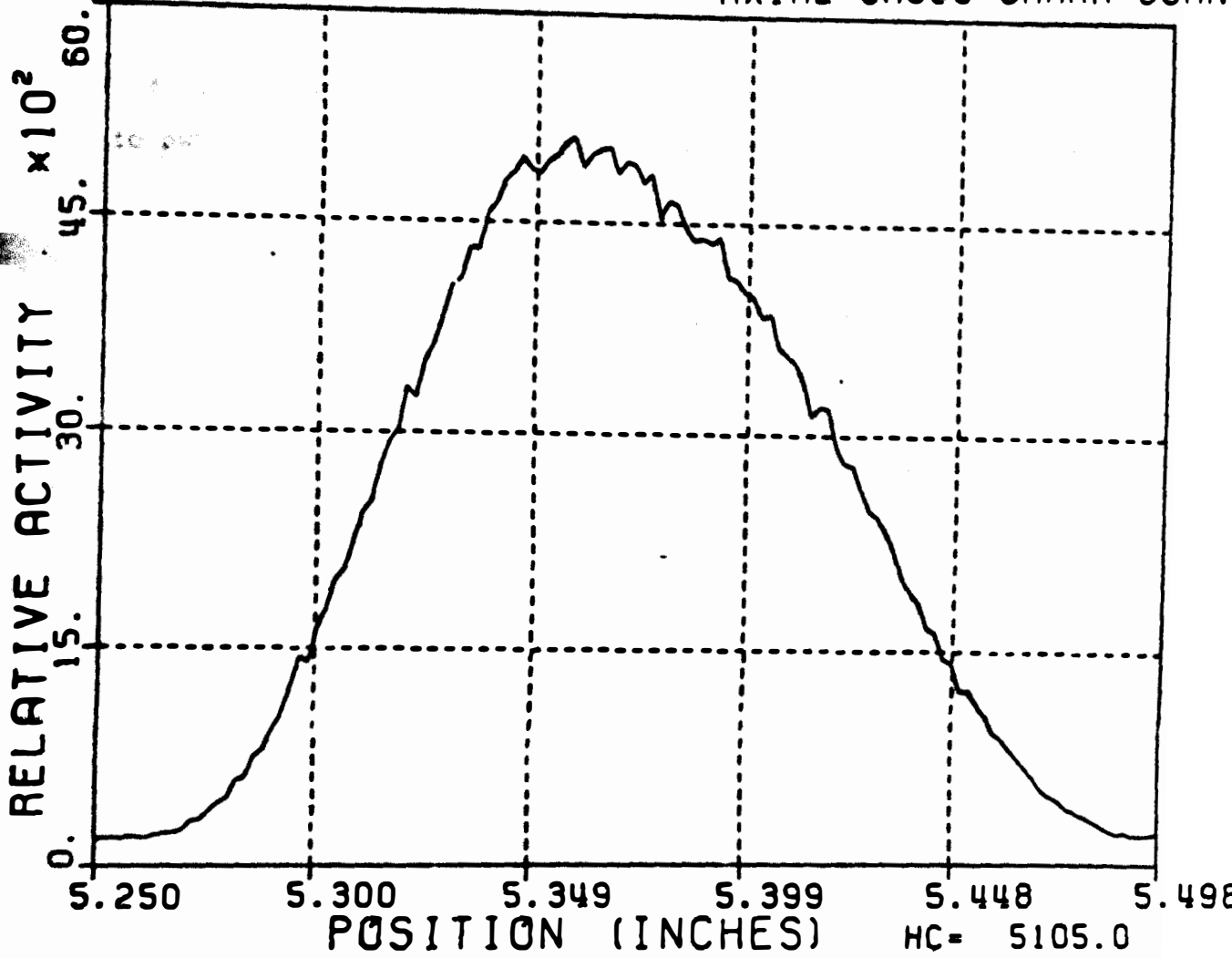


Fig. 5. Axial gross gamma scan of sample TMI-0104.

An isotopic gamma spectrum was taken for 30 minutes using a 15.340-mm primary collimator with a 7.620-mm secondary collimator. The gamma energy peaks that were identified and the isotope to which they are attributed are given in Table I. The uranium x-ray peaks were not evident in this small sample, but are present in other samples that were scanned.

Seven samples were gamma scanned in the second run. Five of the samples were sections of filter paper and debris. Two of the samples were first cuts from the divided MUF-5B Homo. sample. An initial axial gross gamma scan was taken in 0.254-mm steps at 1 second per step using a 15.340-mm high  $\times$  12.7-mm wide primary collimator with 7.620-mm high by 12.7-mm wide secondary collimator. Figure 6 is a plot of the sample activity versus the vertical position of the sample in the tube.

After locating the samples, a total of 21 gamma spectra were taken on the 7 samples, using the same collimators as described above. Table II gives the axial location of each spectra, the sample identification and the counting time for each sample. Figure 7 is a typical spectra collected in the analysis. The energy peaks identified in the spectra are the same as given in Table I. The  $K\alpha_1$ ,  $K\alpha_2$ , and  $K\beta_2$  x-ray peaks of uranium were present in most of the samples.

X-ray peaks for uranium were easily identified in all the spectra except that of the MUF-5B Center No.2 sample and the TMI-0104 sample. Both of these were relatively small samples. The x-rays of uranium are the result of beta particle excitation

TABLE I  
ENERGY PEAKS AND ASSOCIATED ISOTOPES IDENTIFIED  
IN TMI FILTER DEBRIS

<u>Energy (keV)</u>	<u>Radionuclide</u>
133.5 696.5	Ce - 144 + Pr - 144
176.3 208.1 380.4 427.9 463.4 600.6 <sup>a</sup> 606.7 <sup>a</sup> 635.9 671.4	Sb - 125
511.8 621.9	Ru - 106 + Rh - 106
563.3 569.4 604.7 <sup>a</sup> 795.8 801.9 1365.2	Cs - 134
661.6 <sup>b</sup>	Cs - 137
834.8	Mn - 54
657.7 <sup>b</sup> 884.7 937.5	Ag - 110m
1173.2 1332.5	Co - 60
94.6 (K $\alpha$ 2) <sup>c</sup> 98.4 (K $\alpha$ 1) <sup>c</sup> 111.3 (K $\beta$ 1) <sup>c</sup>	U

<sup>a</sup>The Sb-125 peaks at 600.6 keV and 606.7 keV are combined with the Cs-134 peak at 604.7 keV.

<sup>b</sup>The Ag-110m peak at 657.7 falls under the Cs-137 peak at 661.7 keV.

<sup>c</sup>These three peaks are uranium x-rays resulting from excitation of uranium by the radioactivity of the sample.

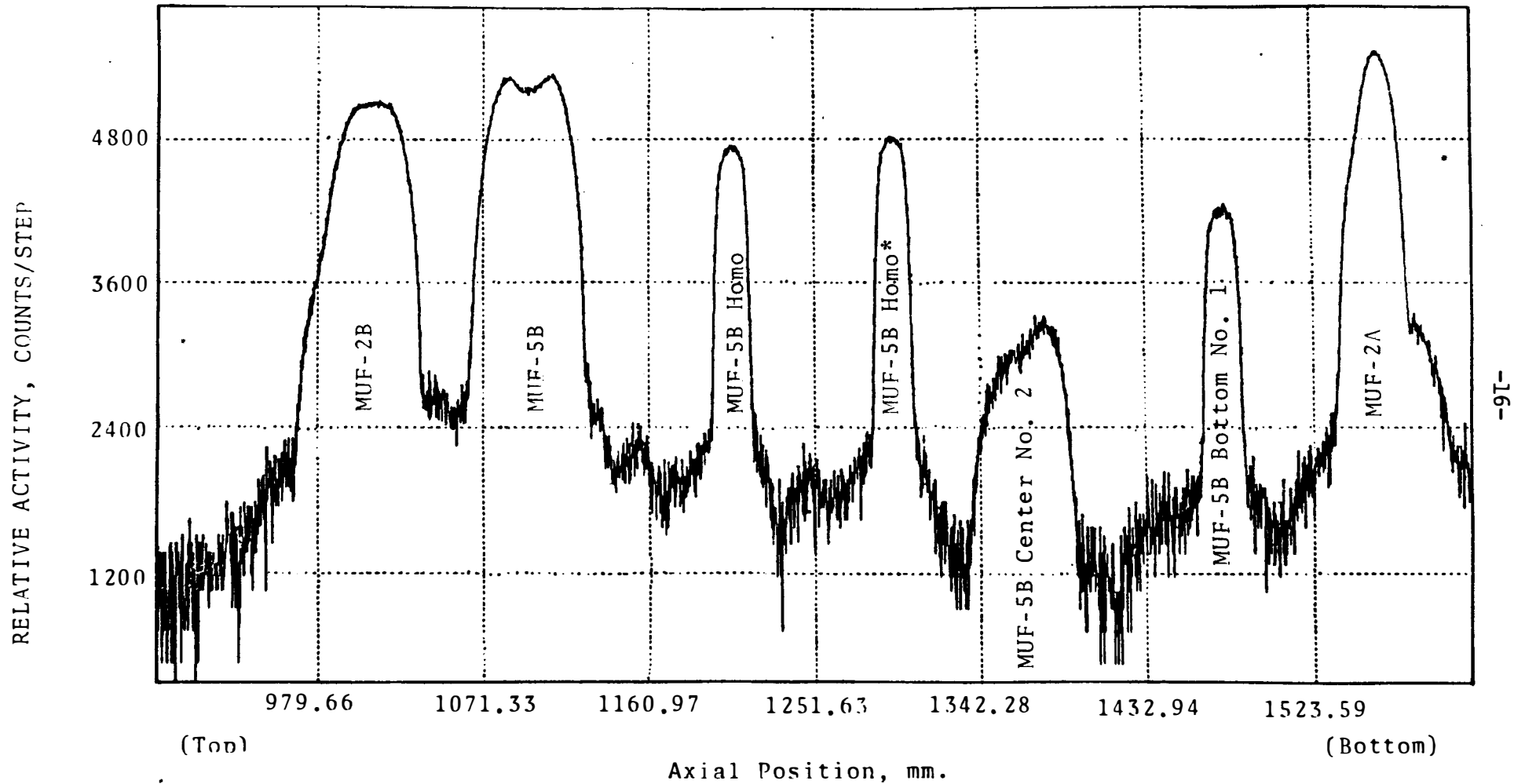


Fig. 6. Results of axial gross gamma scan of seven selected TMI filter debris samples.

TABLE II  
SAMPLE IDENTIFICATION, LOCATION, AND COUNTING TIME  
FOR THE GAMMA SPECTRA TAKEN ON THE SEVEN TMI DEBRIS SAMPLES

<u>Sample Identification</u>	<u>Axial Position-mm</u>	<u>Counting Time, s.</u>
01- TMI MUF-2B	982.98	900 s.
02- TMI MUF-2B	998.22	900 s.
03- TMI MUF-2B	1013.46	900 s.
04- TMI MUF-2B	1028.70	900 s.
05- TMI MUF-5B Grab	1075.69	900 s.
06- TMI MUF-5B Grab	1090.93	900 s.
07- TMI MUF-5B Grab	1106.17	900 s.
08- TMI MUF-5B Grab	1121.41	900 s.
09- TMI MUF-5B Homo(1) <sup>*</sup>	1203.96	900 s.
10- TMI MUF-5B Homo(1)	1219.20	900 s.
11- TMI MUF-5B Homo(2)	1293.37	900 s.
12- TMI MUF-5B Homo(2)	1308.61	900 s.
13- TMI MUF-5B Center(#2)	1350.01	1800 s.
14- TMI MUF-5B Center(#2)	1365.25	1800 s.
15- TMI MUF-5B Center(#2)	1380.49	1800 s.
16- TMI MUF-5B Center(#2)	1395.73	1800 s.
17- TMI MUF-5B Bottom(#1)	1476.76	900 s.
18- TMI MUF-5B Bottom(#1)	1492.00	900 s.
19- TMI MUF-2A	1551.94	900 s.
20- TMI MUF-2A	1567.18	900 s.
21- TMI MUF-2A	1582.42	900 s.

---

<sup>\*</sup>Two 1st cuts of the MUF-5B homo sample were counted.

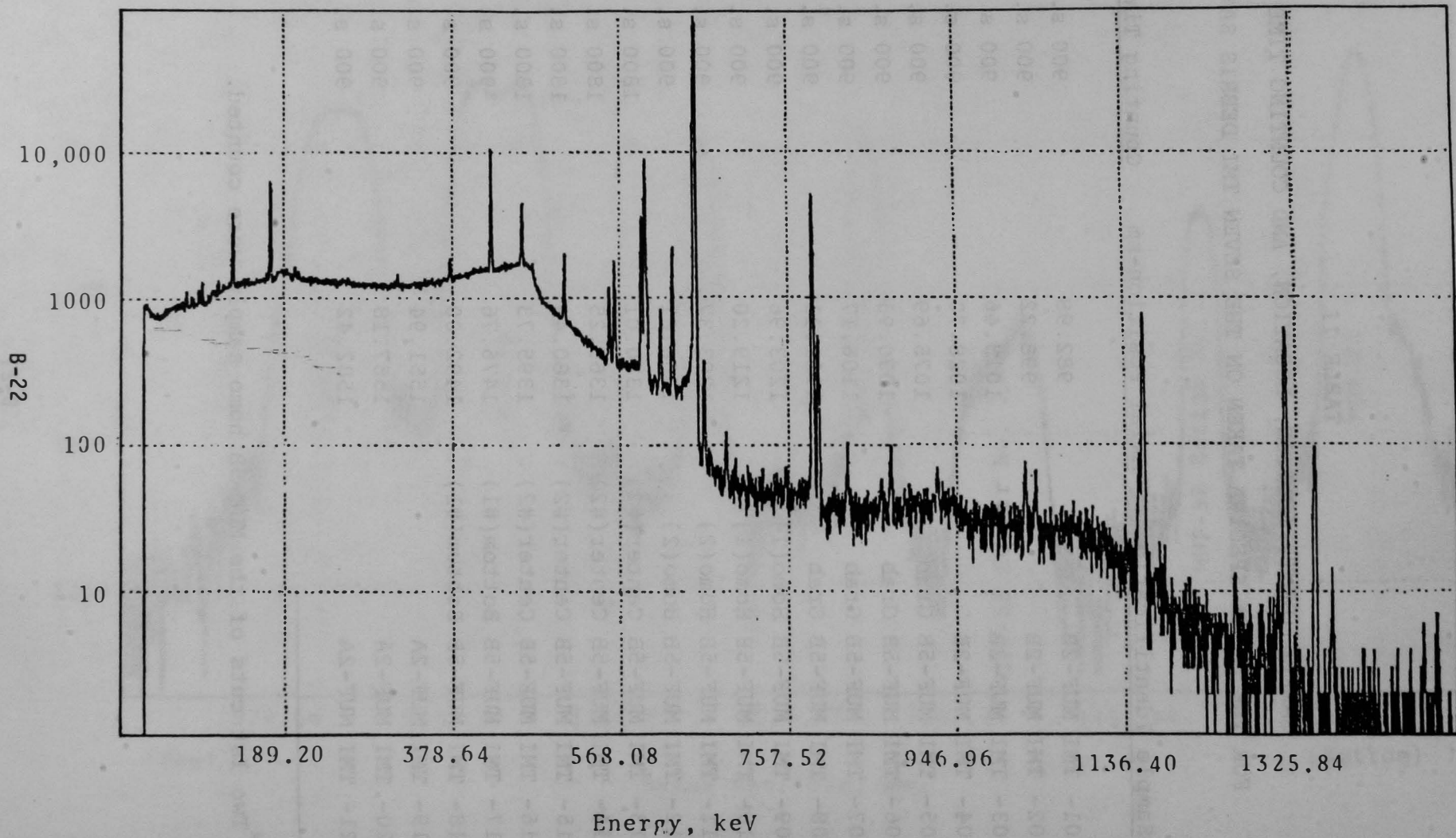


Fig. 7. Typical gamma spectrum obtained with the gamma scanning system. The sample is MUF-2B.

of the fuel present in the sample. This effect might be useful in getting semiquantitative data on the amount of fuel present in the debris.

None of the gamma scan spectra showed any unexpected radionuclides. Some differences were obvious in Cs-137 concentration between samples when compared with the other radionuclides; however, this is not unexpected since cesium is a water soluble element.

Since the detection efficiency of the gamma scanning system could not be readily established, only qualitative results have been obtained from the gamma scans. Quantitative distributions of the radionuclides is found in the Gamma Ray Spectroscopy section (III.C).

#### B. Particle Sizing by Image Analysis

Particle size analysis was done on MUF-5B Grab, MUF-5B Top No. 3, MUF-2A, MUF-2B, and TMI-0104. All particle sizing was done on metallographically mounted filter sections except the TMI-0104 sample which was dispensed with an insufflator as described in the Experimental section. Particle sizing was done with a Zeiss IM-35 metallograph coupled to a Hamamatzu image analyzer.

Particle size results are of limited value for the TMI-0104 sample since it was homogenized. The mean particle size for that material was 4.04  $\mu\text{m}$  with a standard deviation of 2.61  $\mu\text{m}$ . A total of 3645 particles were sized.

Table III gives the results of particle sizing on four other samples. Data collected by the image analyzer were evaluated using the Saltykov type procedure which takes into account the

TABLE III

## RESULTS OF COMPUTER ANALYSIS OF PARTICLE SIZING DATA

<u>Sample Identification</u>	<u>Number of Areas Sized<sup>1</sup></u>	<u>Total Number of Particles</u>	<u>Average Diameter, <math>\mu\text{m}</math></u>	<u>Geometric Mean Diameter, <math>\mu\text{m}</math></u>	<u>Estimated Number of Particles/cm<sup>3</sup> (<math>\times 10^{-6}</math>)</u>
MUF-5B Grab	6	1234	1.61 $\pm$ 1.22	1.21 $\pm$ 2.13	19.1
MUF-5B <sup>2</sup> Top No. 3	14	2092	1.55 $\pm$ 1.02	1.25 $\pm$ 1.93	5.2
MUF-5B <sup>2</sup> Top No. 3	10	935	1.50 $\pm$ 1.02	1.20 $\pm$ 1.97	4.1
MUF-2B	15	1329	1.86 $\pm$ 1.55	1.31 $\pm$ 2.30	2.8
MUF-2A	5	1005	1.48 $\pm$ 1.10	1.12 $\pm$ 2.11	10.5

<sup>1</sup>The size of each area was  $\sim 155 \mu\text{m}$  on a side.

<sup>2</sup>Two separate sizings were done on this filter section. Six regions with 14 areas make up one sample and a seventh region with 10 areas make up the second sample.

sectioning of particles and subsequent sizing at points other than the maximum or real diameter (4). Data analysis was done assuming a log-normal distribution.

Several regions of each filter section were examined. Figure 8 is an example showing the regions analyzed. In each region one or more 155- $\mu\text{m}$   $\times$  155  $\mu\text{m}$  areas were examined. Only particles  $>0.9$   $\mu\text{m}$  were sized. It is known that large numbers of particles less than 0.9  $\mu\text{m}$  exist in all the samples; however, the image analysis as used did not permit sizing of these particles. Results of a typical analysis are shown in Fig. 9. The histogram is the result of sizings from 15 areas with a total of 1329 particles in the MUF-2B sample.

The estimated number of particles per  $\text{cm}^3$  is based on a judgement of how much of an area under examination was actually debris and how much was empty space. Many of the areas were judged to be  $<50\%$  debris with only a few being judged 100%.

The difference between the particle size means is significant for the MUF-2B sample and the other samples as determined by following equation explained in Ref. 5:

$$t = \frac{|\bar{x}_1 - \bar{x}_2|}{\sqrt{\frac{S_1^2}{n_1} + \frac{S_2^2}{n_2}}}$$

where  $\bar{x}$  is the mean particle diameter

S is the standard deviation

n is the number of particles sized

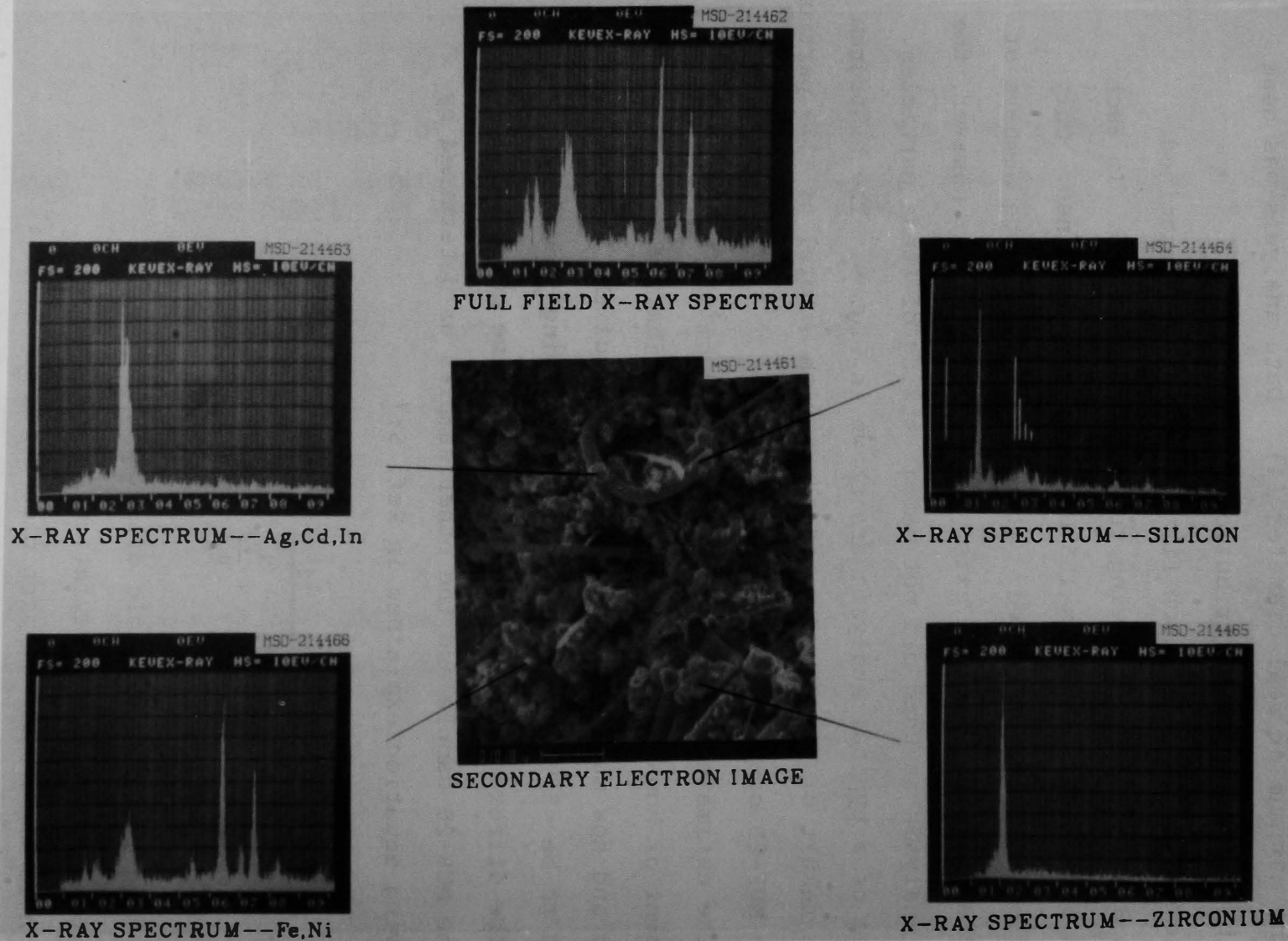


Fig. 5. A second typical area of a piece of the MUF-5B filter with X-ray spectra of some of the particles.

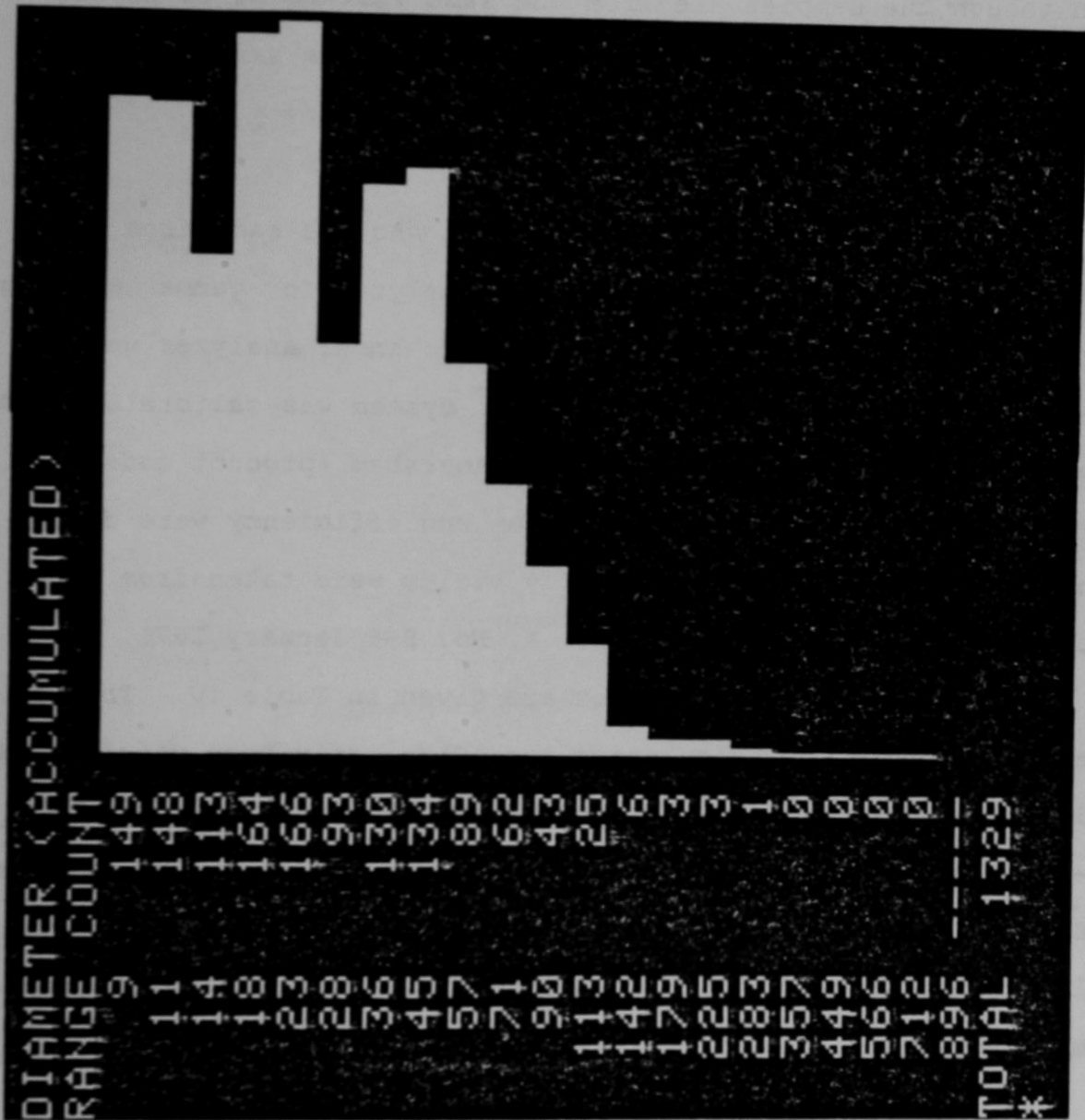


Fig. 9. Histogram of the particle sizing data collected on the MUF-5B sample. The range column gives the particle size interval multiplied by 10 so the first interval is 0.9 to 1.1  $\mu\text{m}$ . The count column gives the number of particles in the range.

For  $t > 2$  the difference between particle size means is considered significant. When the MUF-2B and MUF-5B Grab samples are compared, we find  $t = 4.6$ . A comparison between MUF-5B Grab and MUF-5B Top No. 3 gives  $t = 2.27$  which must also be considered significant even though the samples are from the same filter. This may be due to the location on the filter from which the samples were collected.

### C. Gamma Ray Spectroscopy Analyses

Three cuts from the TMI-0104 sample and one each from of MUF-2A, MUF-2B, and MUF-5B Homo. were analyzed for gamma emitting nuclides. A Ge(Li) detector and a multichannel analyzer were used to record the data. The analyzer system was calibrated with a mixed isotope standard prepared by Amersham (product code QCY.44). Both the energy calibration and efficiency were determined. For calculations, gamma-ray yields were taken from the Nuclear Data Tables, Vol. 8, Sec. A, No. 5-6 January 1971.

The results of the analyses are given in Table IV. The energy peaks used in calculating the  $\mu\text{Ci/g}$  activities were: Mn-54 (835 keV), Co-60 (1332 keV), Ru-106 (512 keV), Sb-125 (428 keV), Cs-134 (796 keV), Cs-137 (662 keV), Ce-144 (133 keV), and Ag-110m (885 keV). The Ag-110m results are not considered reliable values since significant precipitation of AgCl occurred in the sample solutions.

The Cs-137 activity constitutes >49% of the measured gamma activity for all samples as of March 25, 1983. The value will increase with time since Cs-137 is the longest lived isotope detected in these materials. The Cs-137 mass concentration, as

TABLE IV  
 GAMMA SPECTROSCOPY ANALYSIS OF  
 PURIFICATION/MAKEUP FILTER SYSTEM SAMPLES

<u>Radionuclide<sup>a</sup></u>	<u>Identification<sup>b</sup></u>	<u>Activity, <math>\mu</math> Ci/g<sup>c,d</sup></u>
MN-54 (312.5d)	MUF-2A	4.8
	MUF-2B	3.5
	MUF-5B Homo	6.3
	TMI-0104	6.5
Co-60 (5.27 y)	MUF-2A	145
	MUF-2B	111
	MUF-5B Homo	219
	TMI-0104	217
Ru-106 (368 d)	MUF-2A	388
	MUF-2B	280
	MUF-5B Homo	400
	TMI-0104	238
Sb-125 (2.73 y)	MUF-2A	1528
	MUF-2B	970
	MUF-5B Homo	1519
	TMI-0104	575
Cs-134 (2.06 y)	MUF-2A	310
	MUF-2B	367
	MUF-5B Homo	179
	TMI-0104	233
Cs-137 (30.2 y)	MUF-2A	4829
	MUF-2B	5641
	MUF-5B Homo	2808
	TMI-0104	3573
Ce-144 (284.4 d)	MUF-2A	420
	MUF-2B	287
	MUF-5B Homo	540
	TMI-0104	385
Ag-110 m (252 d)	MUF-2A	9.2
	MUF-2B	4.9
	MUF-5B Homo	10.1
	TMI-0104	4.9

<sup>a</sup>The values in parenthesis are the nuclide half-life values. The half-life values were taken from the "Chart of Nuclides" prepared by F. W. Walker, et al., 12th edition, April 1979.

TABLE IV (CONTINUED)

<sup>b</sup>The MUF-5B Homo and TMI-0104 were homogenized debris of the MUF-5B filter. Homogenization was done by EG&G and B&W, respectively.

<sup>c</sup>The specific activity values are for March 25, 1983.

<sup>d</sup>Silver chloride precipitated from the solution; consequently, the Ag-110 m results are not considered accurate.

determined from the activity, ranges from 65 ppm for sample MUF-2B to 32 ppm for MUF-5B Homo. While the cesium activity is highest in the MUF-2B sample, the other radionuclides have their highest concentration in other samples. This lack of correlation between cesium and other radionuclides may be due to association of the cesium primarily with the filter medium and not the core debris.

When the Ce-144 activity in the four samples is divided by the uranium concentration a good correlation between the values is found. The value is  $7.16 \pm 0.50$  m Ci/g. The uranium concentrations are taken from the mass spectrometrically determined value given in Table V except the TMI-0104 value which was taken from emission spectroscopy results of Babcock and Wilcox given in Ref. 6.

The Co-60 and Mn-54 activities in all samples correlate as expected indicating the materials are associated. The Co-60 activity divided by the corresponding Mn-54 activity for the four samples gives 32.52 with a standard deviation of 1.98. Correlation is found for the Sb-125 and Co-60 activities except for the TMI-0104 sample which is significantly different for reason unknown.

#### D. Mass Spectrometry Analyses

Solutions of MUF-2A, MUF-2B, and MUF-5B Homo\* were analyzed by isotope-dilution mass spectrometry for Pu and U contents using calibrated  $^{242}\text{Pu}$  and  $^{233}\text{U}$  spikes. To obtain a measured instead

---

\*These same solutions were analyzed by gamma ray spectroscopy.

of an estimated value for the  $^{242}\text{Pu}$  contents, the small amount of each of the three samples, which remained after the initial analyses, were combined to do an unspiked determination of the  $^{242}\text{Pu}$  content. This approach was considered valid since all of the samples have essentially the same isotopic composition. The results of the analyses are given in Table V.

The fuel collected on the three filters is consistent in isotopic abundances indicating a common source. The U-235 content of 2.30% by weight is in the middle of the enrichment range for the major portion of the core which is 1.98% to 2.64% (see Ref. 6).

#### E. Emission Spectroscopy Analyses

A sample of each of the MUF-2A, MUF-2B, MUF-5B Homo (3rd cut) and TMI-0104 samples was analyzed by emission spectroscopy. The results for elements present in amounts exceeding their detection limits are given in Table VI. Matrix effects and limited amount of sample that could be handled due to the  $\beta$ - $\gamma$  activity make the estimated error a factor of 2. Therefore, a reported value of 5% should be interpreted as a range of 2.5 to 10%.

The MUF-2A and MUF-2B samples were shipped to LANL in aluminum containers which may account for the particularly high Al value for MUF-2A sample; however, the Al may be from burnable poison shaping rods.

The tin concentration is high in all of the samples with value of 0.9 to 1.5%. The tin concentration in Zircaloy is <2%; consequently the tin has at least partially separated from the zirconium.

TABLE V

PLUTONIUM AND URANIUM MASS SPECTROSCOPY ANALYSES  
FROM MUF-2A, MUF-2B, AND MUF-5B HOMO

Isotopic Analyses

<u>Isotope</u>	<u>Concentration, wt%</u>		
	<u>MUF-2A</u>	<u>MUF-2B</u>	<u>MUF-5B Homo</u>
234 <sub>U</sub>	0.023	0.025	0.026
235 <sub>U</sub>	2.30	2.29	2.31
236 <sub>U</sub>	0.07	0.08	0.08
238 <sub>U</sub>	97.61	97.61	97.59
238 <sub>Pu</sub>	0.034	0.034	0.035
239 <sub>Pu</sub>	90.95	90.83	90.87
240 <sub>Pu</sub>	7.55	7.66	7.62
241 <sub>Pu</sub>	1.39	1.41	1.40
242 <sub>Pu</sub>	0.072	0.072	0.072

Analytical Results

<u>Element</u>	<u>Concentration, mg/g of Sample</u>		
	<u>MUF-2A</u>	<u>MUF-2B</u>	<u>MUF-5B Homo</u>
Uranium	54.1	43.8	76.5
Plutonium	0.118	0.101	0.174

TABLE VI  
 EMISSION SPECTROSCOPIC ANALYSIS OF MUF-2A  
 MUF-2B, MUF-5B HOMO AND TMI-0104

Elemental Composition, wt%<sup>a, b</sup>

<u>Element</u>	<u>MUF-2A</u>	<u>MUF-2B</u>	<u>MUF-5B Homo</u>	<u>TMI-0104</u>
Ag	4.2	3.0	3.0	4.8
Al	3.0	0.9	0.3	0.4
B	0.9	1.2	0.5	0.9
Ba	0.2	0.2	0.2	0.2
Ca	0.3	0.3	0.1	0.2
Cd	1.8	1.2	2.4	3.6
Co	0.02	<0.02	0.03	0.03
Cr	0.6	0.4	0.5	0.7
Cu	0.2	0.2	0.9	0.2
Fe	2.4	1.5	0.9	1.8
In	3.0	1.8	1.5	2.4
Mg	0.3	0.1	0.07	0.1
Mn	0.2	0.1	0.09	0.1
Mo	0.7	0.3	0.5	0.9
Nb	0.04	0.03	0.04	0.06
Ni	2.4	1.2	0.9	1.8
Si	0.9	0.9	0.4	0.9
Sn	1.5	1.2	0.9	1.2
Sr	0.09	0.09	0.04	0.03
Ti	0.07	0.03	0.06	0.09
Zr	9.0	7.2	4.8	6.0

<sup>a</sup>The values given are for the element not the oxide.

<sup>b</sup>The accuracy of these analyses is a factor of ~2. If an analysis is listed as 5% then the estimated range is 2.5 to 10%. This is due to the small amount of material that could be worked with and the matrix effects.

The cadmium-to-silver ratio found in the filter debris ranged from ~0.5 to 0.8, which is considerably higher than the 0.06 ratio in the control rod alloy. The cadmium and silver have separated as may have been expected since the cadmium is a volatile metal.

Copper is a third element that has apparently separated from its parent material, Inconel 718, since the copper-to-nickel ratio in the debris is much higher than that present in the parent material. The copper-to-nickel ratios in the debris range from 0.1 to 1 whereas the ratio is 0.003 in Inconel 718.

Manganese, which is a trace element in CF-3M grade stainless steel, is also present in significant concentrations.

The above five elements, (In, Cd, Cu, Sn, and Mn) all have melting points below 1356°K and the melting points are significantly below the melting of the principal elements of the parent alloy which may or may not account for the separations observed.

#### F. Electron Microprobe Analyses

Electron microprobes were used for elemental mapping of relatively large areas (generally ~400  $\mu\text{m}^2$ ) and for single particle analyses. The elemental mapping was used in an attempt to identify stratification of core debris on the filters and the analyses were run on metallographically mounted filter sections. One piece of filter from each the MUF-5B Grab, MUF-5B Top No. 3, and MUF-2B were mapped.

Figure 10 is a picture of the metallographically mounted MUF-5B Grab sample and Fig. 11 is a photomosaic of the region of the cut filter section examined showing the relative positions of

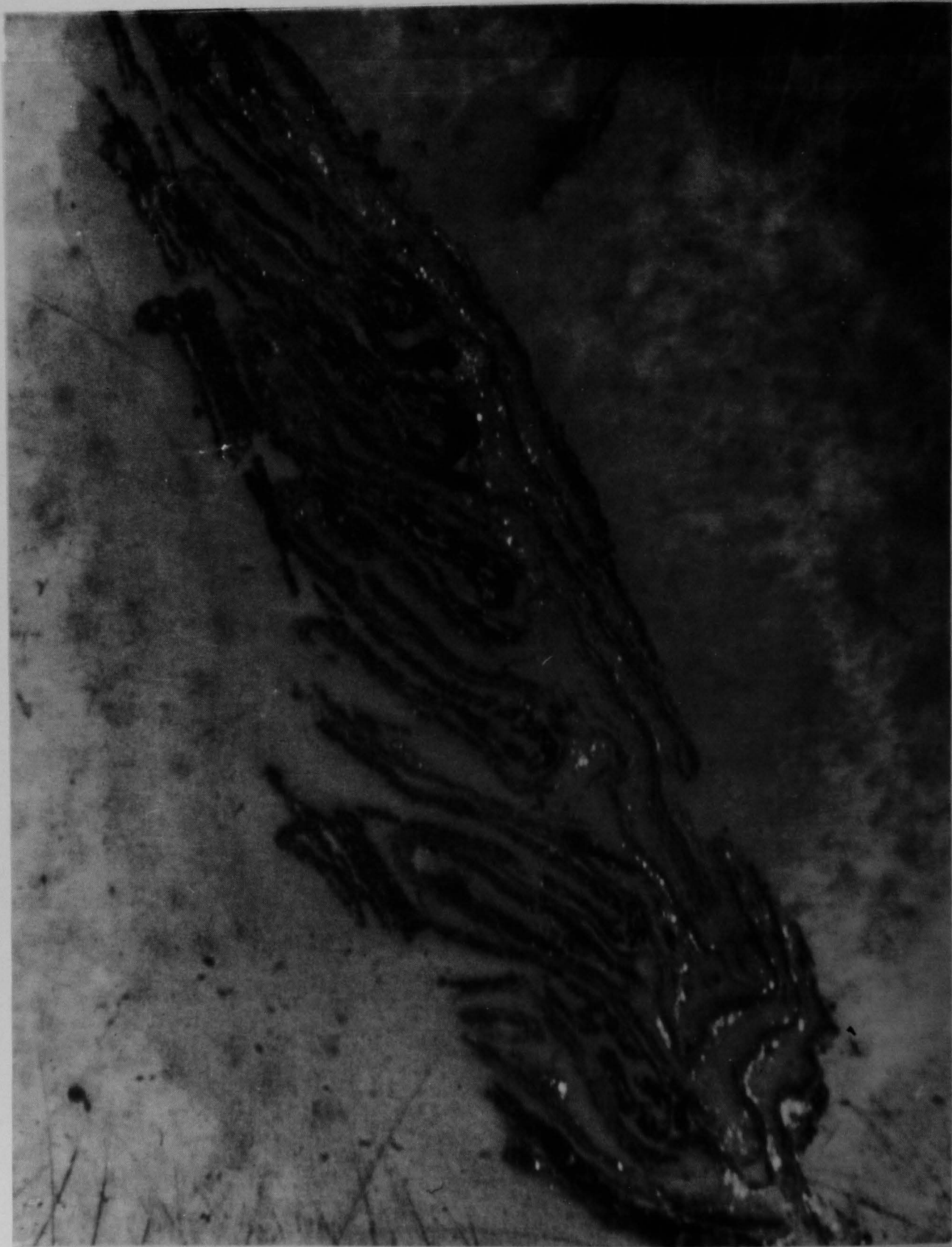


Fig. 10 Metallographic mount of the MUF-5B Grab sample.



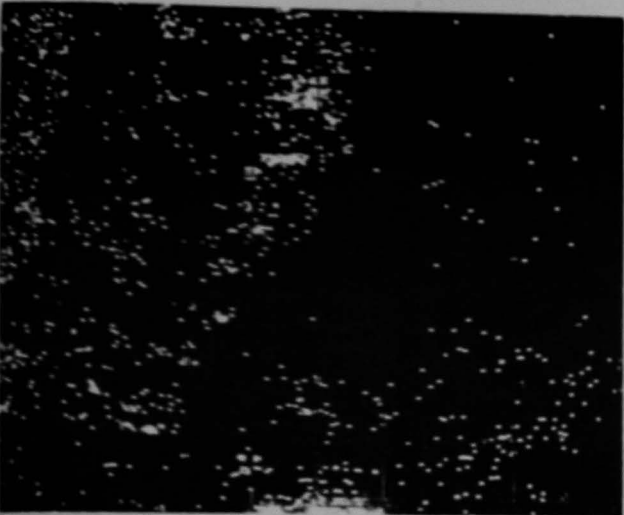
Fig. 11. Photomosaic of the surface of the MUF-5B-Grab sample. The areas examined are outlined. 32X.

the various areas examined by electron microprobe. Many areas were chosen so the layer of debris on the filter would be scanned across its entire width. Other areas were chosen because they visually appeared to be different. The x-ray dot maps of Area 3 in Fig. 11 are reproduced in Fig. 12 as an example of the type of information obtained.

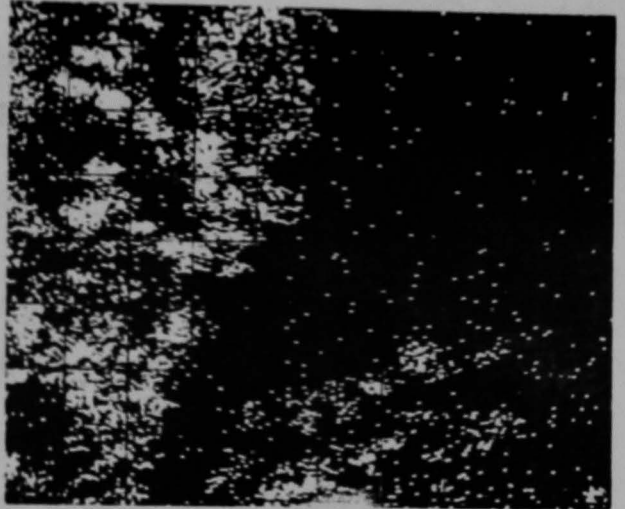
Several observations were made from the data collected on the MUF-5B Grab sample:

1. The elements U, Fe, Ni, Cr, Ag, Cd, In and Zr were found in all areas examined.
2. The control rod materials (Ag, Cd and In) generally showed similar distribution patterns; however the ratio of the relative concentrations varied a great deal. This indicates the control rod materials have segregated at some point in the accident.
3. The zirconium from the fuel cladding was widely dispersed in the areas examined; however, the zirconium was obviously not physically or chemically associated to any other element in large quantities. For example the distributions of uranium and zirconium did not match extensively in any of the areas. In one area large zirconium bearing particles (30-50  $\mu\text{m}$ ) were found surrounded by much smaller particles containing all the other major elements.
4. The stainless steel and inconel major elements of Fe, Ni and Cr had similar distribution patterns. The ratios of the relative concentrations varied from area

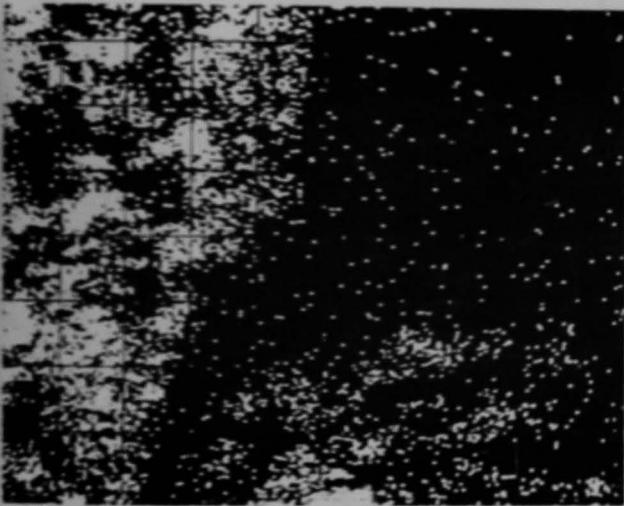
200X



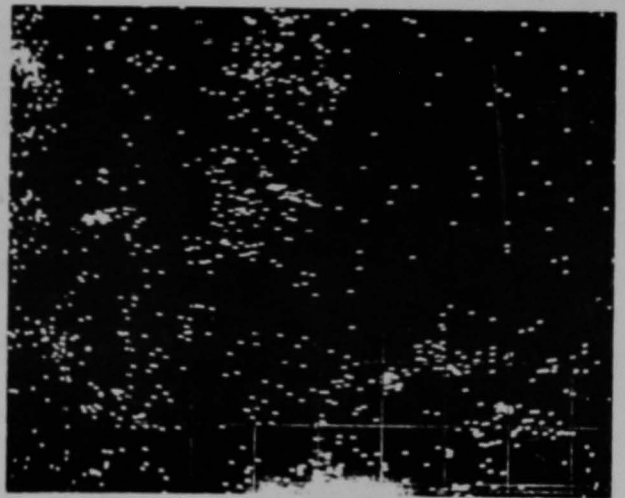
U



Fe

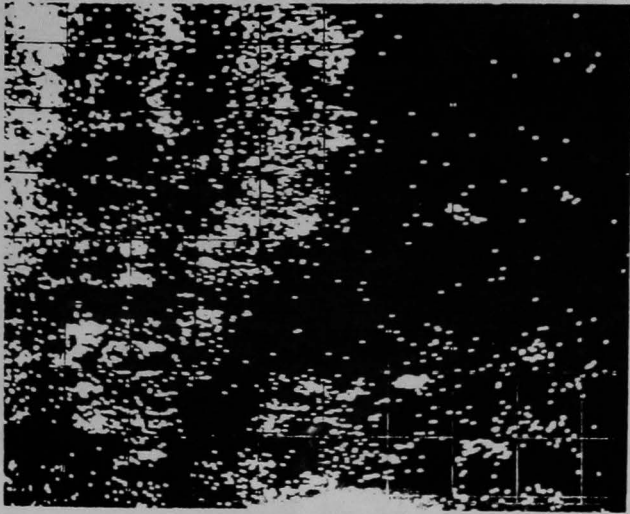


Ni

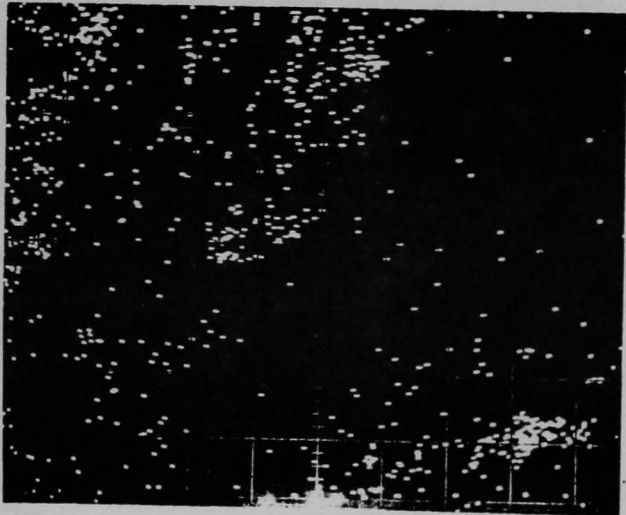
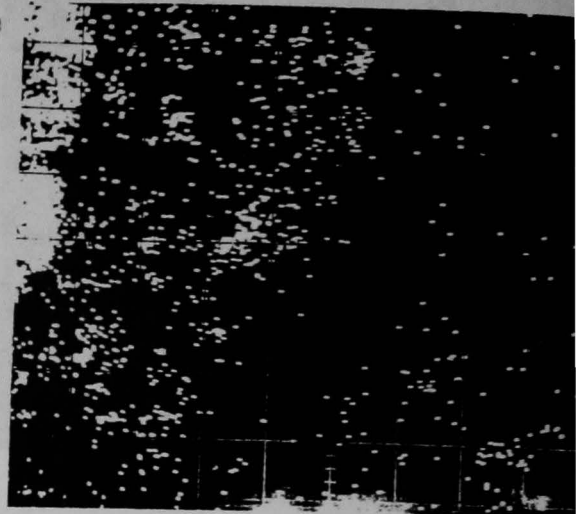


Cr

Fig. 12. Two-dimensional distributions of U, Fe, Ni, Cr, Ag, Cd, In, and Zr over Area 3 outlined in Fig. 11.



Ag



In

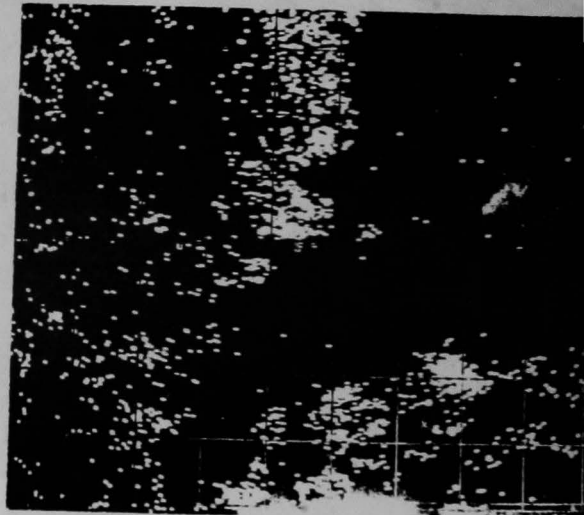


Fig. 12. (Concluded).

to area or in parts of areas. In some areas or parts of areas the x-ray signal strength was stronger for iron than for nickel and presumably these places contained particles from stainless steel. In other places the nickel x-ray signal strength was stronger than the iron which indicates the origin of the particles was inconel. Molybdenum was found in one area where the nickel signal was stronger than iron.

5. The uranium bearing particles were present in all areas. The concentrations varied by an estimated order of magnitude or more. Plutonium was found with the uranium in some instances.

All of the major elements (U, Fe, Ni, Cr, Cd, Ag, and In) showed some intense signal spots indicating relatively large particles; however, the x-ray dot patterns were frequently diffuse giving the indication of a homogeneous distribution of that element. This is apparently due to a wide distribution of very small particles.

The data collected on MUF-5B Top No. 3 and MUF-2B did not differ significantly from the data on MUF-5B Grab. The elemental mapping of the filter sections showed intimate mixture of essentially all core materials and failed to show any stratification of debris on the filters.

Particle analyses by electron microprobe were run on MUF-5B Homo, MUF-5B Top No. 3, and TMI-0104. The TMI-0104 sample was mounted as described in the Experimental section (II. B). The other two samples were polished metallographically mounted samples.

Forty-seven particles of TMI-0104 greater than 1  $\mu\text{m}$  in diameter were analyzed for metallic element composition and size. The results of the analyses are presented in Table VII. The data on particle diameter is given in units of micrometers ( $\mu\text{m}$ ). The elemental composition is given as a normalized intensity, and is semiquantitative with an estimated accuracy of  $\pm 20\%$ . As an example, consider particle 20. The results give the metallic composition of the particle as being 31.2% Mg, 34.3% Si, and 34.4% Mo by weight. These results do not mean the particle contains only those elements; indeed the particle is probably largely carbon based material as indicated by the weak signal obtained. Consequently, drawing conclusions about the overall composition of the sample TMI-0104 from these data should be done with care.

Table VIII shows a histogram of the particle size distribution and Table IX provides breakdown of the data in Table VII according to element, number of particles, and composition.

Zirconium occurs with a wide variety of elements including the elements of the control rod alloy, the elements of the 304 SS cladding, the elements of Inconel and uranium fuel. Interestingly, zirconium does not occur as pure zirconium oxide or metal, which would give an intensity of  $\sim 100\%$ . The highest intensity listed in Table VII for zirconium is only 60.4%

Six particles were analyzed that contained uranium. Three of the particles appear to be pure uranium oxide. The other three particles contain uranium with various other elements; but all three particles contain, U, Zr, Fe, and Ni. These data are not sufficient to confirm or reject the formation of a eutectic between the Zircaloy cladding and the uranium fuel.

TABLE VII

ELECTRON MICROPROBE ANALYSIS OF TMI-0104<sup>a</sup>

Particle	Normalized Intensity Ratios in %												Diameter, ( $\mu\text{m}$ )
	Mg	Al	Si	Zr	Mo	Ag	Cd	In	Cr	Fe	Ni	U	
1	--	2.9	3.8	--	18.1	--	34.3	--	--	23.5	17.5	--	12.3
2	--	--	--	--	--	--	--	--	0.8	1.5	--	97.6	3.1
3	37.8	--	27.4	--	34.7	--	--	--	--	--	--	--	7.7
4	0.4	0.2	0.2	--	4.7	59.1	--	32.2	--	0.6	2.6	--	9.2 <sub>b</sub>
5	38.0	--	18.4	--	43.5	--	--	--	--	--	--	--	12.6 <sub>b</sub>
6	--	1.7	2.0	30.6	1.2	--	26.3	--	1.4	20.7	16.1	--	14.8
7	--	1.2	0.5	4.8	9.4	--	31.8	--	1.0	23.1	28.2	--	16.7
8	--	2.6	86.3	--	--	--	--	--	1.0	2.6	7.4	--	5.1
9	--	--	0.3	--	--	--	--	97.6	--	1.2	0.9	--	4.3
10	0.1	0.2	0.2	0.5	5.4	52.8	--	--	1.6	11.6	27.6	--	18.0
11	--	0.3	0.6	2.0	2.8	--	44.2	--	0.7	7.9	41.4	--	16.0
12	--	0.4	0.3	17.6	--	--	76.1	--	--	1.6	4.0	--	6.6
13	--	2.2	2.6	--	44.3	--	43.1	--	--	4.6	3.1	--	6.2 <sub>b</sub>
14	--	--	7.0	--	18.8	--	--	43.2	6.1	14.1	--	--	19.2 <sub>b</sub>
15	--	11.3	14.4	--	23.4	39.0	--	--	--	--	11.9	--	20.3 <sub>b</sub>
16	--	--	99.9	--	--	--	--	--	--	--	--	--	1.7 <sub>c</sub>
17	--	--	99.9	--	--	--	--	--	--	--	--	--	10.2 <sub>c</sub>
18	--	0.4	0.2	47.0	--	43.1	2.2	--	--	5.4	1.7	--	5.6 <sub>b</sub>
19	--	7.0	6.4	--	22.4	--	28.8	--	--	17.7	17.7	--	4.2 <sub>b</sub>
20	31.2	--	34.3	--	34.4	--	--	--	--	--	--	--	12.0 <sub>b</sub>
21	--	0.5	0.4	--	11.2	19.4	--	18.3	6.2	11.4	32.5	--	3.1
22	--	--	0.1	--	0.7	20.8	78.4	--	--	--	--	--	6.7 <sub>b</sub>
23	41.5	12.4	--	--	46.1	--	--	--	--	--	--	--	10.7 <sub>b</sub>
24	--	--	99.9	--	--	--	--	--	--	--	--	--	1.7 <sub>c</sub>
25	--	0.3	0.2	0.9	2.5	13.9	67.8	--	1.0	4.1	9.4	--	24.8
26	--	--	--	0.4	0.7	15.6	81.7	--	--	0.4	1.1	--	6.4
27	--	0.1	--	--	1.7	--	2.7	--	0.6	84.0	10.9	--	6.7
28	--	1.6	0.6	0.8	19.7	--	65.5	--	2.3	8.1	1.4	--	9.4
29	--	0.2	--	60.4	--	16.8	--	6.5	0.7	4.1	9.4	--	7.0
30	--	--	--	--	--	--	--	--	--	0.2	--	99.8	4.9
31	--	0.3	0.1	6.0	1.3	14.1	73.8	--	0.8	2.1	1.5	--	6.4
32	--	2.1	1.0	8.8	18.6	--	37.4	--	1.0	20.6	10.4	--	2.0

TABLE VII (CONTINUED)

Particle	Normalized Intensity Ratios in %												Diameter ( $\mu\text{m}$ )
	Mg	Al	Si	Zr	Mo	Ag	Cd	In	Cr	Fe	Ni	U	
33	--	1.2	0.7	--	18.5	--	51.8	--	1.8	7.6	12.5	--	4.0
34	--	5.1	4.0	7.4	15.3	--	30.7	--	3.3	15.6	18.6	--	5.6
35	--	1.2	1.4	1.5	14.2	--	27.3	--	1.5	28.1	24.8	--	9.0
36	33.0	--	60.9	--	--	--	--	--	--	6.1	--	--	9.4
37	--	1.3	0.7	3.1	8.3	--	--	27.0	4.8	35.4	7.8	11.5	4.4 <sup>b</sup>
38	26.6	--	73.4	--	--	--	--	--	--	--	--	--	10.0 <sup>b</sup>
39	35.2	--	59.8	--	--	--	--	--	--	4.9	--	--	10.0
40	--	--	--	--	--	--	--	--	--	--	--	99.9	4.0
41	--	0.4	0.3	14.6	0.7	--	54.2	--	2.1	6.6	5.9	15.1	8.5 <sup>b</sup>
42	32.2	--	17.0	--	50.9	--	--	--	--	--	--	--	10.0 <sup>b</sup>
43	--	--	3.4	13.1	--	--	--	--	--	5.2	3.8	74.5	9.0 <sup>b</sup>
44	--	0.7	1.9	--	7.9	--	46.4	--	0.7	10.7	31.8	--	12.9
45	--	--	--	--	2.8	--	90.7	--	--	1.6	4.9	--	7.1 <sup>b</sup>
46	54.7	--	45.3	--	--	--	--	--	--	--	--	--	15.0 <sup>b</sup>
47	--	3.6	2.3	--	15.5	--	36.2	--	3.4	16.2	22.8	--	10.0

<sup>a</sup>Particles less than one micrometer were ignored in this analysis.

<sup>b</sup>Low yield, filter media.

<sup>c</sup>Particle moved during chemical analysis.

Particles 3,5,8,23, and 42 contained low concentrations of Ca.

Particles 8 and 13 contained low concentrations of Na.

TABLE VIII

PARTICLE-SIZED DISTRIBUTION FROM ELECTRON MICROPROBE ANALYSES

<u>Range in Micrometers</u>	<u>Number of Particles</u>
1-5	***** (13)
5-10	***** (18)
10-15	***** (10)
15-20	**** (4)
20-25	** (2)

---

Average diameter of all 47 particles = 9.0  $\mu\text{m}$ . Range 1.7 to 24.8. Only particles greater than 1- $\mu\text{m}$  diameter were selected for microprobe analysis.

TABLE IX

BREAKDOWN OF ELECTRON MICROPROBE ANALYSIS ACCORDING TO  
ELEMENT, INTENSITY, AND NUMBER OF PARTICLES

<u>Normalized Intensity Ratios in %</u>	<u>Number of Particles</u>
Element: Mg	
<20	*(1)
20-40	***** (7)
40-50	** (2)
Element: Al	
<20	***** (21)
Element: Si	
<20	***** (17)
20-40	** (2)
40-60	** (2)
60-80	** (2)
>80	**** (4)
Element: Zr	
<20	***** (13)
20-40	*(1)
40-60	*(1)
60-80	*(1)
Element: Mo	
<20	***** (22)
20-40	***** (5)
40-60	**** (4)
Element: Ag	
<20	**** (4)
20-40	** (2)
40-60	*** (3)
60-80	*(1)
Element: Cd	
<20	** (2)
20-40	***** (7)
40-60	**** (4)
60-80	***** (5)
>80	** (2)
Element: In	
<20	** (2)
20-40	** (2)
40-60	*(1)
60-80	
>80	*(1)

TABLE IX (CONTINUED)

<u>Normalized Intensity Ratios in %</u>	<u>Number of Particles</u>
Element: Cr <20	***** (16)
Element: Fe <20	***** (24)
20-40	**** (4)
40-60	
60-80	
>80	*(1)
Element: Ni <20	***** (26)
20-40	***** (6)
Element: U <20	** (2)
20-40	
40-60	
60-80	*(1)
>80	***(3)

Aluminum is present in 21 of the 47 particles analyzed; however, it never has an intensity >5.1% except on filter media particles. If pieces of the burnable poison (pelletized  $\text{Al}_2\text{O}_3\text{-B}_4\text{C}$ ) were present in the sample, there should be particles with near 100% intensity for aluminum. This lack of particles with high aluminum content could be due to the limited sample examined or reflect the limited amount of burnable poison material in the reactor core. It could also indicate that thermal shock and mechanical shock during the accident were not sufficient to fracture the material to produce micrometer-size particles.

Several particles of what may be ion exchange media were present in the sample. These particles gave low yields of x-rays and generally contain large amounts of magnesium, silicon and molybdenum. Magnesium is present in the cone as MgO an insulating material. Silicon is present in Inconel and stainless steel. The molybdenum, which is apparently soluble, is from Inconel in the core.

Since only particles of  $>1 \mu\text{m}$  were sized, the data presented in Table VIII is obviously shifted toward higher average diameter; however, this information may be useful in determining if certain elements occur more frequently in certain particle sizes. From the limited data of this analysis, there is no obvious composition-size correlation.

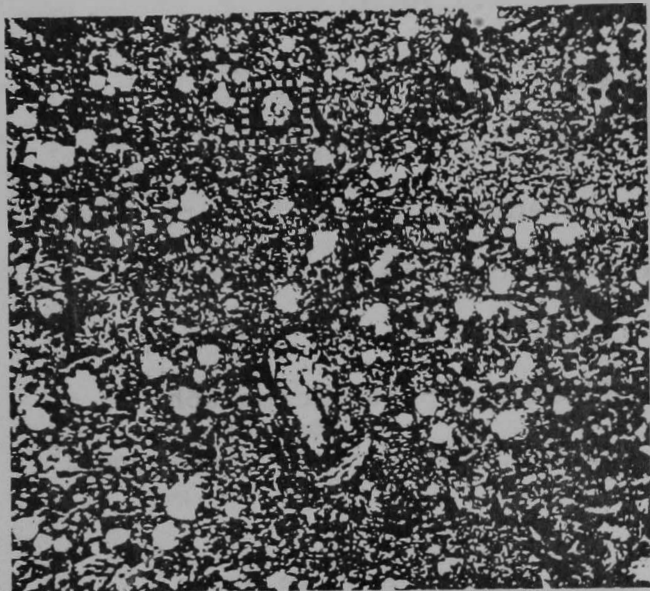
The MUF-5B Homo sample was examined with an optical microscope to select the particles for microprobe analysis. The particles were selected because of some unusual feature such as color or apparent multiphase composition. Each particle was

analyzed with the energy dispersive analyzer monitoring the elements Na through Am. Counts for the elements present were then taken on the wavelength dispersive analyzer to eliminate interferences and to obtain intensity ratios from pure element standards. An example of the kind of information gathered is shown in Figure 13. The area outlined on the photomicrograph corresponds to the area scanned by the specimen current image and x-ray dot maps.

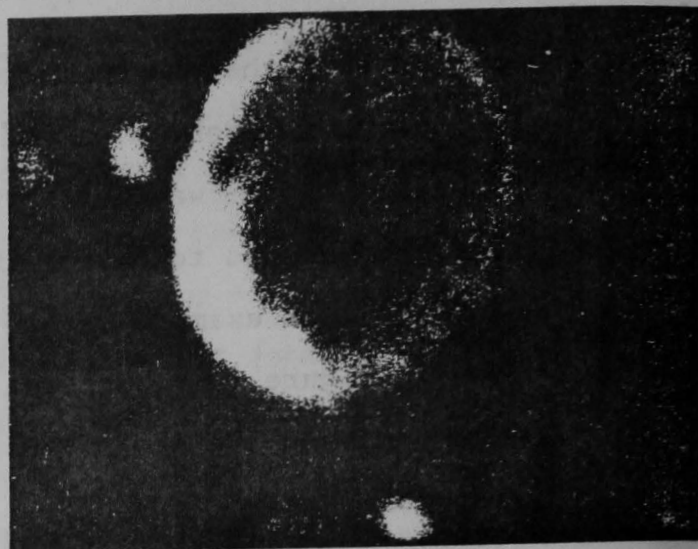
Seven particles were analyzed. The first particle was selected because of a darker colored band around the perimeter of the irregularly shape. The particle contained mostly Zr with lesser amounts O, Cu, Fe, Ni, Ag, In, Th and U. Initial analyses showed no differences between the darker colored band and the center portion of the particle; however, closer examination showed a much higher oxygen concentration in the band than in the center of the particle.

Particle 2 was spherical and had a metallic luster. It was thought that this particle was control rod material. Microprobe analysis confirmed that the particle was Ag, In, and Cd with the surrounding area having Mo, Cd, and O. The Cd was spread uniformly over the area and was not concentrated in the particle as the Ag and In were; therefore it is difficult to determine how the Cd became associated with the particle.

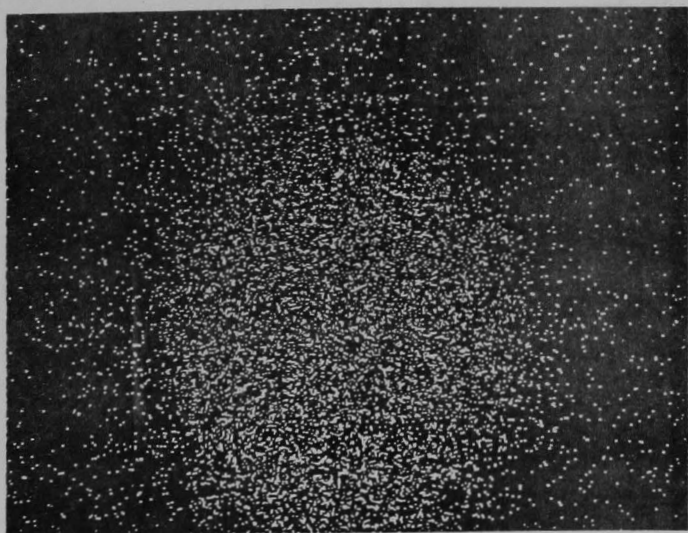
Particle 3 appeared to be an agglomerate of small particles; however, the secondary electron image failed to confirm this observation (see Figure 13). The particle contained mostly Cr, Fe, Zr, and U with lesser amounts of O, Al, Si, Mn, Ni, Cd, and In.



Photomicrograph 600X



Secondary electron image 500X



U



Cr

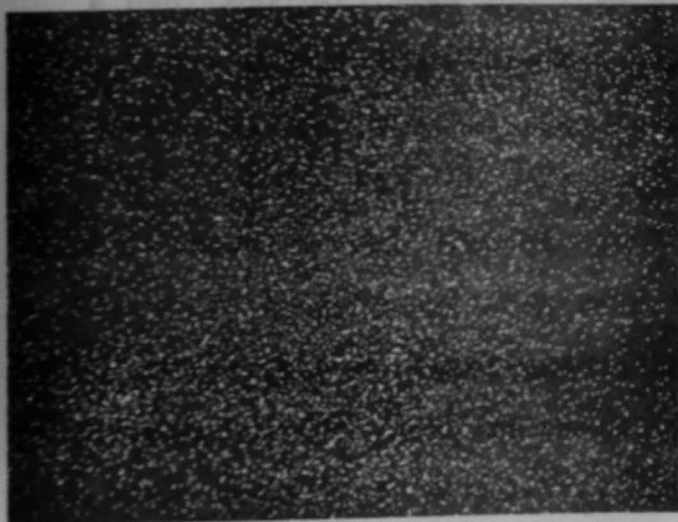
Fig. 13. Electron microprobe analysis of an individual particle in the MUF-5B Homo sample.



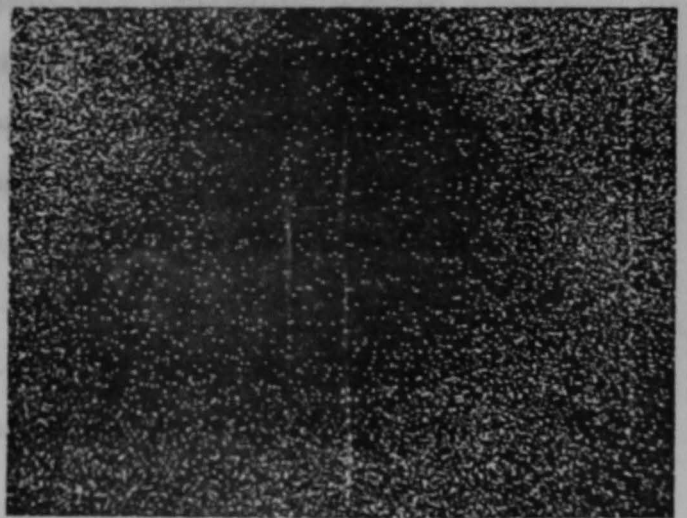
Zr



Mn



Fe



Cd

Fig. 13 (continued).

Particle 4 was reddish under the light optics. The major constituent was Zr with lower concentrations of O, Al, Si, Fe, Ni, Ag, Cd, In, and U.

Particles 5, 6, and 7 contained only zirconium and oxygen. The intensities were in agreement with those from a  $ZrO_2$  standard. One of the particles was ~200- $\mu$ m long by 60- $\mu$ m wide. What appeared to be tiny bubbles could be seen in this particle.

The MUF-5B Top No. 3 sample was examined with the intent of looking at particles containing U and Zr as the major constituents. Seven areas were examined as described for the seven previous particles. The sample  $\beta$ - $\gamma$  activity, which measured 6R/hr, lowered the sensitivity of the analysis and preclude oxygen analyses. Seven areas (each ~25  $\times$  20  $\mu$ m) were examined.

Area 1 contained two Zr particles. One particle contained a high concentration of Ni with no Cr present and little if any Fe. The other particle appeared to contain Ag; however, Ag, Cd, and In dominated the area. Consequently, it is not clear how the Zr and Ag are associated.

Area 2 contained several particles high in Zr or U. Fe, Ni, and Cr were present with the Zr in one particle and absent in another. One U particle contained Cr and Fe, but others did not contain the Cr and Fe.

A large Zr particle was found in Area 3. It did not contain any other element. A small U particle in the area contained Cr and Fe. This area also contained a pure Ti particle.

The fourth area contained three U particles. The largest particle contained Zr, Cr, and Fe.

Area 5 contained two U particles. The larger particle contained significant quantities of Cr, Fe, and some Zr. The other particle was relatively pure.

Area 6 included one particle containing U, Cr, and Fe.

The seventh area contained a relatively pure U particle. Zirconium was present, but was not associated with any elements.

There was evidence in some of the seven areas analyzed of segregation of Cr from Fe and Ni and segregation of Ni from Fe and Cr. Evidence of control rod materials segregation was found, also.

The presence of uranium particles containing Cr and Fe in MUF-5B Homo and MUF-5B Top No. 3 is consistent with the observation of two of six particles in the TMI-0104 sample containing U, Cu, Fe, and Zr. However, the particles of TMI-0104 contained significant quantities of nickel. The uranium bearing particles of the MUF-5B samples did not contain significant amounts of nickel. Two of the TMI-0104 uranium particles contained control rod materials; the uranium bearing particles of MUF-5B samples did not contain control rod alloy elements as major constituents. These discrepancies are believed to be due to the incomplete dispersion of the particles in preparing the TMI-0104 sample for analyses, i.e. the particles may have been agglomerates. Where the samples were metallographically mounted the agglomeration was not a problem. Another piece of evidence that agglomeration was a problem with the TMI-0104 samples is the lack of essentially pure zirconium on zirconium oxide particles. Of the 17 particles containing zirconium in sample TMI-0104 not one has greater than

61% zirconium. In the MUF-5B samples several particles of pure zirconium or zirconium oxide were found.

The TMI-0104 sample had no particles containing Cd and In together whereas the MUF-5B samples apparently did have these elements together in several particles. The reason for this difference is not known.

#### G. Neutron Activation Analysis for I-129.

The I-129 concentration determined in samples MUF-2A and MUF-2B are approximate minimum concentrations. This is due to several causes. First the fraction of the total iodine in the sample that was driven off and collected is unknown. Second, the standard used to determine the counting efficiency of the detector was a solution of a somewhat different geometry than the activated samples. Third, the neutron flux in the reactor was not measured, but was estimated from previous experience.

The values determined for the I-129 concentration were 50 ppm for the MUF-2B sample and 59 ppm for the MUF-2A sample. A minimum value of ~50 ppm for each sample is considered reasonable.

The heating of the debris to drive off the iodine effected a good separation of the iodine from the other elements and is considered a promising method for this analysis.

#### H. Carbon Analysis.

A single carbon analysis was run on a sample of the MUF-5B Homo sample (3rd cut). The sample was heated to ~1300°C in an oxygen atmosphere and the released CO<sub>2</sub> was determined with an infrared detector. The carbon content was 10% by weight.

#### IV. CONCLUSIONS

The physical and chemical character of the debris collected on the MUF-2A, MUF-2B and MUF-5B filters is essentially the same for all three filters. The debris consist of an intimate mixture of most of the major materials found in the reactor core, i.e., fuel, fuel cladding, control rod materials, Inconel and stainless steel. Some differences were found when data from analysis of debris on the filters was compared. Differences were found in particle size distribution, radionuclide content and the percentage elemental composition.

Particle sizing results indicate a statistically significant difference in the mean size of particles collected on the filters. The MUF-2B filter has a mean particle size of 1.86  $\mu\text{m}$  compared to 1.61 to 1.50  $\mu\text{m}$  for MUF-5B samples and 1.48  $\mu\text{m}$  for the MUF-2A sample. The significance of these differences is questioned since the 1.61  $\mu\text{m}$  mean diameter and the 1.50  $\mu\text{m}$  mean diameter determined for the MUF-5B filter samples are also statistically different. This difference in particle size on a single filter may be due to where the particles were collected on the filter. Consequently, the difference in mean particle size between filters may be of similar origin even though the difference between the MUF-2B and the other filters is greater.

The gamma emitting radionuclide concentrations vary from filter to filter. Particularly, the Cs-137 concentration varies when compared to the other radionuclides. This variation may simply reflect the percentage of filter material in the analyzed sample since cesium is water soluble and evaporation of absorbed water would leave cesium on the filter material.

The elemental concentrations on the MUF-2A and MUF-2B filters appears to be similar. For example, if the elemental concentration of Fe, Ni, Ag, Cd and Zr are ratioed to the uranium content, the differences in ratios for a particular element on the two filters are within experimental error. However, when a similar calculation is made for the MUF-5B sample, the uranium content is found to be a factor of 3 or 4 higher when compared to Fe, Ni and Zr. The Ag and Cd are within experimental error.

The mass spectrometry results which give the isotopic abundances show the fuel on all the filters to have a U-235 concentration of 2.30% by weight and to be identical in all other isotopic concentrations (see Table V). The 2.30% U-235 is what might be expected from the core of the reactor (6).

Gamma ray spectroscopy revealed the expected gamma emitting radionuclides. Cesium-137 is the dominate activity with levels as high as 5641  $\mu\text{Ci/g}$  of debris as of March 25, 1983. This corresponds to a concentration of 65 ppm. This is in the range of the I-129 concentration which was estimated to have a minimum concentration on the MUF-2A and MUF-2B filters of 50 ppm. These similar numbers might be taken to indicate that iodine and cesium are associated; however, caution should be exercised in drawing this conclusion since significant quantities of Ag, Cd and In are present which may have reacted with the iodine.

The emission spectroscopy results indicate a broad separation of elements from the parent alloys as does the electron microprobe analyses. The control rod alloy elements separated, tin separated from zirconium, manganese separated from iron in stainless steel,

and copper separated from nickel in Inconel. All of these elements that separated from the parent material have relatively low melting points compared to the principal element in the parent material.

Electron microprobe analyses indicate segregation of some of the major elements such as nickel separating from Cu and Fe. Also, chromium apparently separates from Fe and Ni in some instances.

The electron microprobe also gives evidence for a material formed of U, Cu, Fe and sometimes Zr. Some of particles of this material appear to be roughly spherical which might indicate the particle was formed from molten material. Zirconium appears to be allied with Cr and Fe in some particles. The nature of the materials is not understood at this time.

REFERENCES

1. T. Allen, Particle Size Measurement, Chapman and Hall Ltd., 2nd edition, 1975.
2. C. F. Metz, G. R. Waterbury, "Sealed-Tube Dissolution Method with Applications to Plutonium-Containing Materials," Los Alamos National Laboratory report LA-3554 (July 1966).
3. J. R. Phillips, "New Techniques in Precision Gamma Scanning (Applications to Fast Breeder Reactor Fuel Pins)," Los Alamos National Laboratory report LA-5260-T, UC-4, 80, July 1973.
4. E. E. Underwood, Quantitative Stereology, Addison-Wesley Publishing Co., 1970.
5. G. Herdan, Small Particle Statistics, Academic Press Inc., 2nd edition, 1960.
6. R. E. Mason, et al. "Interim Report on the TMI-2 Purification Filter Examination," EGG-TMI-6181, Feb. 1983.

